

博士論文

Rational Synthesis of Multipore Zeolites Using Simple Organic Structure-Directing Agents by Seed-Directed Method

(種結晶添加法によるシンプルな有機構造規定剤を用いたマルチポアゼオライトの合理的合成)

Sogukkanli Sibel

ソウグクカンル シベル

Department of Chemical System Engineering

The University of Tokyo

**A Dissertation Submitted in Partial Fulfillment of
the Requirements for the Degree of Doctor of Philosophy**

Dissertation Committee:

Tatsuya Okubo, Professor (Supervisor)
Department of Chemical System Engineering
The University of Tokyo

Kazunari Domen, Professor
Department of Chemical System Engineering
The University of Tokyo

Masaru Ogura, Professor
Department of Chemical System Engineering
The University of Tokyo

Kazuya Yamaguchi, Professor
Department of Applied Chemistry
The University of Tokyo

Masashi Okubo, Associate Professor
Department of Chemical System Engineering
The University of Tokyo

Toru Wakihara, Associate Professor
Department of Chemical System Engineering
The University of Tokyo

Dedicated to my dear family

En deęerli varlıęım olan ailem'e

Table of contents

Table of contents	v
Chapter 1. General Introduction.....	1
1.1. Porous materials.....	1
1.2. Zeolites.....	5
1.3. Multipore zeolites	11
1.3.1. Zeolites with medium and large pores.....	15
1.4. Strategies for rational synthesis of zeolites.....	17
1.4.1. The synthesis of zeolites using recyclable organic structure-directing agents.....	17
1.4.2. The synthesis of zeolites without using organic structure-directing agents.....	18
1.4.3. The synthesis of zeolites by replacing organic structure-directing agents.....	20
1.5. Scope and overview of this dissertation.....	22
1.6. References	24
Chapter 2. Synthesis of Aluminosilicate MSE-type Zeolites.....	29
2.1. Introduction.....	29
2.2. Experimental section.....	32
2.2.1. Materials.....	32
2.2.2. Synthesis of seed crystals with organic structure-directing agents.....	32
2.2.3. Synthesis of seed crystals without organic structure-directing agents.....	33
2.2.4. Preparation of physical mixture of tetraethylammonium hydroxide with MCM-68 seed crystals	33
2.2.5. Synthesis of MSE-type zeolites by using tetraethylammonium hydroxide as a simple organic structure-directing agent.....	34
2.2.6. Characterization.....	35
2.3. Results and discussion.....	37
2.3.1. Structural and textural evaluation.....	37
2.3.2. Characterization of occluded tetraethylammonium cations in MSE structure	43
2.3.3. Crystallization kinetics	50
2.4. Conclusion	52
2.5. References	54
Chapter 3. Synthesis of Zincoaluminosilicate MSE-type Zeolites.....	57
3.1. Introduction.....	57
3.2. Experimental section.....	60

3.2.1.	Materials	60
3.2.2.	Synthesis of MCM-68 seed crystals	60
3.2.3.	Preparation of zincoaluminosilicate gels	61
3.2.4.	Synthesis of MSE-type zeolites using zincoaluminosilicate gels and tetraethylammonium hydroxide as a simple organic structure-directing agent	62
3.2.5.	Synthesis of comparison sample by using zinc acetate	63
3.2.6.	Ion-exchange	63
3.2.7.	Characterization.....	64
3.3.	Result and discussion	66
3.3.1.	Characterization of zincoaluminosilicate gels	66
3.3.2.	Characterization of zincoaluminosilicate MSE-type zeolites	67
3.3.3.	Structural evaluation.....	67
3.3.4.	Chemical and textural evaluation	76
3.3.5.	Ion-exchange characteristics	80
3.4.	Conclusion	82
3.5.	References	84
Chapter 4.	Synthesis of Aluminoborosilicate CON-type Zeolites.....	86
4.1.	Introduction	86
4.2.	Experimental section.....	89
4.2.1.	Materials	89
4.2.2.	Preparation of <i>N,N,N</i> -Trimethyl(-)-cis-myrtanylammonium as organic structure directing agent	89
4.2.3.	Synthesis of borosilicate beta seed crystals	90
4.2.4.	Synthesis of borosilicate CIT-1 seed crystals	91
4.2.5.	Synthesis of aluminoborosilicate CON-type zeolites using tetraethylammonium hydroxide as an organic structure-directing agent.....	92
4.2.6.	Characterization.....	93
4.3.	Result and discussion	94
4.3.1.	Chemical and textural evaluation	94
4.3.2.	Characterization of occluded tetraethylammonium cations.....	102
4.4.	Conclusion	104
4.5.	References	105
Chapter 5.	General Conclusion and Future Perspectives	107
	List of publications	112
	Acknowledgment	113

Chapter 1. General Introduction

1.1. Porous materials

Porous materials with nanosized structure offer unique “spaces” in their interiors which enable the material to interact with atoms, ions, and molecules not only at the surface but also throughout the entire body.^[1,2] Besides their traditional usage as catalysts, ion-exchangers, and adsorbents, these type of materials have been intensively investigated in both academia and industry for their usage in new areas ranging from device technology to drug delivery.^[1,6] The porous solids were classified into three groups based on their pore structures since the shape, size, and volume of the pores are primary factors to characterize the materials. According to the International Union of Pure and Applied Chemistry (IUPAC), the materials with pore sizes are exceeding 50 nm referred as macroporous, those are between 50 and 2 nm called as mesoporous, and those are less than 2 nm denoted as microporous.^[7] Among them, the only ones having microporous and mesoporous pores are scope of being nanosized.^[8] During the past decades, the interest in developing these materials with uniform pore structures is firmly increased because of their potential ability to control the adsorbates and bring superior application properties to those materials.^[1] Therefore, various mesoporous and microporous materials with ordered structures were established from different organic and inorganic species as shown in Figure 1.1. These two classes of materials can be further subdivided into three general groups such as carbonaceous adsorbents, porous organic materials, zeolite molecular sieves.^[8,9]

Carbonaceous adsorbents as organic-based materials can be prepared using low-cost precursors such as coal^[10] and agricultural solid wastes.^[11] Those materials with their unique micropore and mesopore volumes provide quite high surface areas of over 2000 m²g⁻¹.^[12,13] As one of the carbonaceous adsorbents, activated carbons are very useful materials in gas storage^[14] and separation applications.^[15] Another type is synthetic carbons such as ordered mesoporous carbon (OMC)^[16] which offers better sorption characteristics than those of activated carbons since their tailored pore architectures.

Porous organic materials enable us to design novel structures by selecting the components based on the requirements. Those materials can be synthesized from purely organic materials. They are covalently bonded and hydrothermally stable materials, showing high and accessible surface areas, and properties.^[17,18] Porous polymer networks (PPNs) is another type of porous organic materials which offer superior thermal and chemical stability beside large surface areas. There are a number of PPNs such as hyper-crosslinked polymers (HIPs), polymers with intrinsic microporosity (PIMs), and conjugated microporous polymers (CMPs) designed to be utilized in various applications.^[19] Covalent organic frameworks (COFs) are one of the most utilized PPNs. By assembling reversible self- or/and co-condensation reactions, they constructed from covalently bonded light elements such as B, C, N and O which are favorable for the formation of stable structures as in those of diamonds and graphite.^[20] Because of their being low-cost, easy processing and low molecular density, COFs are emerged as promising materials in gas storage^[21,22], photonic and catalytic applications.^[23]

Additionally, the novel porous materials structured from inorganic bodies with organic core materials are established as hybrid porous materials. Metal-organic

frameworks (MOFs) are typical hybrid porous materials with crystalline structures wherein metal cations or clusters of cations are connected with organic linker ions or molecules by coordinating bonds.^[24] An extensive class of MOFs can be designed by using infinite possible combinations of various organic and inorganic species in reticular synthesis.^[25,26] MOFs possess unique features such as organic functionality and tunable pore characteristics. Especially, their extremely high surface areas (Langmuir surface area: 10400 m² g⁻¹ for MOF-210) and large pore volumes allow these hybrid materials to find a wide range of applications as gas storage^[27,28], separation^[29,30], catalysis^[31], drug delivery^[32], and chemical sensors.^[33] Another example of hybrid porous materials is periodic mesoporous organosilicas (PMOs) which can be synthesized by the sol–gel process from organo-bridged alkoxysilane in the presence of structure-directing agents.^[34] Because of their advantageous robust frameworks, those materials can be utilized in light-harvesting^[35] and electronics.^[36]

On the other hand, porous materials can also be structured as micropore and mesopore from only inorganic components such as metals^[37] and metal oxides.^[38] MCM-41 is one of the particular mesoporous silica materials exhibits an ordered pore system with adjustable sizes from 2 to 50 nm and a number of desirable physical properties such as large internal surface areas and thermal stabilities.^[39] Therefore, these molecules have found great utility in catalysis and sorption applications, and they recently proposed as convenient materials for drug and gene delivery.^[40]

Zeolites will be deeply discussed in the following section 1.2.

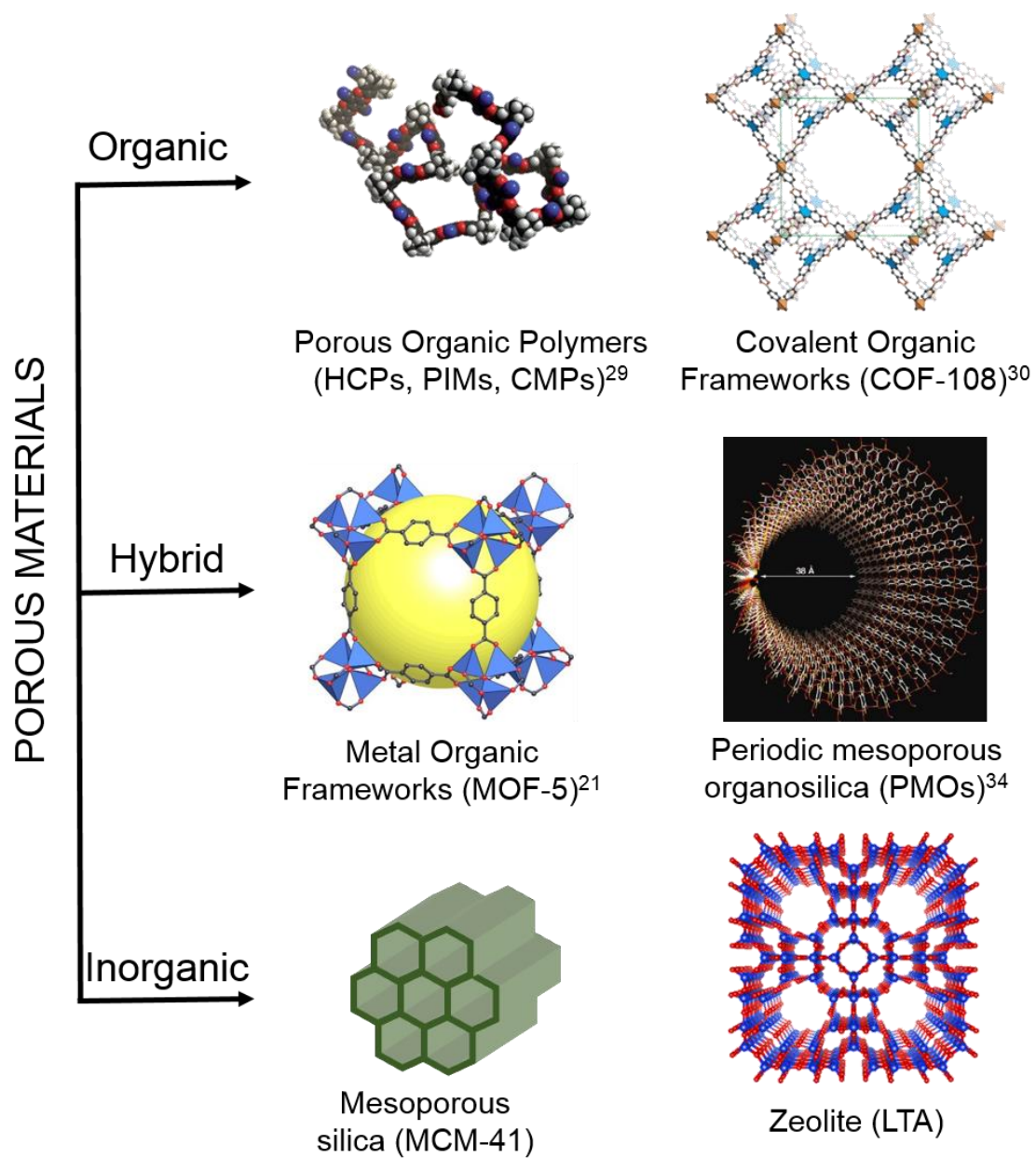


Figure 1.1 Illustrations of some representative ordered porous materials.

1.2. Zeolites

Zeolites are very important class of crystalline microporous inorganic materials. These materials constructed of tetrahedral TO_4 (T (tetrahedral atom) = Si, Al, Zn, Ti, Ge, Ga, *etc.*) primary building units, and each unit is connected with four neighbors by sharing their vertex oxygen atoms (Figure 1.2).^[41,42] Zeolites have found tremendous usage in many traditional industrial applications such as catalysis, separation, adsorption, and ion exchange due to their well-defined pores and cavities of molecular dimensions within their frameworks (ca. 3-12 Å).^[43,44] The zeolite science is started by the discovery of the first zeolite from an unknown silicate material in 1756,^[41] developed an identity with great efforts of Barrer and Milton on the synthesis of zeolites in the 1940s,^[45,46] and it came up to these days with continuous growth. Today, the Structure Commission of the International Zeolite Association (SC-IZA) has already recognized 232 types of zeolite structure with different pore architecture. The topological uniqueness of each zeolite structures is identified by coordination sequences and vertex symbols and given three-letter code.^[47]

Zeolites are conventionally synthesized under hydrothermal conditions from supersaturated reaction gels in the high-pressure water at temperatures between about

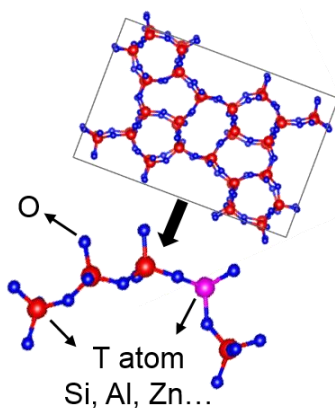


Figure 1.2 Illustrations of the linked TO_4 tetrahedral primary units in ZSM-5 unit cell.

80 and 200 °C.^[48] The reaction gels are generally containing T atom sources such as silica and alumina sources (e.g. fumed silica, colloidal silica, aluminum hydroxide, sodium aluminate, *etc.*) mixed with mineralizing agents such as hydroxide and fluoride anions, and organic molecules as shown in Figure 1.3.

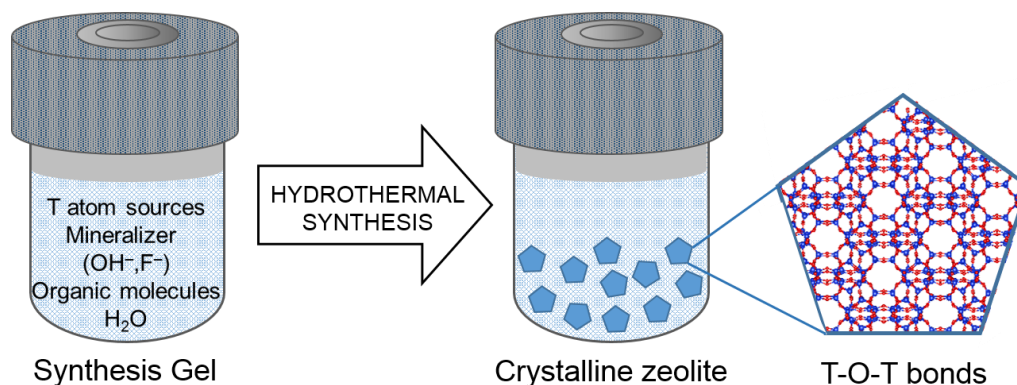


Figure 1.3 Illustration of conventional hydrothermal synthesis of zeolites.

In fact, the first zeolites such as zeolite X and Y had been synthesized from the reaction gels containing only inorganic components.^[49,50] Then, in the early 1960s, simple quaternary ammonium cations were introduced to be used as organic molecules in zeolite synthesis.⁵¹ This introduction had surely a great impact on the zeolite synthesis since it allowed discovery of many industrially important zeolites such as zeolite beta (*BEA) and ZSM-5 (MFI).^[52,53] By the time of progress, the variable range of organic molecules rapidly expanded from simple to rigid, bulky and complex organic molecules owing to their ability to lead new zeolite structures. According to Davis, organic molecules can behave as either organic structure-directing agents (OSDAs) or pore filler species during the formation of zeolites.^[54] For instance, 18-crown-6 is a specific molecule to be utilized only in the synthesis of a particular zeolite (EMT); thus, it can be claimed that the molecule is acting as OSDA.^[55] On the other hand, one organic molecule can be used to synthesize different zeolites, or one zeolite can be

prepared from various organic molecules. In that case, the organic molecules can be asserted as pore-fillers since they stabilize the structures by fitting in the voids. In order to bring a better understanding on the structure-directing mechanism of OSDAs, the formation of pure silica MFI zeolite (silicate-1) was studied from the gel prepared with tetrapropylammonium (TPA) as OSDA, and without any inorganic cations.^[56] The proposed hydrophobic hydration mechanism is shown in Figure 1.4. In this mechanism, it is speculated that TPA cations and hydrophobic silicate species firstly order the water molecules around itself with the help of hydrophobic hydration. When their hydrophobic hydration spheres come close to each other, they overlap and release the water into the bulk water phase (entropic driving force). Then, this overlapped organic and silicate species make van der Waals contacts (enthalpic driving force) and form the organic-inorganic composite which promotes further crystal growth of MFI structure.

In addition to the conventional hydrothermal synthesis of zeolites, many other synthesis paths such as solventless synthesis^[57,58] solvothermal synthesis,^[59] and ionothermal synthesis^[60] are reported in the literature. In any case, it is well-known that the zeolite synthesis is a complicated self-assembly process in which many factors can influence the formation mechanism, such as raw materials, composition of reactants, synthesis conditions, *etc.* When appropriate conditions are prepared, the zeolite crystallization starts immediately after the induction period, which is the time from the start of reaction till obtaining the first crystal particles, and continues with crystal growth.^[48]

The characteristics of zeolites are directly related to their chemical composition, crystal structure and effective pore diameter, which result in high surface area, the possible selectivity for products, high adsorption capacity, the possible location and numbers of the active sites.^[43]

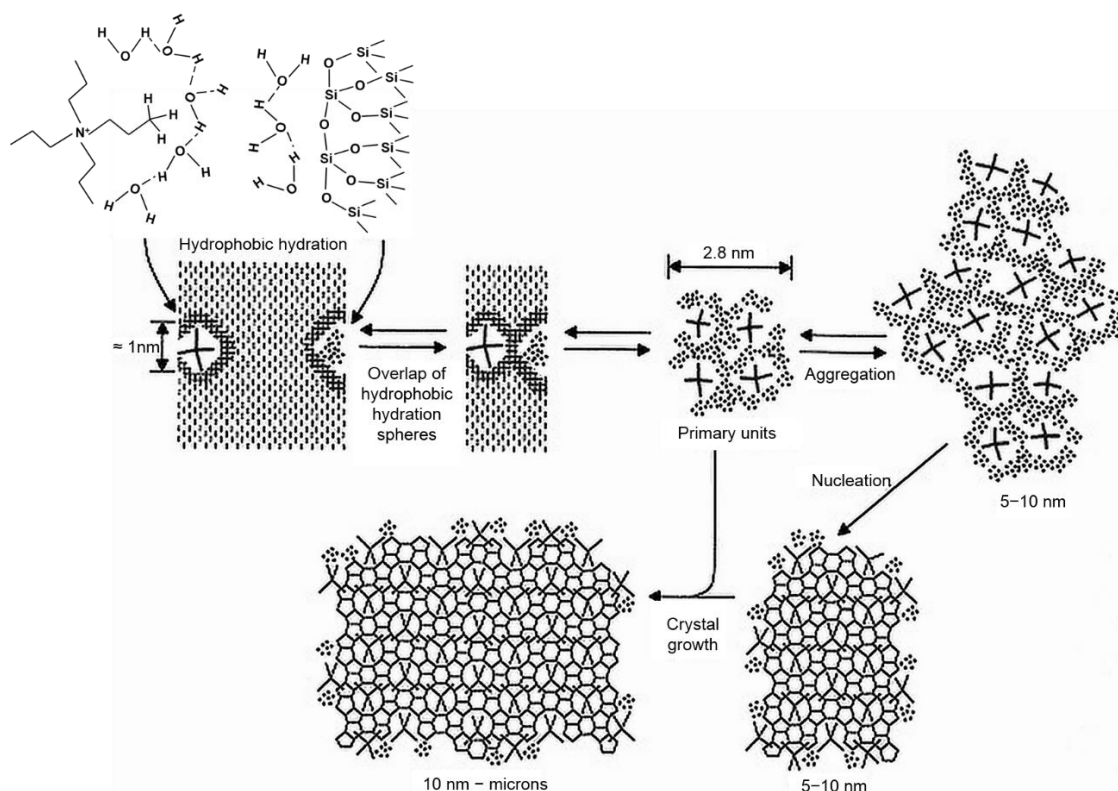


Figure 1.4 Proposed formation mechanism of pure silica MFI (silicate-1) from the gel with TPA as OSDA, and without any inorganic cations.^[56]

The most extended gel composition of zeolites is as aluminosilicates. Recently, several heteroatoms such as Ti, Zn, Ga, Ge, Sn, *etc.* are inserted into zeolitic frameworks by isomorphous substitution of Si atoms by those elements.^[61] Indeed, this replacement allows to subtly adjust the physicochemical features of the zeolites such as internal acidity, redox properties, and hydrophobic–hydrophilic nature.^[62–64] For example, pure silicate materials (SiO_2) exhibit hydrophobic properties, and they do not contain any framework charge since silicon is a tetravalent atom. Aluminosilicates and other metal inserted zeolites (except tetravalent metal atoms) generate negative charges per atoms in their lattice which can be compensated with the exchangeable extra-framework cations such as alkaline metals (e.g. Na^+ , K^+) and alkaline earth cations (e.g. Ca^{2+} , Ba^{2+}). Also, these zeolites behave more hydrophilic and can be utilized as

adsorbents for the water purification and softening the washing water.^[65] Among these zeolites, aluminosilicates usually exhibit high Brønsted acidity because of the ammonium ions (protons) which balanced with negative charges generated by the insertion of trivalent Al atoms into the framework.^[42] They are of great importance for many catalytic applications such as oil refining and petrochemistry.^[43] On the other hand, the isomorphic substitution of transition metal ions allows the introduction of Lewis acidic properties into high silica materials which brings to the zeolite high catalytic activity and selectivity for the oxidation and redox reactions.^[66,67] Moreover, the zeolites containing tetravalent transition atoms (e.g. Ti, Sn, *etc.*) shows hydrophobic characteristics with Lewis acid sites which are recently proposed to be used to catalyze isomerization of aldoses.^[68]

In addition to their chemical compositions, zeolites can be identified depending on the size, shape, and dimensions of their pores, channels, and cavities since most of the chemical reactions related to industrial applications occur in those pores, channels, and cavities. Therefore, their characteristics play a key role to determine the usage of zeolites in specific reactions as catalysts. Based on their pore sizes, zeolites can be divided into four major groups. The zeolites having 8 T-atoms within their pore openings are defined as “small pore zeolites” (8-R, ca. 3.0–4.5 Å), those with 10 T-atoms are called as “medium pore zeolites” (10-R, ca. 4.5–6.0 Å), those with 12 T-atoms are referred as “large pore zeolites” (12-R, ca. 6.0–7.0 Å), and those presenting more than 12 T-atoms are denoted as “extra-large pore zeolites”. Also, the number of channel dimensions are used for their structural definition such as “onedimensional” (1D), “twodimensional” (2D), or “threedimensional” (3D) zeolites.^[69] Indeed, multidimensional zeolites are desired for many reactions since their different dimensional channels may intersect and form cavities within zeolitic structures which

provide larger diffusivity of the reactants and products.^[70,71] For example, multidimensional zeolites with large and extra-large pores (pore openings ca. 7Å) such as ITQ-33 generally used for the reactions involving large and bulky organic molecules such as acetalization of aldehydes,^[72] while the ones with small pores (pore openings smaller than 4Å) such as CHA process small organics as in the methanol-to-olefins (MTO) and selective catalytic reduction (SCR) of NO_x.^[73] Also, the five zeolites (FAU, MFI, MOR, *BEA, and FER) as the most commercialized zeolite catalysts are widely used in fluid catalytic cracking (FCC) process with their intersecting multidimensional structures.^[74]

1.3. Multipore zeolites

A different class of multidimensional zeolites was introduced as multipore zeolites which contain intersecting pores of differently sized in the same structure.^[75] These zeolites are very useful materials as shape-selective catalysts since they allow different diffusion rates to the reactants and products along different channels. This feature of multipore zeolites can be explained by their molecular traffic control (MTC) effect.^[76,77] MTC occurs in the materials containing more than one type of intersected channels. By the help of MTC, reactants may preferentially enter the zeolite through one of those pore systems, whereas products diffuse out through another one. In Figure 1.5, the proposed shape selective molecular traffic control effects of the zeolite with only one type of channel system such as MEL (a), and with different type of intersected channels system such as ZSM-5 (b) are illustrated. Also, the partial pressure of reactants which are inside and outside the zeolites are given as P_r^i and P_r^o , respectively, P_p^i and P_p^o being corresponding values for products. In the case of (a), counterdiffusion effects will occur due to larger value of P_r^o than that of P_p^i , and the diffusion of the products will be restricted by the faster diffusion of reactants since they have smaller size than

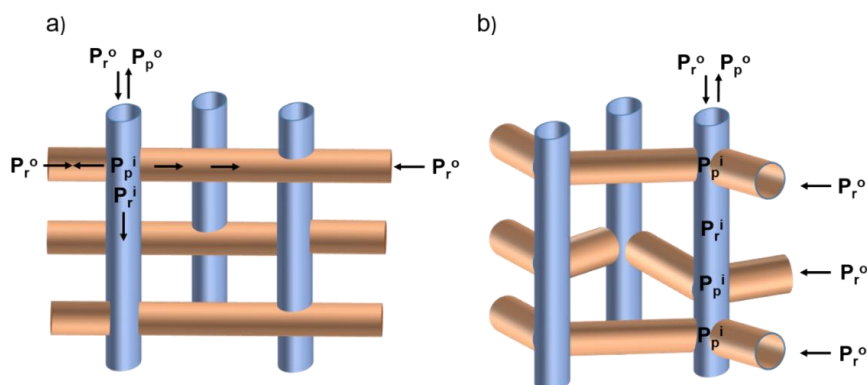


Figure 1.5 Illustration of the proposed shape selective molecular traffic control effects of (a) the zeolite with only one type of channel system such as MEL, and (b) with different type of intersected channels system such as ZSM-5.^[77]

that of products. On the other hand, ZSM-5 is a particular structure since it contains linear and sinusoidal channels. In the case of (b), reactants may enter either from linear or sinusoidal, while the bulky products are desorbing through linear channels. After entering of reactants, they convert at the channel intersections (where active sites are located), then occurred products diffuse out through specific channels without counterdiffusion. Therefore, it can be said that there is a continuous flow of reactants and products.

Besides this traffic control effect, some of these zeolites can have different amount of active acid sites in different channels as a result of different framework Al amount. Also, it is possible for those zeolites to possess specific cavities which can increase the catalytic activity and selectivity of the zeolites for a particular reaction due to their active acid sites as in the case of the low-temperature carbonylation of dimethyl ether with CO by using multipore acidic zeolites with particular cavities.^[78,79] As shown in Table 1.1, these multipore zeolites can be categorized by their combined pore sizes such as small and medium, small and large, medium and large, medium and extra-large, large and extra-large pores.

There are several zeolites containing interconnected small and medium pores in their structure. FER is probably the most paid attention zeolite with its 2D interconnected 8- and 10-R (8×10-R) channels. Also, they can be synthesized under very board synthesis conditions with several OSDAs.^[80] Because of the intersection of its channels, FER has specific FER cavities which can be accessible only through the 8-R window. Therefore, FER is a popular catalyst for the skeletal isomerization of 1-butene into isobutene which can be utilized as an octane enhancer for gasoline.^[81] Regarding recent report on the production of light olefins, FER exhibited higher selectivity for desired olefins than the conventionally utilized zeolite (ZSM-5); however,

their small pore nature restricts their catalytic activities. Therefore, it is suggested their usage along with ZSM-5 zeolites for this industry.^[82,83] The other zeolites with small and medium pores can be synthesized by using different linear dicationic OSDAs, or by using layered silicates as precursors.

Even though numerous zeolites with intersected small and large pores have been reported, most of them showed low-silica frameworks which decrease their hydrothermal stabilities such as OFF.^[84] MOR with its intersected small and large pores nature can be prepared in a wide range of synthesis ways. However, MOR is accepted as 1D large pore catalyst for its industrial applications such as alkylation, cracking, and hydroisomerization reactions since their 8-R channels are not active for those applications.^[85]

Zeolites with intersected extra-large pore and smaller pore zeolites are having increased number of diversity day by day thanks to the recent advances in the zeolite synthesis such as designing rigid and bulky OSDAs, using fluoride mineralizer instead of hydroxides, and framework isomorphous substitutions.^[86,87] Especially, the introduction of Ge into zeolitic frameworks allowed the synthesis of zeolites with extra-large pores and low framework densities due to the preferential occupation of Ge in double-3-rings (D3R) and double-4-rings (D4R). For example, ITQ-33 with 18×10×10-R channel system has the lowest FD ever reported. The zeolite with its unique features is utilized for the alkylation of benzene with propylene to produce cumene, and it showed better performance than commercial zeolite beta.^[88] Even though these zeolites are very promising catalysts, their low hydrothermal stabilities limits their usages in industries.

Table 1.1 Zeolites with multipore systems.^[75]

	IZA Code	Zeolites Names	Pore Architecture
Small and Medium Pores	CGF	Co-Ga-phosphate-5	10×8
	FER	Ferrierite	10×8
	MFS	ZSM-57	10×8
	PCR	IPC-4	10×8
	RRO	RUB-41	10×8
	STI	TNU-10	10×8
	SZR	SUZ-4	10×8×8
	UOS	IM-16	10×8×8
	CGS	Co-Ga-phosphate-5 TNU-1	10×8×8
Small and Large Pores	AFR	SAPO-40	12×8
	AFS	MAPSO-46	12×8
	SFO	SSZ-51	12×8
		EMM-8	12×8
	MOR	Mordenite	12×8
	OFF	Offretite	12×8
	SBE	UCSB-8	12×8
	AFY	CoAlPO-50	12×8×8
	BPH	UZM-4, STA-5	12×8×8
	EON	ECR-1	12×8×8
	MOZ	ZSM-10	12×12×8
	SBS	UCSB-6	12×12×8
SBT	UCSB-10	12×12×8	
Medium and Large Pores	BOG	ITQ-47	12×10
	OKO	COK-14, IPC-2	12×10
	SEW	SSZ-82	12×10
	SFS	SSZ-56	12×10
	UWY	IM-20	12×10
	ITG	ITQ-38	12×10×10
	IWR	ITQ-24	12×10×10
	MSE	MCM-68	12×10×10
	*SFV	SSZ-57	12×10×10
	*-ITN	ITQ-39	12×10×10
	CON	CIT-1, SSZ-26, SSZ-33	12×12×10
Extra-large and Smaller Pores	ETR	ECR-34	18×8×8
	ITT	ITQ-33	18×10×10
	UTL	IM-12	14×12
	IRR	ITQ-44	18×12×12

1.3.1. Zeolites with medium and large pores

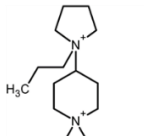
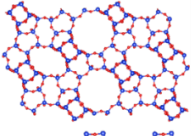
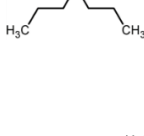
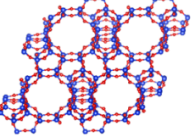
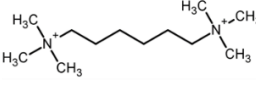
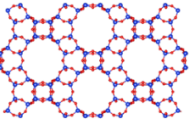
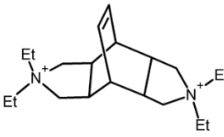
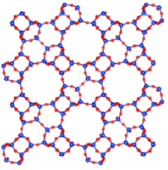
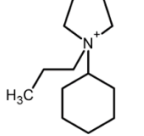
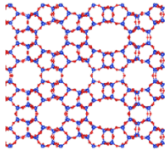
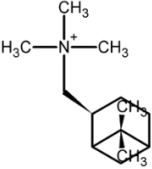
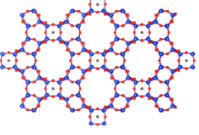
BOG was the first mineral which has naturally occurred 2D interconnected medium and large pores in its structure.^[89] After the discovery of BOG, intensive studies were carried out to find new zeolites with intersected medium and large pores since those materials probably provide such reaction activity, selectivity, and stability which could not find in any other materials. Especially, the synthesis of 3D zeolites containing intersected discrete channels formed by medium and large pores is a matter of potential interest since they possess the catalytic properties of both most successful aluminosilicate catalysts, zeolite beta (*BEA, 3D, 12-R) and ZSM-5 (MFI, 3D, 10-R).

To date, there are relatively few zeolites can be described with these structural features. In fact, the preparation of those zeolites was recently accomplished by innovation in OSDA design which allows the synthesis of CON family such as aluminosilicate SSZ-26 and the related borosilicates SSZ-33^[90] and CIT-1.^[91] The progress on the zeolites containing medium and large pores then continued with the synthesis of five more zeolites with different topologies such as ITQ-24 (IWR),^[92] MCM-68 (MSE),^[93] ITQ-38 (ITG),^[94] SSZ-57 (SFV),^[95] and ITQ-39 (*-ITN)^[96] by using several complex and bulky OSDAs. These zeolites with their topology, structures, and OSDAs are illustrated in Table 1.2. Regarding their structural features and catalytic abilities mostly tested in laboratory scales, it can be said that each of those zeolites is very promising catalysts to be used in industrial applications ranging from MTO^[97] to the conversion of low-value naphtha fractions into diesel.^[98]

Even though zeolites with intersected medium and large pores hold such importance, their actual usage in industries is very limited due to their difficulties for mass production. The most significant handicap to produce these zeolites is the essentialness of using complex and bulky OSDAs. In fact, the cost of these OSDAs

engages the biggest portion of the total cost of the starting materials. Also, removal of these OSDAs by calcination, which generally requires high-temperature combustion, destroys this high-cost component and results in waste water and gas which needs an extra process to be removed from the system. Therefore, there is always the push to develop the rational synthesis of existing multipore zeolites as well as establish new structures.

Table 1.2 Topology, OSDAs, and structure of zeolites containing 3D medium and large pore channels system.

Zeolite Topology	Zeolites	OSDAs	Zeolite Structures
ITG	ITQ-38		
*-ITN	ITQ-39		
IWR	ITQ-24		
MSE	MCM-68		
*SFV	SSZ-57		
CON	CIT-1		

1.4.Strategies for rational synthesis of zeolites

The structure-directing concept of organic molecules has provided a wealth of new structures with new properties as described above. However, the usage of OSDAs in crystallization of the zeolites of interest might hinder their commercialization. Not only synthesis costs of these OSDAs but also the processing or treatment of the waste water and gas after their calcination should be taken into account. In order to bring a solution to this synthesis burden, Zones recently addressed three simplified synthesis strategies which aim to reduce the production costs arising from the usage of high-cost OSDAs in the zeolite synthesis.^[99] These approaches were to develop a recyclable OSDAs which can be fragmented and recovered at the end of synthesis, to replace much of the SDA with a less selective but less-expensive pore-filler, and to remove the OSDAs by successful seeding.

1.4.1. The synthesis of zeolites using recyclable organic structure-directing agents

In the case of recyclable OSDAs, Lee et al. proposed the combustion free methodology for ZSM-5 zeolite.^[100] The schematic representation of this synthesis approach is shown in Figure 1.6. For doing this, they first designed an OSDA containing ketal groups which can be disassembled within the zeolite pores to allow removal of their fragments which then reassemble with the aim of reusing as OSDA. This methodology also could be applied for ZSM-5, ZSM-12, mordenite, and VPI-8 zeolites. However, this method has not been commercialized yet, due to the complicated synthesis and the drawbacks of the extraction process of those recyclable OSDAs. Moreover, there is not any reported example of the usage of complex and bulky OSDAs which can be recovered and reutilized.

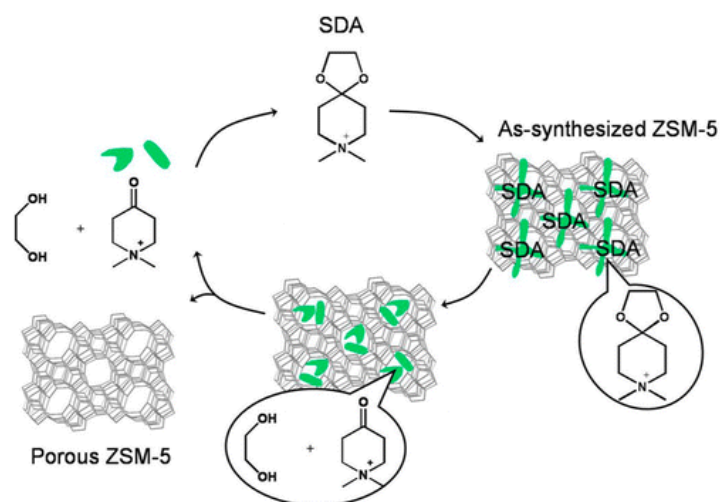


Figure 1.6 Representative scheme of a recyclable OSDA.^[100]

In addition to designing OSDAs with ketal groups, the recyclable concept can be realized by extraction of the OSDAs via acid treatments. Davis et al. showed that extraction of tetraethylammonium (TEA) cations from zincosilicate zeolite beta (CIT-6) and aluminosilicate zeolite beta frameworks.^[101] The TGA results revealed that the remaining TEA cations within aluminosilicate zeolite beta pores were much higher than those in CIT-6. Therefore, it can be said that applying this method to zincosilicate structure rather than aluminosilicates is more practicable, even though some zinc species were extracted from framework along with TEA cations.

1.4.2. The synthesis of zeolites without using organic structure-directing agents

Another approach is the synthesis of zeolites with the assistance of zeolite seed crystals without adding costly and environmentally-unfriendly OSDAs (OSDA-free) as shown in Figure 1.7.^[102] In this approach, the zeolite crystals were firstly synthesized using conventional method requiring OSDAs. After calcining those crystals, they are utilized as seed crystals for the next synthesis from the gels which does not include any OSDAs. Because of the absence of expensive organic molecules, seed-directed, OSDA-free approach is expected to reduce the cost, and allow to reach a cost efficient

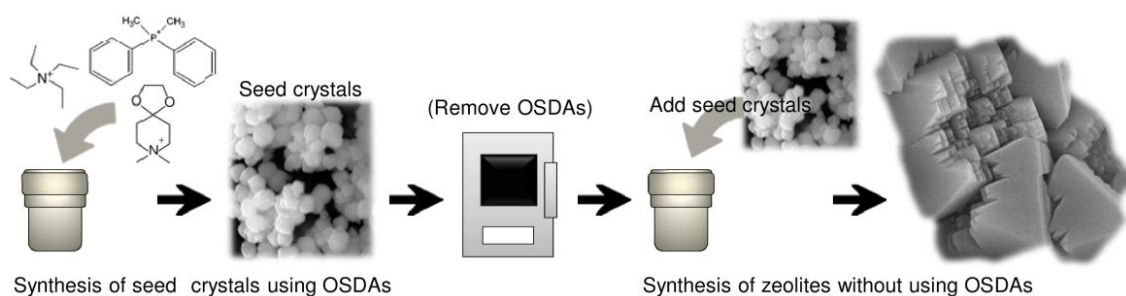


Figure 1.7 Schematic illustration of the seed-directed, OSDA-free synthesis of zeolites.^[102]

synthesis processes for zeolites. Moreover, the usage of seed crystals enables us to skip the nucleation step in the zeolite synthesis and promote fast crystal growth on the surface of the seed crystals. Thanks to these features of OSDA-free synthesis, many zeolites including industrially important zeolite beta, ZSM-5, and ferrierite could be synthesized under economic conditions. Since there are numerous possible combinations of seeds, gel compositions, and reaction conditions, a working hypothesis so-called “composite building unit (CBU) hypothesis”^[103] is proposed by our group to assist determining the synthesis conditions in the organic free manner and widen the type of zeolites can be synthesized by this method. On the basis of this hypothesis, the seed crystals of target zeolite and the zeolite intended to be obtained from the seed-free gel should share at least one common CBU. Also, the optimized synthesis gels and reaction conditions should be employed to prevent any spontaneous nucleation before the accomplishment of the targeting zeolite growth. As shown in Figure 1.8, *mor* unit is elucidated as the common CBU for *BEA, FER, and MOR structures; thus, the OSDA-free synthesis of those zeolites could be achieved by using same Na-aluminosilicate gel composition which leads mordenite when it further prolonged. Moreover, the increasing number of OSDA-freely synthesized zeolites was surely shown this approach to be an actual achievement in the zeolite synthesis under economically favorable conditions. However, besides its economic advantageous, the

commercialize. Therefore, it might be suggested that using simple OSDAs can be helpful to reach the existing complex structures which generally requires complex OSDAs and let them industrialize.

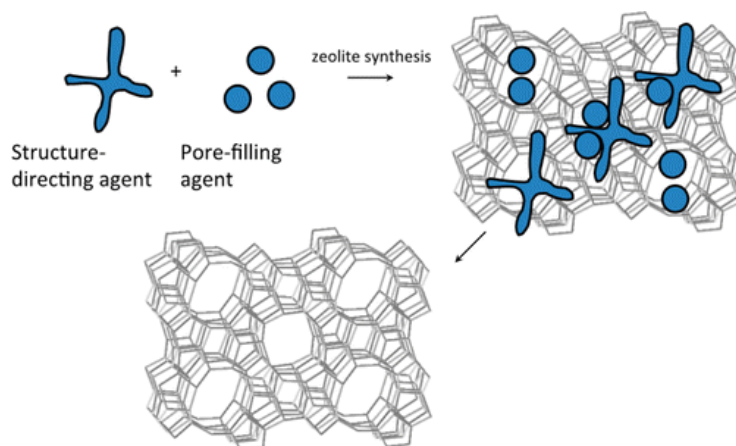


Figure 1.9 Schematic representation of the replacement of much of complex OSDA with simple, cheap, and a commercially available organic molecule that can fill pore space during the synthesis of a zeolite.^[99]

1.5. Scope and overview of this dissertation

The scope of this dissertation is to develop a rational synthesis route for multipore zeolites containing medium and large pores by solely using simple, inexpensive, and commercially available OSDAs in the seed-directed method. The idea has been inspired by the strategy which aims to simplify the synthesis of zeolites by replacing much of bulky and rigid OSDAs with less expensive pore fillers. Moreover, CBU hypothesis, by which structural similarities are considered to associate different zeolite architectures to determine the synthesis conditions for seed-directed synthesis, is not only utilized for this purpose but also extended to select an appropriate less expensive and commercially available OSDA from a huge “zeolite synthesis library” for the rational synthesis of objective multipore zeolites. The concept applied in this research aims to suppress the formation of undesired products, and to promote the direct crystal growth of target materials on the partially dissolved seed crystal surfaces with the help of simple OSDA. For doing this, the synthesis conditions were optimized by aging, modifying reaction composition, and controlling the kinetics. These adjustments, combined with the advantages of simple OSDA in the seed-directed method, allow obtaining highly crystalline pure multipore zeolites with satisfying solid yields that could not be achieved in any other simplified synthesis paths, so far.

The structure of this doctoral dissertation reveals in Figure 1.10. In Chapter 1, general background and the rationalization of objective and strategy of this thesis are presented. In this dissertation, developing a rational synthesis route for multipore zeolites having intersected medium and large pores is described. In Chapter 2, the rational synthesis of aluminosilicate MSE-type zeolites by using TEAOH as a simple OSDA in the seed-directed method is investigated, and the obtained results compared

with those of other alternative methods for MSE-type zeolites. In Chapter 3, the insertion of zinc species as a heteroatom into MSE structure is studied by combining and modifying the rational synthesis of aluminosilicate MSE-type zeolites and a co-precipitated zincoaluminosilicate gel preparation technique, which allows evaluating the efficiency and usage of rational synthesis for a different purpose. In Chapter 4, a simplified synthesis of aluminoborosilicate CON-type zeolites by applying the gels containing TEAOH as an easily reachable OSDA is demonstrated with a view to extending the rational synthesis approach to other multipore zeolites containing medium and large pores. Finally, the general conclusions, as well as a future perspective of this research are summarized in Chapter 5.

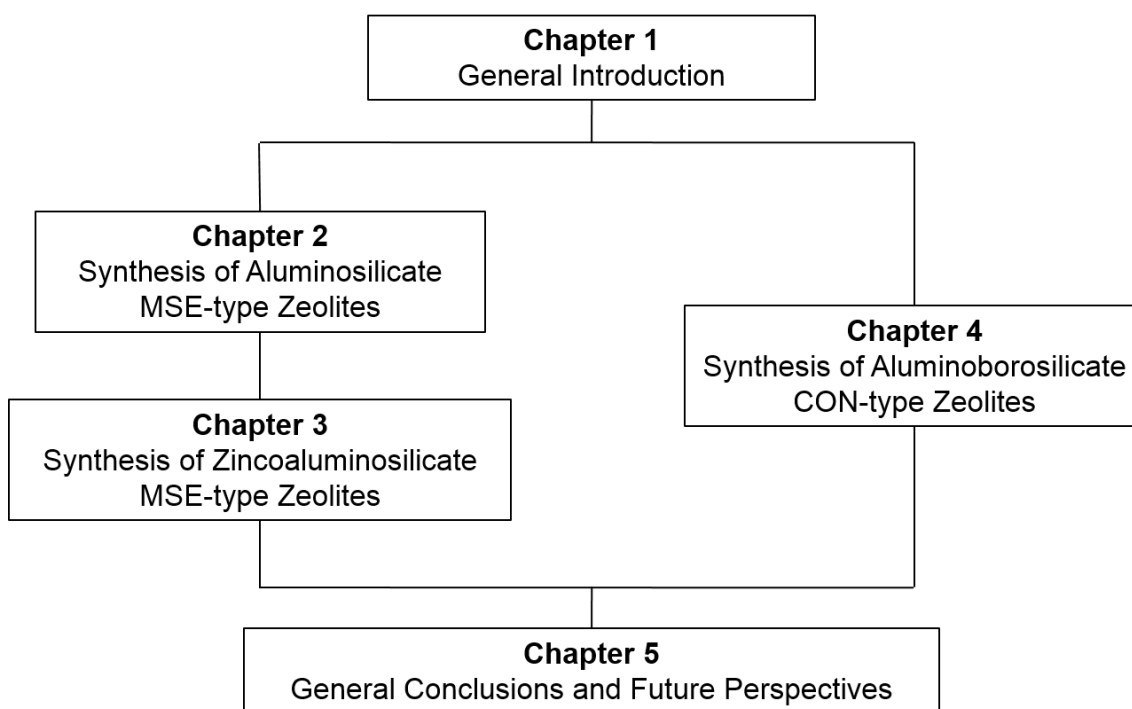


Figure 1.10 Framework of this dissertation.

1.6. References

- [1] M. E. Davis, *Nature* 417 (2002) 813–821.
- [2] G. A. Ozin, *Adv. Mater.* 4 (1992) 612–649.
- [3] C. R. Martin, *Science* 266 (1994) 1961–1966.
- [4] R. E. Morris, P. S. Wheatly, *Angew. Chem. Int. Ed.* 47 (2008) 4966–4981.
- [5] A. Corma, *Chem. Rev.* 97 (1997) 2373–2419.
- [6] Y. Hoshikawa, H. Yabe, A. Nomura, T. Yamaki, A. Shimojima, T. Okubo, *Chem. Mater.* 22 (2010) 12–14.
- [7] K. S. W. Sing, D. H. Everett, R. A. W. Haul, L. Moscou, R. A. Pierotti, J. Rouquerol, T. Siemieniewaka, *Pure Appl. Chem.* 57 (1985) 603–619.
- [8] V. Valtchev, L. Tosheva, *Chem. Rev.* 113 (2013) 6734–6760.
- [9] F. Chang, J. Zhou, P. Chen, Y. Chen, H. Jia, S. M. I. Saad, Y. Gao, X. Cao, T. Zheng, *Asia. Pac. J. Chem. Eng.* 8 (2013) 618–626.
- [10] K. Kadirvelu, M. Kavipriya, C. Karthika, M. Radhika, N. Vennilaman, S. Patabhi, *Bioresource Technology* 87 (2003) 129–132.
- [11] A. Ahmadpour, D. D. Do, *Carbon* 34 (1996) 471–479.
- [12] J. Lee, J. Kim, T. Hyeon, *Adv. Mater.* 18 (2006) 2037–2094.
- [13] T. Kyotani, *Carbon* 38 (2000) 269–286.
- [14] L. Méndez-Liñan, F. J. López-Garzón, M. Domingo-García, M. Pérez-Mendoza, *Energy Fuels* 24 (2010) 3394–3400.
- [15] Y. -C. Chiang, P. -C. Chiang, C. -P. Huang, *Carbon* 39 (2001) 523–534.
- [16] D. Saha, S. Deng, *J. Colloid Interface Sci.* 345 (2010) 402–409.
- [17] J. Tian, P. K. Thallapally, B P. McGrath, *CrystEngComm* 14 (2012) 1909–1919.
- [18] S. Das, P. Heasman, T. Ben, S. Qiu, *Chem. Rev.* 117 (2017) 1515–1563.
- [19] W. Lu, D. Yuan, D. Zhao, C. I. Schilling, O. Plietzsch, T. Muller, S. Bräse, J. Guenther, J. Blumel, R. Krishna, Z. Li, H. -C. Zhou, *Chem. Mat.* 22 (2010) 5964–5972.
- [20] H. M. El-Kaderi, J. R. Hunt, J. L. Mendoza-Cortés, A. P. Côté, R. E. Taylor, M. O’Keeffe, O. M. Yaghi, *Science* 316 (2007) 268–272.
- [21] H. Furukawa, O. M. Yaghi, *J. Am. Chem. Soc.* 131 (2009) 8875–8883.
- [22] S. S. Han, H. Furukawa, O. M. Yaghi, W. A. Goddard, *J. Am. Chem. Soc.* 130 (200) 11580–11581.

- [23] A. P. Côté, A. I. Benin, N. W. Ockwig, M. O’Keeffe, A. J. Matzger, O. M. Yaghi, *Science* 310 (2005) 1166–1170.
- [24] S. L. James, *Chem. Soc. Rev.* 32 (2003) 276–288.
- [25] O. M. Yaghi, M. O’Keeffe, N. W. Ockwig, H. K. Chae, M. Eddaoudi, J. Kim, *Nature* 423 (2003) 705–714.
- [26] Y Sun, H. -C. Zhou, *Sci. Technol. Adv. Mater.* 16 (2015) 054202.
- [27] D. J. Collins, H. -C. Zhou, *J. Mater. Chem.* 17 (2007) 17 3154–3160.
- [28] J. -R. Li, Y. Ma, M. C. McCarthy, J. Sculley, J. Yu, H. -K. Jeong, P. B. Balbuena, H. -C. Zhou, *Coord. Chem. Rev.* 255 (2011) 255 1791–1823.
- [29] J. -R. Li, R. J. Kuppler, H. -C. Zhou, *Chem. Soc. Rev.* 38 (2009) 38 1477–1504.
- [30] B. Chen, C. Liang, J. Yang, D. S. Contreras, Y. L. Clancy, E. B. Lobkovsky, O. M. Yaghi, S. Dai, *Angew. Chem.* 11 (2006) 1418–1423.
- [31] J. Y. Lee, O. K. Farha, J. Roberts, K. A. Scheidt, S. T. Nguyen, J. T. Hupp, *Chem. Soc. Rev.* 38 (2009) 1450–1459.
- [32] P. Horcajada, T. Chalati, C. Serre, B. Gillet, C. Sebrie, T. Baati, J. F. Eubank, D. Heurtaux, P. Clayette, C. Kreuz, J. S. Chang, Y. K. Hwang, V. Marsaud, P. N. Bories, L. Cynober, S. Gil, G. Férey, P. Couvreur, R. Gref, *Nature Materials* 9 (2010) 172–178.
- [33] L. E. Kreno, K. Leong, O. K. Farha, M. Allendorf, R. P. Van Duyne, J. T. Hupp, *Chem. Rev.* 112 (2012) 1105–1125.
- [34] J. G. Croissant, X. Cattoën, M. W. C. Man, J. O. Durand, N. M. Khashab, *Nanoscale* 7 (2015) 20318–20334.
- [35] M. Waki, N. Mizoshita, Y. Maegawa, T. Hasegawa, T. Tani, T. Shimada, S. Inagaki, *Chem. Eur. J.* 18 (2012) 1992–1998.
- [36] N. Mizoshita, T. Tani, H. Shinokubo, S. Inagaki, *Angew. Chem. Int. Ed.* 124 (2012) 1182–1186.
- [37] Y. Yamauchi, A. Sugiyama, R. Morimoto, A. Takai, K. Kuroda, *Angew. Chem. Int. Ed.* 47 (2008) 5371–5373.
- [38] P. Yang, T. Deng, D. Zhao, P. Feng, D. Pine, B. F. Chmelka, G. M. Whitesides, G. D. Stucky, *Science* 282 (1998) 2244–2246.
- [39] A. Sayari, Y. Yang, M. Kruk, M. Jaroniec, *J. Phys. Chem. B* 103 (1999) 3651–3658.
- [40] I. I. Slowing, J. L. Vivero-Escoto, C. -W. Wu, V. S.-Y. Lin *Adv. Funct. Mater.* 60 (2008) 1278–1288.

- [41] D. W. Breck, *Zeolite Molecular Sieves: Structure, Chemistry, and Use*, Wiley–Interscience publication, New York, (1974).
- [42] M. E. Davis, R. F. Lobo, *Chem. Mater.* 4 (1992) 156–768.
- [43] C. Martínez, A. Corma, *Coord. Chem. Rev.* 255 (2011) 1558–1580.
- [44] A. Corma, *Chem. Rev.* 97 (1997) 2373–2419.
- [45] R. M. Barrer, *J. Chem. Soc.* (1948) 127–132.
- [46] R. M. Barrer, L. Hinds, E. A. White, *J. Chem. Soc.* (1953) 1466–1475.
- [47] <http://www.iza-structure.org/databases/> (accessed in April 2017).
- [48] C. S. Cundy, P. A. Cox, *Microporous and Mesoporous Mater.* 82 (2005) 1–78.
- [49] R. M. Milton, US Patent 2,882,243 (1959).
- [50] R. M. Milton, US Patent 2,882,244 (1959).
- [51] R. M. Barrer, P. J. Denny, *J. Chem. Soc.* (1961) 971–982.
- [52] R. L. Wadlinger, G. T. Kerr, E. J. Rosinski, US Patent 3,308,069 (1967)
- [53] R. J. Argauer, G. R. Landolt, US Patent 3,702,886 (1972)
- [54] M. E. Davis, R. F. Lobo, *Chem. Mater.* 4 (1992) 756–768.
- [55] C. -N. Wu, K. -S. Chao, *J. Chem. Soc. Faraday Trans.* 91 (1995) 167–173.
- [56] S. L. Burkett, M. E. Davis, *J. Phys. Chem.* 98 (1994) 4647–4653.
- [57] R. E. Moris, S. L. James, *Angew. Chem. Int. Ed.* 52 (2013) 2163–2165.
- [58] M. Matsukata, M. Ogura, T. Osaki, P. R. H. P. Rao, M. Nomura, E. Kikuchi, *Top. Catal.* 9 (1999) 77–92.
- [59] D. M. Bibby and M. P. Dale, *Nature* 317 (1985) 157–158.
- [60] R. E. Morris, S. J. Weigel, *Chem. Soc. Rev.* 26 (1997) 309–317.
- [61] M. Moliner, *Dalton Trans.* 43 (2014) 4197–4208.
- [62] P. Y. Dapsens, C. Mondelli, J. Perez-Ramírez, *Chem. Soc. Rev.* 44 (2015) 7025–7043.
- [63] J. Penzien, A. Abraham, J. A. van Bokhoven, A. Jentys, T. E. Müller, C. Sievers, J. A. Lercher, *J. Phys. Chem. B* 108 (2004) 4116–4126.
- [64] X. Collard, P. Louette, S. Fiorillic, C. Aprile, *Phys. Chem. Chem. Phys.* 17 (2015) 26756–26765.
- [65] J. Weitkamp, *Solid State Ionics* 131 (2000) 175–188.
- [66] A. Corma, L. T. Nemeth, M. Renz, S. Valencia, *Nature* 412 (2001) 423–425.
- [67] A. Corma, H. García, *Chem. Rev.* 103 (2003) 4307–4365.
- [68] M. Moliner, Y. Román-Leshkov, M. E. Davis, *Proc. Natl. Acad. Sci.* 107 (2010) 6164–6168.

- [69] R. Xu, W. Pang, J. Yu, Q. Huo, *Chemistry of Zeolites and Related Porous Materials: Synthesis and Structure*; John Wiley, Singapore, 2007.
- [70] A. Corma, M. J. Díaz-Cabañas, J. Martínez-Triguero, F. Rey, J. Rius, *Nature* 418 (2002) 514–517.
- [71] E. G. Derouane, Z. Gabelica, *J. Catal.* 65 (1980) 486–489.
- [72] J. Jiang, J. Yu, A. Corma, *Angew. Chem. Int. Ed.* 49 (2010) 3120–3145.
- [73] M. Moliner, C. Martínez, A. Corma, *Chem. Mater.* 26 (2014) 246–258.
- [74] E. T. C. Vogt, B. M. Weckhuysen, *Chem. Soc. Rev.* 44 (2015) 7342–7370.
- [75] M. Moliner, C. Martínez, A. Corma, *Angew. Chem. Int. Ed.* 54 (2015) 3560–3579.
- [76] E. G. Derouane, Z. Gabelica, *J. Catal.* 65 (1980) 486–489.
- [77] E. G. Derouane, Z. Gabelica, *J. Catal.* 70 (1981) 238–239.
- [78] A. Corma, F. J. Llopis, C. Martínez, G. Sastre, S. Valencia, *J. Catal.* 268 (2009) 9–17.
- [79] M. Boranat, C. Martinez-Sanchez, D. Law, A. Corma, *J. Am. Chem. Soc.* 130 (2008) 16316–16323.
- [80] G. Guo, Y. Sun, Y. Long, *Chem. Commun* (2000) 1893–1894.
- [81] L. Gómez-Hortigüela, A. B. Pinar, F. Corá, J. Pérez-Pariente, *Chem. Commun* 46 (2010) 2073–2075.
- [82] H. H. Mooiweer, K. P. de Jong, B. Kraushaar-Czarnetzki, W. H. J. Stork, B. C. H. Krutzen, *Stud. Surf. Sci. Catal.* 84C (1994) 2327–2334
- [83] A. Matijasic, J. Patarin, *Microporous Mesoporous Mater.* 29 (1999) 405–412.
- [84] L. Zhang, A. N. C. van Laak, P. E. de Jongh, K. P. De Jong, *Microporous Mesoporous Mater.* 126 (2009) 115–124.
- [85] S. I. Zones, R. J. Darton, R. Morris, S. J. Hwang, *J. Phys. Chem. B* 109 (2005) 652–661.
- [86] A. Corma, M. E. Davis, *ChemPhysChem* 5 (2004) 304–313.
- [87] T. Blasco, A. Corma, M. J. Díaz-Cabañas, F. Rey, A. Vidal-Moya, C. M. Zicovich-Wilson, *J. Phys. Chem. B* 106 (2002) 2634–2642.
- [88] A. Corma, M. J. Díaz-Cabañas, J. L. Jordá, C. Martínez, M. Moliner, *Nature* 443 (2006) 842–845.
- [89] J. J. Pluth, J. V. Smith, *Am. Mineral.* 75 (1990) 501–507.
- [90] R. F. Lobo, M. Pan, I. Chan, H. X. Li, R. C. Medrud, S. I. Zones, P. A. Crozier, M. E. Davis, *Science* 262 (1993) 1543–1546.
- [91] R. F. Lobo, M. E. Davis, *J. Am. Chem. Soc.* 117 (1995) 3766–3779.

- [92] R. Castaneda, A. Corma, V. Fornes, F. Rey, J. Rius, *J. Am. Chem. Soc.* 125 (2003) 7820–7821.
- [93] D. L. Dorset, S. C. Weston, S. S. Dhingra, *J. Phys. Chem. B* 110 (2006) 2045–2050.
- [94] M. Moliner, T. Willhammar, W. Wan, J. González, F. Rey, J. L. Jorda, X. Zou, A. Corma, *J. Am. Chem. Soc.* 134 (2012) 6473–6478.
- [95] C. Baerlocher, T. Weber, L. B. McCusker, L. Palatinus, S. I. Zones, *Science* 333 (2011) 1134–1137.
- [96] T. Willhammar, J. Sun, W. Wan, P. Olevnikov, D. Zhang, X. Zou, M. Moliner, J. Gonzalez, C. Martínez, F. Rey, A. Corma, *Nat. Chem.* 4 (2012) 188–194.
- [97] M. Yoshioka, T. Yokoi, T. Tatsumi, *ACS Catal.* 5 (2015) 4268–4275.
- [98] M. E. Martínez-Armero, M. Moliner, G. Sastre, F. Rey, C. Martínez, *Journal of Catalysis* 333 (2016) 127–138.
- [99] S. I. Zones, *Microporous and Mesoporous Materials* 144 (2011) 1–8.
- [100] H. Lee, S. I. Zones, M. E. Davis, *Nature* 425 (2003) 385–388.
- [101] T. Takewaki, L. W. Beck, M. E. Davis, *J. Phys. Chem. B* 103 (1999) 2674–2679.
- [102] K. Iyoki, K. Itabashi, T. Okubo, *Microporous Mesoporous Mater.* 189 (2014) 22–30.
- [103] K. Itabashi, Y. Kamimura, K. Iyoki, A. Shimojima, T. Okubo, *J. Am. Chem. Soc.* 134 (2012) 11542–11549.
- [104] Y. Kubota, K. Itabashi, S. Inagaki, Y. Nishita, R. Komatsu, Y. Tsuboi, S. Shinoda, T. Okubo, *Chem. Mater.* 26 (2014) 1250–1259.
- [105] R. Bai, Q. Sun, N. Wang, Y. Zou, G. Guo, S. Iborra, A. Corma, J. Yu, *Chem. Mater.* 28 (2016) 6455–6458.

Chapter 2. Synthesis of Aluminosilicate MSE-type Zeolites

2.1.Introduction

MCM-68 (i.e., MSE-type, assigned by the Structure Commission of the International Zeolite Association (IZA-SC)^[1] was first reported by ExxonMobil researchers^[2] as a type of multipore zeolite with a 12×10×10-membered ring (R) pore system.^[3] The MSE framework consists of 12-R straight channels intersecting with two independent tortuous 10-R channels besides super cages with 18×12-R accessible only through the 10-R channels as shown in Figure 2.1.^[2,4] MCM-68 is a promising material with unique acid-catalytic properties,^[5-7] and is widely utilized as a shape-selective catalyst for the alkylation of aromatics^[8-10] and the production of propylene by paraffin cracking.^[11] Furthermore, the potential of MCM-68 as a hydrocarbon trap^[12] and the remarkable performance of titanium-substituted MCM-68 in the oxidation of phenol and olefins have been reported.^[13, 14]

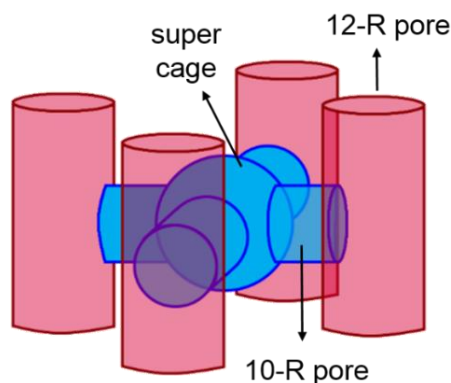


Figure 2.1 The illustration of MSE structure with 12-R and 10-R pores, and super cage.^[7]

Additionally, Kubota et al. achieved the synthesis of pure silica (YNU-2)^[15] and Al-rich (YNU-3)^[16] versions of MSE-type zeolites by steam-assisted crystallization (SAC)^[17] with some post-synthetic modifications and hydrothermal conversion of FAU-type zeolite, respectively. Both of them are found promising parent materials for industrial applications as highly selective and long-lived catalysts. As it is mentioned in the previous chapter, organic molecules/cations are often employed as OSDAs which makes their usage indispensable for the synthesis of many zeolites. Conventionally, the synthesis of aluminosilicate MCM-68 was possible only under hydrothermal conditions using quite complex and expensive OSDA so-called *N,N,N',N'*-tetraethylbicyclo[2.2.2]oct-7-ene-2,3:5,6-dipyrrolidinium diiodide (TEBOP²⁺(I⁻)₂).^[4] In fact, the necessity of using OSDAs in the synthesis of MCM-68 is a significant handicap to manufacture the zeolite with low cost. Therefore, alternative synthesis methods for MSE-type zeolites have been studied in both academia and industries with the motivation of decreasing the production costs by replacing current OSDAs with inexpensive molecules.^[18] In this sense, Moscoso et al.^[19] recently reported the synthesis of UZM-35 (i.e., an MSE-type zeolite with a SiO₂/Al₂O₃ ratio similar to that of MCM-68) by using dimethyldipropylammonium (DMDP) hydroxide as a relatively simple OSDA with small amounts of K⁺ and Na⁺ following the Charge Density Mismatch (CDM) Approach, where essentially dilute condition is employed. In addition, numerous patents are reported on the synthesis of MSE-type zeolites using several newly designed OSDAs. However, their structures are not simple, their preparation cost is not low enough yet, and most of them are not commercially available.^[20-24] On the other hand, the seed-directed, OSDA-free synthesis of MSE-type zeolite^[25] is

also reported by our group; however, the resulting product yield was not high enough (ca. 15 wt.%) to help the zeolite industrialize.

The report herein describes the achievement in the synthesis of MSE-type zeolites with a simplified, easily reachable, and comparatively inexpensive OSDA by applying the extended CBU hypothesis. In the case of the OSDA-free synthesis of *BEA-type zeolites based on the CBU hypothesis,^[26] *BEA seeds were added to the Na-aluminosilicate gel that yields MOR-type zeolites when heated without seeds. The correlation of common CBU between MOR and *BEA is *mor* as shown in Figure 2.2. Since *BEA and MSE contain entirely the same CBUs, it is assumed that MSE-type zeolite can be obtained by adding MCM-68 seed crystals to the initial gels, which commonly yield MOR-type zeolites, containing TEAOH as an OSDA. The strategy described here is based on suppressing *BEA (and MOR) formation and making MSE crystal growth favorable by aging, modifying reaction composition and controlling kinetics.

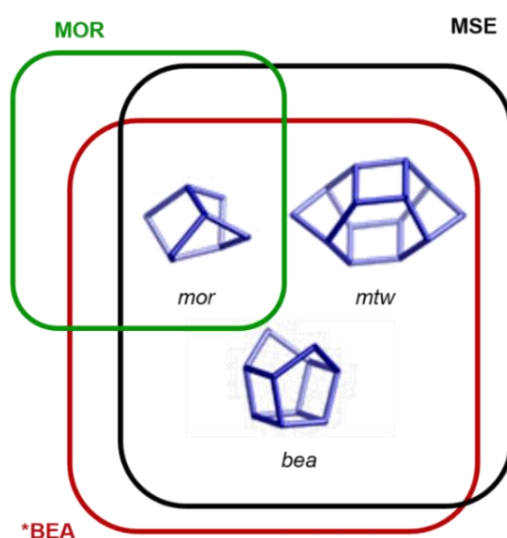


Figure 2.2 The correlation of common CBUs among MOR, *BEA and MSE.

2.2. Experimental section

2.2.1. Materials

The following commercially available reagents were used as received without further purification: colloidal silica (Ludox[®] HS-40, 40 wt.%, DuPont) and fumed silica (Cab-O-Sil[®] M5, Cabot) as the silica sources; aluminum hydroxide (Al(OH)₃, Pfaltz, and Bauer or Sigma-Aldrich) and sodium aluminate (NaAlO₂, Wako) as the alumina sources; sodium hydroxide solution (NaOH, 50 w/v% in water, Wako) and potassium hydroxide solution (KOH, 50 wt.% in water, Wako) as the alkali sources; tetraethylammonium hydroxide solution (TEAOH, 35 wt.% in water, Aldrich) as the OSDA; and deionized water. In addition, commercially available *exo,exo*-bicyclo[2.2.2]oct-7-ene-2,3:5,6-tetracarboxylic anhydride (Aldrich), ethylamine solution (70 wt.% in water, KANTO Chem.), lithium aluminum hydride (LiAlH₄, Wako), tetrahydrofuran (THF, JIS Special Grade, KANTO Chem.), benzene (JIS Special Grade, Wako), iodoethane (JIS Special Grade, Wako), ethanol (JIS Special Grade, Wako), and acetone (JIS Special Grade, Wako) were used to synthesize TEBOP²⁺(Γ⁻)₂.

2.2.2. Synthesis of seed crystals with organic structure-directing agents

MCM-68 crystals were synthesized according to a previous report^[25] from a gel with the following composition: 1.0SiO₂: 0.05Al₂O₃: 0.188K₂O: 0.1TEBOP²⁺(Γ⁻)₂: 30H₂O. First, colloidal silica, Al(OH)₃, and deionized water were mixed in a 180 mL Teflon[®] beaker and stirred for 10 min. KOH solution was added to this starting mixture and stirred for additional 30 min. TEBOP²⁺(Γ⁻)₂, which was synthesized as reported elsewhere^[11, 13], was subsequently mixed with the solution and further stirred for 4 h. Lastly, the obtained gel was placed in a 125 mL Teflon[®]-lined autoclave (No. 4749, Parr

Instrument) and maintained at 160 °C for 16 days in a convection oven. After the hydrothermal treatment, the solution was cooled to room temperature and the solid products were separated by centrifugation, washed with deionized water several times, and finally dried at 80 °C overnight. In order to remove the OSDA occluded in the pores, the as-synthesized MCM-68 was heated from ambient temperature to 650 °C at a rate of 1 K min⁻¹ and maintained at this temperature for 10 h. After cooling down, the calcined MCM-68 powder was obtained as seed crystals.

2.2.3. Synthesis of seed crystals without organic structure-directing agents

According to a previous report^[25], OSDA-free synthesis of an MSE-type (MSE-OSDAF) zeolite was accomplished by the addition of calcined MCM-68 seeds to the (Na, K)-aluminosilicate gel having a molar composition of 1.0SiO₂: 0.01Al₂O₃: 0.3(Na₂O+K₂O): 20H₂O. Firstly, sodium aluminate was dissolved in a solution containing the required amounts of NaOH and KOH to obtain a clear solution. Secondly, Cab-O-Sil[®] M-5 and the above-mentioned, calcined MCM-68 seeds (10 wt.% relative to the silica source) were simultaneously added and slowly mixed using a mortar and a pestle. After obtaining a homogeneous gel, the mixture was transferred to a 23 mL Teflon[®]-lined stainless steel autoclave and kept at 140 °C for 48 h in an oven under static conditions. Subsequently, the product was filtered and washed multiple times with hot distilled water. Finally, the gel was dried at 80 °C in an oven overnight to obtain pure MSE phase.

2.2.4. Preparation of physical mixture of tetraethylammonium hydroxide with MCM-68 seed crystals

The physical mixture of TEAOH and calcined MCM-68 seed crystals were prepared by adding the same amount of seed crystals and TEAOH amount as applied for sample No. 3 (see in Table 2.1). Then, this mixture was stirred by using

a spatula for 30 min. After that, the centrifugation was applied to obtain solid products and subsequently washed with water until the pH of the filtrate became neutral. Recovered products were dried at 80 °C overnight before further characterizations.

2.2.5. Synthesis of MSE-type zeolites by using tetraethylammonium hydroxide as a simple organic structure-directing agent

The initial gels for the synthesis of MSE-type zeolites using TEAOH as an OSDA were prepared with using $\text{Al}(\text{OH})_3$, NaOH, KOH, and TEAOH solutions and fumed silica. In a typical synthesis, aluminum hydroxide powder was dissolved in an aqueous alkali solution under stirring for ca. 10 min, and fumed silica was subsequently added slowly. The resulting mixture was homogenized using a mortar and a pestle for additional 30 min. Thereafter, this synthesis mixture was transferred to a 23 mL Teflon[®]-lined stainless steel autoclave (No. 4749, Parr Instrument), which was heated at 80 °C for 24 h. The starting gel had the following molar ratios: $1.0\text{SiO}_2: x\text{Al}_2\text{O}_3: y(\text{K}_2\text{O}+\text{Na}_2\text{O}): z(\text{TEA})_2\text{O}: 15\text{H}_2\text{O}$ (where $x = 0.02\text{--}0.05$, $y = 0.225\text{--}0.280$, $z = 0.11\text{--}0.12$, and the $\text{K}_2\text{O}/(\text{K}_2\text{O}+\text{Na}_2\text{O})$ ratio ranged from 0.15 to 0.5). After cooling the autoclave to room temperature, calcined MCM-68 seed crystals (from 10 to 20 wt.% relative to the silica source) were added. The resultant mixture was hydrothermally treated at 160 °C for 168 h under static conditions in a preheated air circulated oven. After the prescribed synthesis time, the solid products were centrifuged and subsequently washed with distilled water until the filtrate pH became neutral. Recovered products were dried at 80 °C overnight. In order to obtain the calcined powder, the as-synthesized product was heated at 550 °C for 10 h under flowing dry air. The solid yield of the obtained zeolite was described as the weight ratio percentage ($\text{g/g} \times 100$) of the calcined

solid product to the sum of the SiO₂, Al₂O₃, Na₂O, K₂O, and calcined seeds in the starting gel. Relative crystallinities were calculated based on the ratio of the area percentages of the sum for the four peaks in the X-Ray diffraction (2 theta ca. 19.45, 21.68, 22.47, and 22.99) for solid products to those of seed crystals.

2.2.6. Characterization

Powder X-Ray diffraction (XRD) patterns were recorded on a Rigaku Ultima IV diffractometer using CuK α radiation with a D/Tex Ultra detector ($\lambda = 0.015406$ nm, 40 kV, 40 mA). The amounts of silicon and aluminum in the products were measured on a Thermo Scientific iCAP-6300 inductively coupled plasma-atomic emission spectrometer (ICP-AES) system after dissolving the products in a potassium hydroxide solution. Additionally, a Hitachi Z-2000 atomic absorption spectrometer equipped with a heated graphite tube atomizer was used for the determination of sodium and potassium after dissolving them in hydrofluoric acid. Na and K hollow cathode lamps operating at 6.5 mA were used as the radiation sources. CHN elemental analyses were carried out on a CE-440 elemental analyzer (Exeter Analytical). Thermogravimetric and differential thermal analysis (TG-DTA) were performed on a Rigaku Thermo plus TG 8120 from 30 to 800 °C at a heating rate of 10 K min⁻¹ under a flow (200 mL min⁻¹) of 10% O₂/90% He gas mixture. Raman spectra of the solid products were collected on a device NRS-5100 (JASCO) by using a 532 nm laser. Nitrogen adsorption–desorption isotherms of the calcined samples were obtained on an Autosorb-iQ2-MP instrument (Quantachrome Instruments) at liquid nitrogen temperature. The crystal sizes and morphologies of the obtained products were observed on a JSM-7500FA (JEOL) field emission scanning electron microscope (FE-SEM) after Os coating over the powder samples on the carbon tape.

Transmission electron microscopy (TEM) observations were carried out on a JEM-200EX-II (JEOL) instrument at an accelerating voltage of 200 kV. The samples were prepared for TEM observations as the following sequence. Firstly, the zeolite powder was finely ground with an agate mortar and pestle. Then, the fine powder was dispersed into ethanol (1 mg zeolite in 3 mL ethanol). Two droplets of this zeolite-ethanol mixture were dropped onto a Cu mesh. After drying in the air the zeolite sample deposited on the Cu mesh was ready for TEM observation. Solid-state magic angle spinning nuclear magnetic resonance (MAS NMR) measurements were conducted on an ADVANCEIII-600 (600 MHz (1H), Bruker) device with a 4 mm diameter ZrO₂ rotor. ²⁷Al direct-excitation (DE) MAS NMR spectra (156.4 MHz) were recorded at 0.5 s contact time for 1024 times at a spinning rate of 13 kHz. The ²⁷Al chemical shifts were determined using aqueous Al(NO₃)₃ solutions whose resonance peak was adjusted to 0 ppm. The ²⁹Si dipolar-decoupling (DD) MAS NMR spectra (119.2 MHz) were recorded at 30 s contact time for 1024 times at 10 kHz. The reference for ²⁹Si chemical shifts was measured with regard to the signal of hexamethylcyclotrisiloxane at -9.66 ppm. The ¹³C CP MAS NMR spectra (150.6 MHz) were recorded at 3 s contact time for 4096 times at 10 kHz. The ¹³C chemical shifts were determined using glycine (carbonyl-C) at 176.03 ppm.

2.3. Results and discussion

2.3.1. Structural and textural evaluation

The chemical compositions of the reaction mixtures, the synthesis conditions as well as the phases and yields of the resultant products are summarized in Table 2.1. First, the chemical compositions of the reaction mixture without TEAOH or seed crystals that largely yielded MOR-type zeolites was confirmed by the synthesis experiments (Table 2.1, samples Nos. 1 and 2), and the XRD patterns in Figure 2.3. These results strongly point that rational synthesis might be realized only in the existence of both TEAOH as a simple OSDA and calcined MCM-68 seed crystals.

Based on these results, the rational synthesis of MSE-type zeolites using TEAOH as an OSDA (i.e., MSE-TEA) was performed by varying the $\text{SiO}_2/\text{Al}_2\text{O}_3$, $(\text{K}_2\text{O}+\text{Na}_2\text{O})/\text{SiO}_2$, $\text{K}_2\text{O}/(\text{K}_2\text{O}+\text{Na}_2\text{O})$ ratios. It is worth noting that highly-crystalline, pure products were obtained by using a certain amount of NaOH along

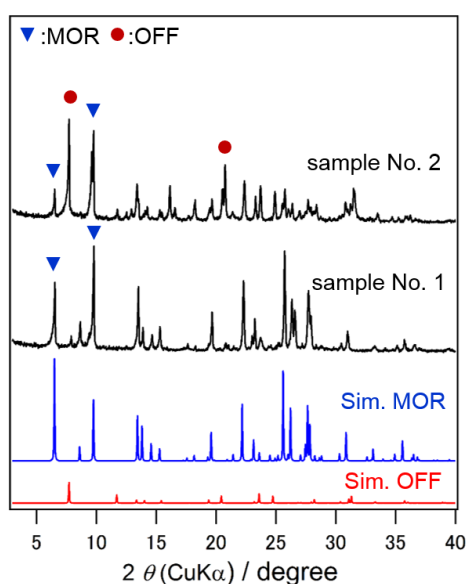


Figure 2.3 Powder XRD patterns of the samples No. 1, 2 synthesized in accordance with Table 2.1 and simulated XRD patterns of MOR and OFF.

Table 2.1 Summary for the seed-directed synthesis of MSE-type zeolites with TEOAH as OSDA.

Sample No.	Reaction Mixture Composition ^a				Seed	Aging ^b		Product		
	SiO ₂ /Al ₂ O ₃	(K ₂ O + Na ₂ O)/SiO ₂	K ₂ O/(K ₂ O + Na ₂ O)	TEA ₂ O/SiO ₂	Additive Amount [wt.%]	Time [h]	Yield [wt.%] ^c	Micropore volume (cm ³ g ⁻¹) ^e	BET surface area (m ² g ⁻¹) ^e	Phase
1	50	0.250	0.25	-	20 ^d	24	-	-	-	MOR
2	50	0.250	0.25	0.11	0	24	-	-	-	MOR+OFF
3	50	0.250	0.25	0.11	20 ^d	24	30.5	0.20	544	MSE
4	50	0.240	0.25	0.11	20 ^d	24	25.8	0.22	604	MSE
5	50	0.225	0.25	0.12	20 ^d	24	-	-	-	MSE+*BEA
6	50	0.250	0.50	0.11	20 ^d	24	27.4	0.19	534	MSE
7	50	0.250	0.15	0.11	20 ^d	24	34.2	0.19	540	MSE
8	40	0.250	0.25	0.11	20 ^d	24	38.1	0.19	539	MSE
9	40	0.238	0.25	0.11	20 ^d	24	39.5	0.21	556	MSE
10	40	0.280	0.25	0.11	20 ^d	24	36.6	0.20	555	MSE
11	30	0.250	0.25	0.11	20 ^d	24	42.9	0.21	600	MSE
12	20	0.250	0.25	0.11	20 ^d	24	54.0	0.19	525	MSE
13	50	0.250	0.25	0.11	20 ^d	0	-	-	-	MSE+*BEA
14	50	0.250	0.25	0.11	15 ^d	24	-	-	-	MSE+*BEA
15	50	0.250	0.25	0.11	10 ^d	24	-	-	-	MSE+*BEA
16	50	0.250	0.25	0.11	20 ^e	48	37.1	0.20	546	MSE
17	50	0.250	0.25	0.11	20 ^f	48	32.8	0.18	501	MSE

^aAll samples were synthesized by using a H₂O/SiO₂ molar ratio of 15, at 160° C for 7 days. ^bAging is applied at 80° C. ^cThe calculation of the solid yield was based on the oxides (excluding TEOAH and H₂O). ^dCalcined MCM-68. ^eUncalcined MSE-OSDAF. ^fUncalcined MSE-TEA (sample No. 3). ^gMicropore volumes and ^hBET surface areas were calculated using *t*-plot and multi-point BET plot methods, respectively.

with KOH (K₂O/(K₂O+Na₂O) = 0.15–0.50), whereas the conventional synthesis method only required KOH as an alkali source.^[4, 25] Therefore, it is clarified that the usage of binary alkali cations containing gels is essential to reach a successful rational synthesis. As it can be seen from Table 2.1 and the XRD pattern in Figure 2.4 (a), the sample No. 12 synthesized from a gel having higher aluminum contents showed significant improvements in the product yield (up to 54.0 wt.%) with a sufficient relative crystallinity (99%). On the other hand, the gel containing higher TEOAH concentrations and lower alkalinity (TEA₂O/SiO₂ = 0.12; (K₂O+Na₂O)/SiO₂ = 0.225) yielded a MSE-TEA product with a minor amount of *BEA impurity, as shown in

Figure 2.4 (a) for sample No. 3, indicating dominant structure-directing effect of TEAOH for the nucleation of zeolite beta. However, as seen in samples No. 5 and 12, the usage of highly alkaline gels is one of the keys to suppress this structure directing effect of TEAOH, and turn the synthesis conditions favorable for MSE crystallization. Moreover, the FE-SEM images of those samples revealed that the obtained materials were composed of crystal particles approximately 200–300 nm in size with smooth rectangular facets, which are comparatively larger than the seed crystals (ca. 50–100 nm in size, Fig. 2(b)–(d)). These large crystals of MSE-TEA products might be indicative of that crystal growth took place on the (partially dissolved) seed crystal surfaces, as reported earlier.^[27] Regarding results mentioned above, we can say that the usage of calcined MCM-68 seed crystals is very critical to promote the MSE crystal growth from the gel mostly yielding MOR in the absence of seed crystals.

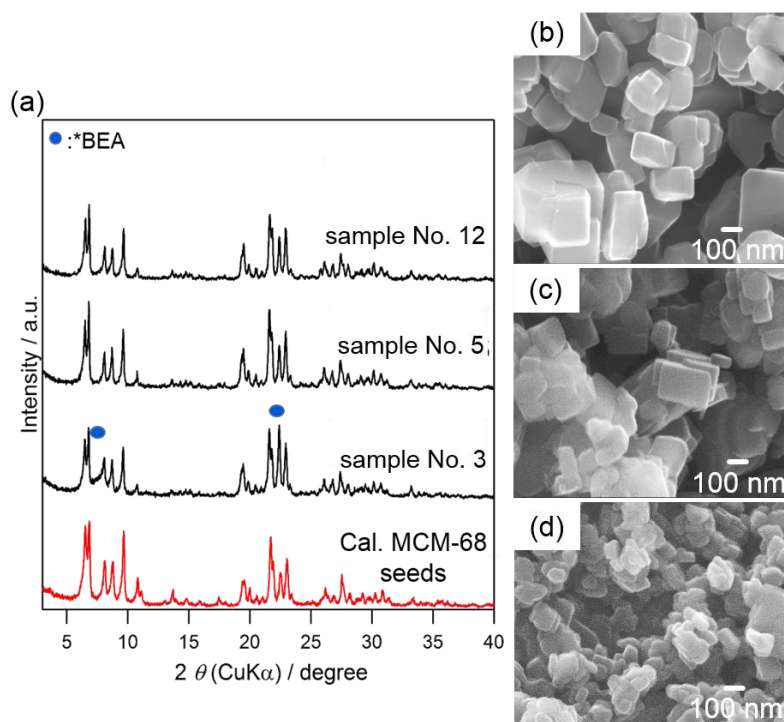


Figure 2.4 (a) Powder XRD patterns of the samples No. 3, 5, and 12 synthesized as described in Table 2.1. FE-SEM images of: (b) calcined MCM-68 seed crystals, (c) sample No. 3, and (d) sample No. 12.

The HRTEM images showed distinctive crystalline orders for both MCM-68 seed crystals and sample No. 3, as shown in Figure 2.5 (d) and (e), respectively. As expected, the image corresponding to sample No. 3 displayed a well-developed lattice, indicating highly-crystalline MSE structures without having any amorphous matter surroundings as in the case of MCM-68 seed crystals. Additionally, N₂ adsorption-desorption measurements were carried out to bring a better understanding of the structural and textural characteristics of the synthesized samples. MCM-68 seed crystals and seed-directed, OSDA-freely synthesized MSE (i.e., MSE-OSDAF) were also measured for comparison with sample No. 3 which is selected as a representative sample for the whole set of synthesized MSE-TEA series. Regarding those isotherms shown in Figure 2.5 (a), (b) and (c), it can be said that all the samples displayed type I(a) isotherms, as defined in the International Union of Pure and Applied Chemistry

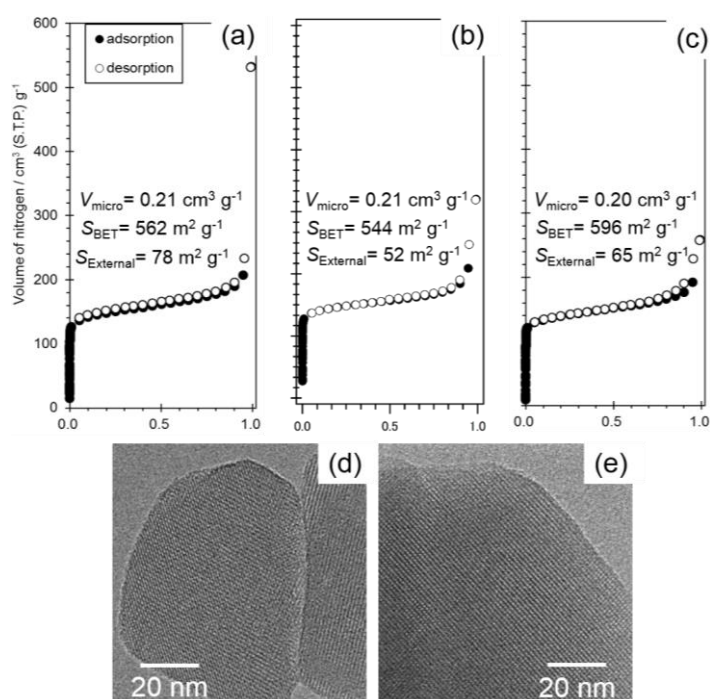


Figure 2.5 Nitrogen adsorption-desorption isotherms of: (a) MCM-68 seed crystals, (b) sample No. 3 as MSE-TEA, and (c) MSE-OSDAF samples. HRTEM images of (d) MCM-68 seed crystals, and (e) sample No. 3.

(IUPAC) classification, confirming no observation of hysteresis loops caused by mesoporous structures or hollows.^[28,29] By using *t*-plot method,^[30] the micropore volumes for MSE-TEA series (see Table 2.1), MCM-68, and MSE-OSDAF were calculated as 0.20, 0.19, and 0.17 cm³g⁻¹, respectively, showing the pore characteristic of MSE-TEA samples nearly similar to those of conventional MCM-68 seed crystals. Also, these results indicate that MCM-68 seed crystals provided active surface for the growth of MSE-TEA crystals, proving the validity of CBU hypothesis shown in Figure 2.2 even for those samples containing TEAOH as an OSDA.

The role of the seed crystals or TEAOH in the synthesis were assessed by carrying out some control experiments under various conditions (samples Nos. 13–17, 5, and 1 in Table 2.1). As shown in Table 2.1, seed crystal amounts lower than 20 wt.% (based on SiO₂) led to the onset of *BEA phase traces (samples Nos. 14–15) along with MSE-TEA after 7 days hydrothermal treatment. Here seed crystals have an essential role to kinetically accelerate the crystal growth of MSE-type zeolite prior to the spontaneous nucleation of *BEA. Therefore, the usage of 20 wt.% of MCM-68 seed crystals as sublimit is required to reach the successful seed-directed synthesis of MSE-type zeolites using TEAOH as an OSDA under the described synthesis conditions. It is also worth mentioning that aging at 80 °C for 24 h before the addition of seed crystals to the initial gels was highly effective in avoiding spontaneous nucleation of other phases (see sample No. 13). Also, the as-synthesized MSE-TEA and MSE-OSDAF materials were further employed as seed crystals in order to study their efficiency compared to conventional MCM-68. As a result, both MSE-TEA and MSE-OSDAF zeolites yielded “second-generation” MSE-TEA zeolites with high purities after optimizing the aging period to 48 h (see Table 2.1 of samples Nos. 16 and 17) to prevent *BEA nucleation. Although the reasons behind the longer aging time

requirements for these seed crystals are still under investigation, different stabilities between the calcined and as-synthesized seed crystals have been already suggested in previous papers.^[31] It is noteworthy that second-generation zeolites have not been reported in seed-directed systems except for few zeolites^[32, 33], thereby indicating the advantage of this seed-directed system using TEOAH as an OSDA. Regarding these results, it can be claimed that the seed crystals actually act as growth centers by providing surface for the crystallization of MSE-TEA, while TEOAH is promoting the growth on these surfaces. Therefore, we can suggest that using a certain amount of calcined seed crystals and TEOAH together is having a collaborative crystal growth effect in the rational synthesis of MSE-type zeolites.

Further structural characterizations were performed on each sample by ^{27}Al and ^{29}Si MAS NMR measurements. As shown in Figure 2.6 (a), the ^{27}Al spectrum of the as-synthesized sample consisted of a single resonance centered at $\delta = 53.5$ ppm corresponding to tetrahedrally coordinated framework Al. However, after calcination, the

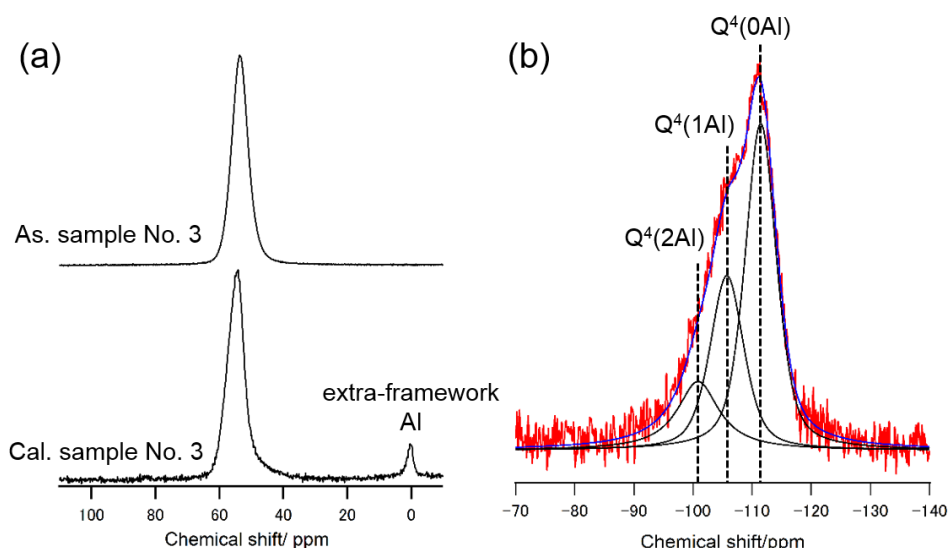


Figure 2.6 (a) ^{27}Al MAS NMR spectra of the as-synthesized and calcined sample No. 3. (b) Peak fittings of the ^{29}Si DD MAS NMR spectra with Gaussian line shapes corresponding to the as-synthesized sample No. 3.

signal slightly shifted to $\delta = 54.4$ ppm, and a minor additional resonance appeared at ca. 0 ppm ascribed to octahedrally coordinated aluminum since a little dealumination occurred during decomposition of TEA^+ from the pores of MSE-TEA. In fact, these results confirm the common behavior of conventional MCM-68 for MSE-TEA samples before and after calcination.^[25] The peak areas were evaluated by the integration of ^{29}Si MAS NMR spectra fitted with Gaussian functions for deconvolution of overlapped peaks (Figure 2.6 (b), dotted lines), which revealed three different components. The peak at -111.5 ppm assigned to $\text{Q}^4(0\text{Al})$ silicon atoms with no aluminum in the second coordination sphere ($\text{Si}(\text{OSi})_4$).^[34] Additional signals appeared at ca. $\delta = -105.7$ and -100.9 ppm which corresponded to $\text{Q}^4(1\text{Al})$; ($\text{Si}(\text{OAl})(\text{OSi})_3$) and $\text{Q}^4(2\text{Al})$; ($\text{Si}(\text{OAl})_2(\text{OSi})_2$) silicon species, respectively. As evidenced by the solid-state NMR spectra, it can be concluded that aluminosilicate and silicate precursors were formed by the dissolution and condensation of four-coordinated $\text{SiO}_{4/2}$ and $\text{AlO}_{4/2}$ species with the aid of organic and inorganic cations. Also, the integrated intensity ratios of these peaks enabled us to calculate the real $\text{SiO}_2/\text{Al}_2\text{O}_3$ ratio of MSE-TEA sample as 14.6, which is slightly lower than that measured value by ICP-AES (16.1, Table 2.2) due to negligible analysis mistakes.

2.3.2. Characterization of occluded tetraethylammonium cations in MSE structure

^{13}C DD MAS NMR was performed for the as-synthesized sample No. 3 with the aim to characterize the TEA^+ occluded in the zeolite cavities. As shown in Figure 2.7 (b), the NMR spectra presented two narrow resonance positioned at 7.4 and 52.2 ppm attributed to carbon atoms of the methyl ($-\text{CH}_3$) and methylene ($-\text{CH}_2-$) groups (shown in Figure 2.7 (a)) of TEA^+ , respectively. Also, no differences were observed between the chemical shifts of TEA^+ in solution and that of TEA^+ occluded in

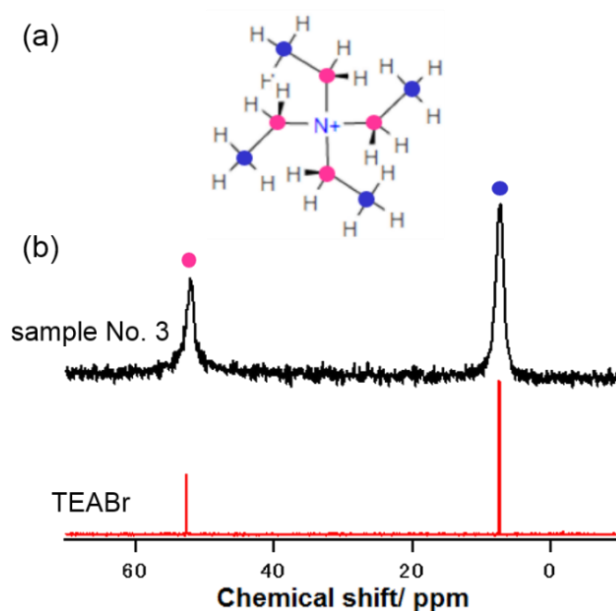


Figure 2.7 (a) Molecular model of TEA⁺. (b) ¹³C CP MAS NMR spectra of as-synthesized sample No. 3.

MSE-TEA (see Figure 2.7 (b)). This can be the result of the weak interaction of TEA⁺ species with the zeolite framework, as reported previously.^[35] Considering these results, it can be said that TEA cations are successfully occluded into MSE cavities. However, ¹³C MAS NMR measurements did not allow to gain information about the conformational state of those occluded TEA⁺ species. Therefore, Raman spectroscopy was employed on the as-synthesized samples. As it is widely known, TEA⁺ in aqueous solution consisted of two conformers with all-trans (tt.tt) and trans-gauche (tg.tg) arrangements in a ratio of 50:50.^[36-38] The conformers exhibited two distinct Raman bands as a result of the C₄N tetrahedral symmetric stretching mode of TEA⁺. As shown in Figure 2.8 (a), the Raman spectrum of the as-synthesized sample No. 3 presented one intense peak (676.5 cm⁻¹) along with a small peak (664.5 cm⁻¹) assigned to tt.tt and tg.tg conformers, respectively. The area fraction of these two Raman bands revealed that ca. 90% of the TEA⁺ occluded in MSE-TEA were formed by tt.tt conformers. Thus, the conformations of TEA⁺ occluded in MSE-TEA zeolite was

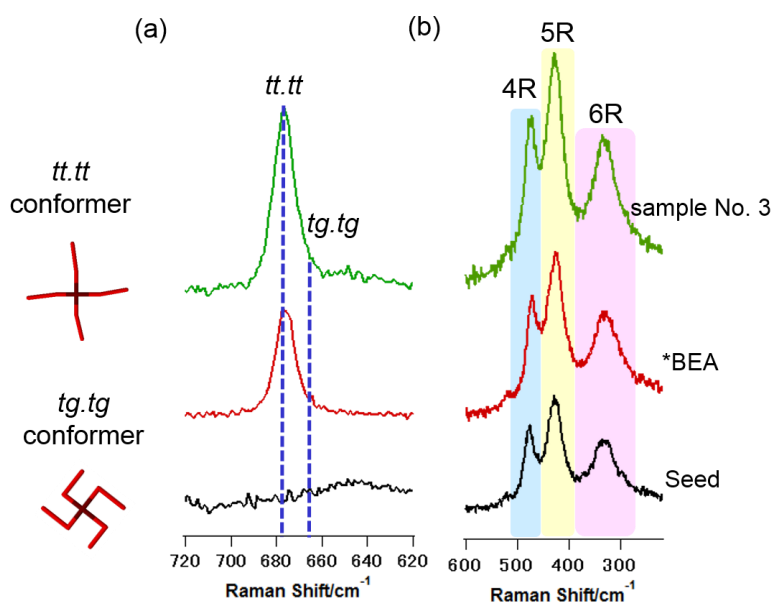


Figure 2.8 Raman spectra of: (a) as-synthesized, (b) calcined sample No. 3, standard *BEA, and seed crystals.

similar to that of TEA⁺ in standard *BEA (tt.tt conformers constituted 95% of all occluded TEA⁺).^[39]

Moreover, Raman spectroscopy is used to study the structural evaluation of aluminosilicate frameworks of calcined samples, standard *BEA zeolite, and MCM-68 seed crystals. Figure 2.8 (b) shows the spectra of those samples in the silicate ring region (220–600 cm⁻¹).^[40] The bands at 327.5, 422.5, and 472.5 cm⁻¹ were attributed to 6, 5, and 4-Rs, respectively. Obviously, the framework of sample No. 3 obtained with TEAOH contained the same ring structures as those of seed crystals since both have MSE topology. Interestingly, standard *BEA possessed a ring structure very similar to that of MSE-type zeolites, which can be due to their consisting of utterly same CBUs and nearly similar ring size distributions as respectively shown in Figure 2.9 (a) and (b). In fact, this result supported well the herein purposed strategy which is based on the utilization of TEAOH as a simple OSDA and selecting the synthesis conditions similar to those of *BEA for the preparation of MSE-TEA based on the CBU hypothesis.

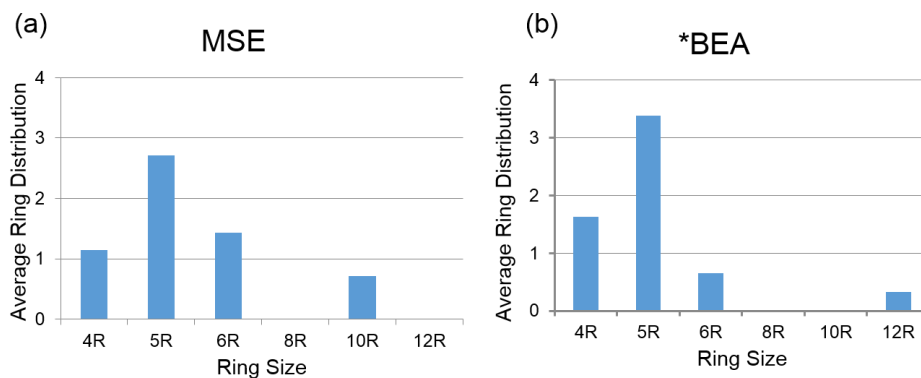


Figure 2.9 Ring distribution of (a) MSE and (b) *BEA- type framework structures.

In order to assess the contents of water and OSDAs interacting with the aluminosilicate frameworks, TG-DTA measurements were carried out on the MSE-TEA and seed crystal samples. Standard *BEA zeolite and a physical mixture of TEAOH with seeds were also measured for comparison with sample No. 3. As shown in Figure 2.10 (A), the DTA curves presented an endothermic peak at ca. 100 °C and exothermic peaks at ca. 450 °C. The endothermic peak was attributed to the dehydration of adsorbed water, while the exothermic peaks centered at 415 °C (physical mixture), 440 °C (*BEA), and 450 °C (Sample No. 3) were ascribed to the combustion of balanced TEA^+ with negatively charged Al sites.^[41–43] The higher combustion temperature of TEA^+ on MSE-TEA (sample No. 3) compared to the physical mixture of TEAOH and MCM-68 seed crystals indicated that TEA^+ was occluded in the cavities of MSE-TEA. Also, it is speculated in the literature^[39] that the high selectivity for tt.tt conformers in the case of *BEA is most probably because they allow closer interaction between positively charged atom of TEA cations and negatively charged framework elements compared to tg.tg conformers. As shown here in DTA analysis, this can be also the case for MSE since the decomposition temperatures of occluded TEAs were as high as zeolite beta one. Therefore, high interaction might be shown as a reason for the high selectivity of tt.tt conformers for MSE. Figure 2.10 (B) exhibits no peak around 360 °C

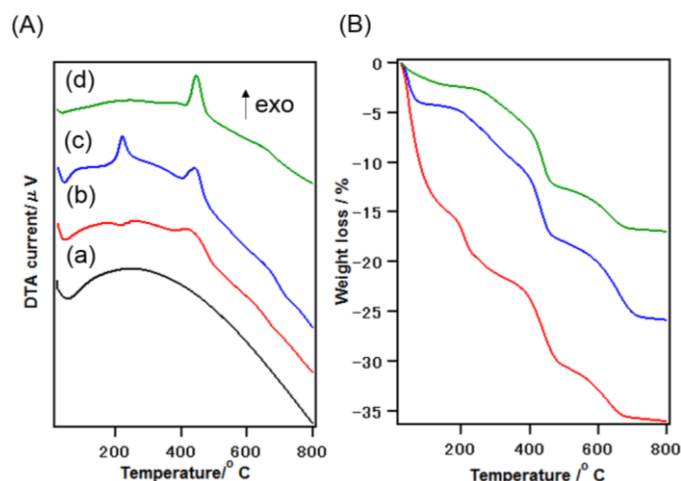


Figure 2.10 (A) DTA and (B) TG curves of (a) MCM-68 seed crystals, (b) the physical mixture of MCM-68 seeds with TEAOH, (c) standard zeolite BEA, (d) sample 3.

arising from desorption and/or combustion of TEA^+ balanced with silanol defect at the framework.^[38–40] From TG data in the Figure 2.11 (B), the weight loss of sample No. 3 due to organics were measured about 14.5 wt.% while those of *BEA and the physical mixture were 21.2 wt.% and 21.0 wt.%, respectively. All above-mentioned results along with ICP-AES, AAS, and CHN elemental analyses employed for each MSE-TEA zeolites was used in the calculations to attain the chemical composition of the MSE-TEA products, and results of these calculations were presented in Table 2.2. Regarding this, the $\text{SiO}_2/\text{Al}_2\text{O}_3$ ratios of the obtained products ranged from 13.9 to 17.3 depending on the synthesis, which is lying between MSE-OSDAF (11.9) and seed crystals (20.2). Also, the chemical analysis of the obtained series of MSE-TEA products revealed that almost 8 TEA^+ cations are occluded into MSE structure regardless of $\text{SiO}_2/\text{Al}_2\text{O}_3$ ratios of those products. And it is found that all occluded inorganic and organic cations compensated with the negatively charged framework element, which suggests no silanol defect occurring. Regarding these results, it is clear to say for the Al-rich samples, the incorporation of Al into the framework mostly controlled by Na and K alkali cations, while TEA cations primarily stabilized the structure with its

Table 2.2 Summary of the chemical compositions of the samples MSE-TEA, MSE-OSDAF, *BEA, and calcined MCM-68 seed crystals successfully prepared.

Sample No.	SiO ₂ / Al ₂ O ₃ ^a	Na ⁺ /u.c. ^b	K ⁺ / u.c. ^b	TEA ⁺ /u.c. ^c	Al/ u.c.	M ⁺ +TEA ⁺ / u.c.
3	16.2	1.6	2.8	8.2	12.3	12.6
4	17.8	1.2	2.3	8.3	11.3	11.8
6	13.6	2.4	4.5	8.3	14.7	15.2
7	16.1	1.9	3.0	8.4	12.8	13.3
8	16.3	1.7	2.4	8.4	12.2	12.5
9	16.8	1.4	2.6	8.4	11.9	12.2
10	14.9	1.9	3.7	7.9	13.1	13.5
11	15.3	2.1	3.1	8.1	12.9	13.3
12	14.1	2.3	4.3	7.6	13.8	14.2
16	15.1	1.8	4.2	7.4	13.1	13.4
17	14.6	2.3	4.6	6.8	13.4	13.7

^aSi and Al contents were quantified by ICP-AES. ^bNa and K measurements were carried out using AAS. ^cTEA⁺/u.c values were calculated from the CHN and TGA results (u.c: unit cell of MSE and *BEA consisting of 112 and 64 T-atoms, respectively.)

limited crystal growth effect by occluding constant number into MSE structure, which indicates that TEAOH plays pore filler role of OSDA.

As the newly established path, rational synthesis is further compared with other alternative MSE synthesis methods to understand the effectiveness of it. As you can see in Table 2.3, the conventional synthesis path showed almost 100 percent silicon yield while OSDA-free method had only 17 percent. As it is previously reported, seed-directed, OSDA-free synthesis tends to yield Al-rich products due to the absence of organic components.^[27] This is generally because of the high charge densities of the alkali cations (Na⁺, K⁺, Li⁺, etc.) which cause the electrostatic interactions between aluminosilicate species, resulting in the formation of Al-rich structures. Conversely, the synthesis carried in the existence of organic molecules induce hydrophobic interactions between silicate species due to their low charge densities, and yield the high silica zeolites. Therefore, this difference in silicon yield can be attributed to the large difference in the charge densities of the used cations which are alkali cations in the case

Table 2.3 Comparison of simplified synthesis methods for MSE-type zeolites.

Sample	Si/ Al _{gel}	Si/ Al _{product}	OSDA ⁺ / u.c.	Al/ u.c.	Si Yield [wt.%]	Solid Yield [wt.%]
MSE _{TEBOP}	10	10	5.0	10	~100	~100
MSE _{TEA}	25-10	7.1~8.9	8.0	11-15	30-60	30~54 (20 wt.% seed)
MSE _{OSDAF}	50	6.0	-	16	17	15 (10 wt.% seed)
YNU-3 _{TEBOP}	6.7	6.5	n.d.	15	n.d.	80~90 (5 wt.% seed)

Unit cell of MSE consisting of 112 T atoms.

of OSDA-free synthesis, and TEBOP²⁺ in the conventional synthesis. Since TEBOP²⁺ having a bulky structure is balancing with two negatively charged Al sites, it is allowing more silicon incorporation in the framework. By introducing TEA cations in the synthesis of MSE, this large gap in the silicon yield of OSDA-free and conventional synthesis could be filled due to having relatively intermediate charge density of TEA cations which allowed to expand the synthesis space and increase the solid product yield compared to OSDA-free method, and decrease the production costs compared to conventional OSDA synthesis as seen in Figure 2.11. In this case, we plot concentration of Si against the concentration of M (inorganic or organic cations) and by altering the concentrations of both we consider the range of points where the zeolite forms.

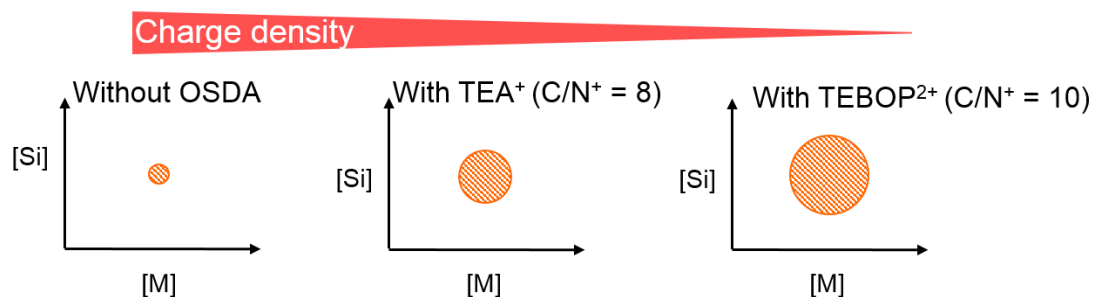


Figure 2.11 Synthesis space (hatched circle) for alternative methods which are utilized to produce MSE-type zeolites by using different inorganic or organic cations.

Therefore, to the best of our knowledge, it can be said that our approach showing this much high solid yield of MSE-type zeolite is the most efficient route among the alternative methods using either relatively inexpensive OSDA or OSDA-free synthesis.^[19-24]

2.3.3. Crystallization kinetics

The samples synthesized from a gel with the same composition as that used for sample No. 3 (Table 2.1) and with different periods of crystallization at 160 °C are depicted in Figure 2.12. The sample was amorphous before the addition of seed crystals (data not shown). The amount of this amorphous matter was very low owing to the clear liquid-like nature of the preheated sol. Therefore, the sample collected right after the addition of seed crystals was nearly similar to seed crystals itself (data not shown). In Figure 2.12 (a), the XRD patterns of the samples after 6 h of hydrothermal treatment in the presence of seed crystals exhibited 80% of relative crystallinity with amorphous matter. The peaks attributed to *BEA appeared after 24 h of heating, while MCM-68 seed crystals seemed to be partially dissolved and therefore the crystallinity of MSE-TEA products slightly decreased (71 and 75% for 24 and 72 h of heating). It can be seen that a small amount of *BEA impurity were initially nucleated from the amorphous matter (24–120 h of heating), suggesting the strong structure-directing effect of TEAOH for *BEA structure. However, the intensity of those peaks decreased by prolonging the synthesis time, and finally disappeared after 168 h of hydrothermal treatment since the medium conditions turned to be favorable for MSE-TEA growth. After 168 h, the peak intensity of MSE-TEA reached a maximum without the presence of any impurities, indicating the higher stability of MSE-TEA products compared to *BEA under the present conditions. As shown in Figure 2.12 (b), the SEM images of the sample heated for 6 h revealed the presence of amorphous matter together with

partially dissolved seed crystals. Although a small amount of *BEA was detected in the XRD patterns for further heating, finally after 168 h of hydrothermal treatment the existence of beta crystals could not be confirmed from the SEM images. Also, the products exhibited pseudo-cubic or rectangular crystals.

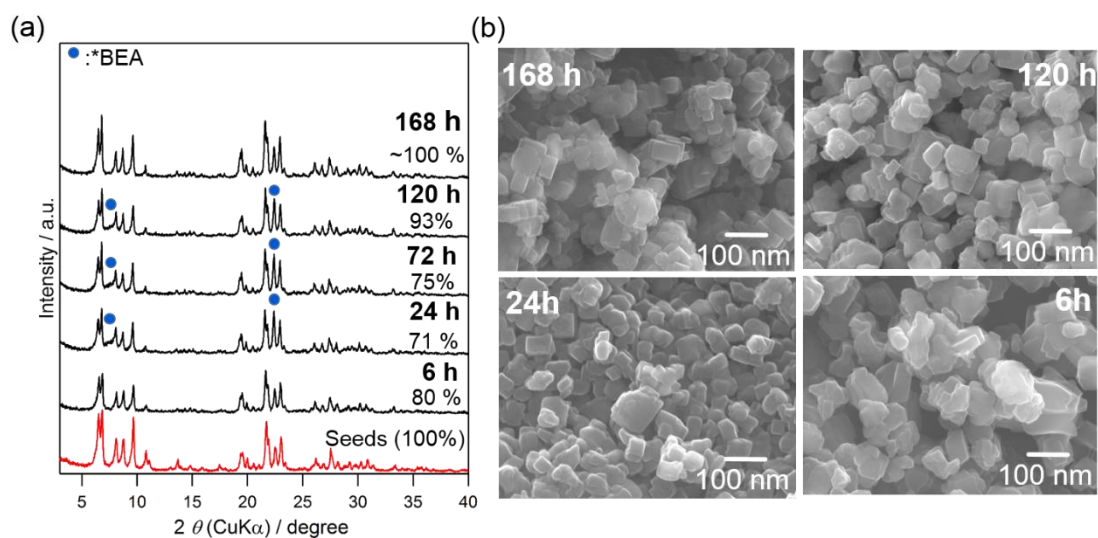


Figure 2.12 (a) XRD patterns of the samples after 6 h, 24 h, 72 h, 120 h, and 168 h of heating.

(b) FE-SEM images of the samples after 6 h, 24 h, 120 h, and 168 h of heating.

2.4. Conclusion

Simplified, seed-directed synthesis of MSE-type zeolites was accomplished in an attempt to replace complex OSDAs with commercially available TEAOH based on common CBU between *BEA and MSE with the CBU hypothesis. The representative scheme for the proposed synthesis path is shown in Figure 2.13. The obtained physicochemical analysis of the synthesized products revealed similar properties to that of conventional MCM-68. Furthermore, the effect of the chemical compositions, the role of the TEA⁺, and the textural properties of obtained MSE zeolites were investigated in detail to better understand the formation of the structure. Regarding this, it is found that TEA⁺ act as pore filler to stabilize the MSE structure during the crystallization. Also, the effectiveness of the seed-directed approach is once more confirmed since the obtained product from the present system is changed in the absence of seed crystals. Furthermore, the results revealed that the amounts and ratios of all the raw materials in the reactant gel mixture (i.e., TEAOH, NaOH, KOH, SiO₂, Al₂O₃) are keys in this new synthesis approach. A highly crystalline MSE-TEA sample with a maximum solid yield of 54 wt.% was obtained from the gel containing TEAOH. This high yield, which is to the best of our knowledge the highest one reported so far, was obtained by applying

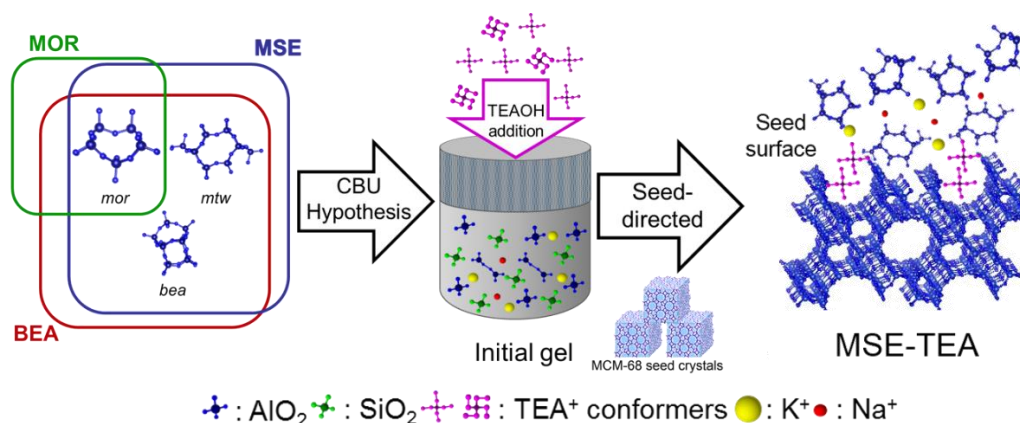


Figure 2.13 Representative scheme for the rational synthesis of MSE-type zeolites.

seed-directed, rational synthesis approach. Therefore, it can be assumed that the herein proposed rational synthesis offers the most simplified and efficient synthesis path by using the commercially available TEAOH (3600 ¥ for 100 mL, Sigma Aldrich) as an OSDA.

Regarding the evolution of the MSE crystallization process, it can be said that the surface of the seed crystals leads the gel to an MSE structure (instead of *BEA) after exposing with the liquid. It is also showed the applicability of seed-directed approach to in the simplified synthesis of multipore zeolites. Therefore, the concepts demonstrated herein are believed to be extended to many other systems for multi-dimensional, large-pore zeolite synthesis, currently requiring complex and expensive OSDAs. Moreover, the CBU hypothesis was surely shown to be valid even for zeolite synthesis methods involving OSDA.

2.5. References

- [1] C. Baerlocher, W. M. Meier, D. H. Olson, *Atlas of Zeolite Framework Types*; sixth ed.; Elsevier, Amsterdam, 2007.
- [2] D. C. Calabro, J. C. Cheng, R. A. Jr. Crane, C. T. Kresge, S. S. Dhingra, M. A. Steckel, D. L. Stern, S. C. West, U.S. Patent 6049018, 2000.
- [3] M. Moliner, C. Martínez, A. Corma, *Angew. Chem. Int. Ed.* 54 (2015) 3560–3579.
- [4] D. L. Dorset, S. C. Weston, S. S. Dhingra, *J. Phys. Chem. B* 110 (2006) 2045–2050.
- [5] N. Žilková, M. Bejblová, B. Gil, S. I. Zones, A.W. Burton, C.-Y. Chen, M. Musilová-Pavlavčková, G. Košová, J. Čejka, *J. Catal.* 266 (2009) 79–91.
- [6] B. Gil, G. Košová, J. Čejka, *Microporous Mesoporous Mater.* 129 (2010) 256–266.
- [7] Y. Kubota, S. Inagaki, Y. Nishita, K. Itabashi, Y. Tsuboi, T. Syahylah, T. Okubo, *Catal. Today* 243 (2015) 85–91.
- [8] T. Shibata, S. Suziki, H. Kawagoe, K. Komura, Y. Kubota, Y. Sugi, J. -H. Kim, G. Seo, *Microporous Mesoporous Mater.* 116 (2008) 216–226.
- [9] T. Shibata, N. H. Kawagoe, K. Komura, Y. Kubota, Y. Sugi, *J. Mol. Catal. A: Chem.* 297 (2009) 80–85.
- [10] S Ernst, S. P. Elangovan, M. Gerstner, M. Hartmann, S. Sauerbeck, *Stud. Surf. Sci. Catal.* 154C (2004) 2861.
- [11] S. Inagaki, K. Takechi, Y. Kubota, *Chem. Commun.* 46 (2010) 2662–2664.
- [12] S. P. Elangovan, M. Ogura, S. Ernst, M. Hartmann, S. Tontisirin, M. E. Davis, T. Okubo, *Microporous Mesoporous Mater.* 96 (2006) 210–215.
- [13] Y. Kubota, Y. Koyama, T. Yamada, S. Inagaki, T. Tatsumi, *Chem. Commun.* (2008) 6224–6226.
- [14] S. Inagaki, Y. Tsuboi, M. Sasaki, K. Mamiya, S. Park, Y. Kubota, *Green Chem.* 18 (2016) 735–741.
- [15] Y. Koyama, T. Ikeda, T. Tatsumi, Y. Kubota, *Angew. Chem. Int. Ed.* 47 (2008) 1042–1046.
- [16] S. Inagaki, Y. Tsuboi, Y. Nishita, T. Syahylah, T. Wakihara, Y. Kubota, *Chem. Eur. J.* 19 (2013) 7780–7786.
- [17] M. Matsukata, M. Ogura, T. Osaki, P. R. H. P. Rao, M. Nomura, E. Kikuchi, *Top. Catal.* 9 (1999) 77–92.
- [18] S.I. Zones, *Microporous Mesoporous Mater.* 144 (2011) 1–8.
- [19] J.G. Moscoso, D.Y. Jan, U.S. Patent 7922997, 2011.

- [20] K. G. Strohmaier, S. C. Weston, J. C. Vartuli, J. T. Ippoliti, U.S. Patent 9025863, 2011.
- [21] A. W. Burton, U.S. 8900548, 2014.
- [22] S. C. Weston, K. G. Strohmaier, H. B. Vroman, U.S. Patent 8916130, 2014.
- [23] S. C. Weston, K. G. Strohmaier, H. B. Vroman, U.S. Patent 2013/0115163, 2013.
- [24] S. C. Weston, K. G. Strohmaier, H. B. Vroman, J. C. Vartuli, J. T. Ippoliti, A. J. W. Lobo, D. W. Lewis, International Symposium on Zeolite and Microporous Crystals, Japan, 2015.
- [25] Y. Kubota, K. Itabashi, S. Inagaki, Y. Nishita, R. Komatsu, Y. Tsuboi, S. Shinoda, T. Okubo, *Chem. Mater.* 26 (2014) 1250–1259.
- [26] K. Itabashi, Y. Kamimura, K. Iyoki, A. Shimojima, T. Okubo, *J. Am. Chem. Soc.* 134 (2012) 11542–11549.
- [27] K. Iyoki, K. Itabashi, T. Okubo, *Microporous Mesoporous Mater.* 189 (2014) 22–30.
- [28] K. S. W. Sing, D. H. Everett, R. A. W. Haul, L. Moscou, R. A. Pierotti, J. Rouquerol, T. Siemieniewka, *Pure Appl. Chem.* 57 (1985) 603–619.
- [29] F. Rouquerol, J. Rouquerol, K. Sing, *Adsorption by Powders & Porous Solids*, Academic Press, London, 1999.
- [30] W. D. Harkins, G. Jura, *J. Am. Chem. Soc.* 66 (1944) 1366–1373.
- [31] K. Iyoki, K. Itabashi, T. Okubo, *Chem. Asian J.* 8 (2013) 1419–1427.
- [32] Y. Kamimura, W. Chaikittisilp, K. Itabashi, A. Shimojima, T. Okubo, *Chem. Asian J.* 5 (2010) 2182–2191.
- [33] Y. Kamimura, K. Itabashi, T. Okubo, *Microporous Mesoporous Mater.* 147 (2012) 149–156.
- [34] G. Engelhardt, D. Michel, *High-Resolution Solid-State NMR of Silicates and Zeolites*; John Wiley & Sons, New York, 1987.
- [35] J. Pérez-Pariente, J. Sanz, V. Fornés, A. Corma, *J. Catal.* 124 (1990) 217–223.
- [36] C. Naudin, F. Bonhomme, J. L. Bruneel, L. Ducasse, J. Grondin, J. C. Lassègues, L. Servant, *J. Raman Spectrosc.* 31 (2000) 979–985.
- [37] T. Takekiyo, Y. Yoshimura, *J. Phys. Chem. A* 110 (2006) 10829–10833.
- [38] T. Goto, T. Takekiyo, Y. Yoshimura, *J. Phys.: Conf. Ser.* 121 (2008) 042005.
- [39] T. Ikuno, W. Chaikittisilp, Z. Liu, T. Iida, Y. Yanaba, T. Yoshikawa, S. Kohara, T. Wakihara, T. Okubo, *J. Am. Chem. Soc.* 137 (2015) 14533–14544.
- [40] Y. Yu, G. Xiong, C. Li, F.-S. Xiao, *Microporous Mesoporous Mater.* 46 (2001) 23–34.
- [41] W. Chaikittisilp, T. Yokoi, T. Okubo, *Microporous Mesoporous Mater.* 116 (2008) 188–195.

- [42] M. Matsukata, M. Ogura, T. Osaki, E. Kikuchi, A. Mitra, *Microporous Mesoporous Mater.* 48 (2001) 23–29.
- [43] M. Matsukata, T. Osaki, M. Ogura, E. Kikuchi, *Microporous Mesoporous Mater.* 56 (2002) 1–10.

Chapter 3. Synthesis of Zincoaluminosilicate MSE-type Zeolites

3.1. Introduction

As much as discovering new structures, and/or developing simplified synthesis routes for existing structures with medium and large pores remain important, introducing isolated heteroatoms in those of existing frameworks is recently attracting increasing attentions.^[1-4] MCM-68 (MSE topology) with its multipore architecture^[5,6] has received a great interest in this manner owing to its unique acid properties,^[7,8] which allow the zeolite to be widely utilized as a shape-selective catalyst for the alkylation of aromatics,^[9,10] and for the production of propylene by paraffin cracking.^[11] In response to this, the insertion of Ti^{4+} into MSE framework (Ti-MCM-68) as a heteroatom has been achieved via post-synthetic treatments. The obtained Ti-MCM-68 unexpectedly showed superior activity to other titanosilicates such as TS-1, Ti-*BEA, and Ti-MWW for phenol oxidation using H_2O_2 as an oxidant owing to higher diffusivity in 12-R over 10-R as well as the absence of a large cavity at 12- and 10-R intersections.^[3] Even though several attempts have been done for direct crystallization of MCM-68 with different framework atoms, only a pure silica version of MSE topology could be synthesized by utilizing “steam-assisted crystallization (SAC)” method.^[12] However, this material exhibited many site defects in the framework due to unbalanced cationic charges, which also requires some post-synthetic treatments to stabilize the MSE structure. Therefore, there is a call to develop a synthesis path for the insertion heteroatoms into MSE-type zeolites or

multipore zeolites which have a potential for various applications with their framework structure containing heteroatoms.

Indeed, the isomorphic substitution of framework Si^{4+} by different transition atoms allows us to subtly adjust the physicochemical features of the zeolites such as internal acidity, redox properties, and hydrophobic–hydrophilic nature.^[12–16] Particularly interesting in this regard is zinc-based zeolites, in which framework Zn^{2+} as divalent atom originates two anionic charges per zinc atom, whereas trivalent atoms (Al^{3+} , B^{3+} and so on) generate only one charge per aluminum atom, and tetravalent atoms (Ti^{4+} , Sn^{4+} and so on) do not contain any framework charges. Therefore, the ion exchange for divalent-cations such as Cu^{2+} , Ni^{2+} , Fe^{2+} can be realized for zincosilicates in one to one ratio per framework zinc without leaving any unpaired charge.^[15,17] As previously reported, CIT-6 (Zn-*BEA) and Zn-MCM-41 showed much-improved performance in different reactions compared to their analogous Sn- and Ti-incorporated solids.^[18,19] After Ni^{2+} exchanged of those zeolites and their Al analogous, they were tested for light olefin oligomerization. The results proved that Ni^{2+} exchanged zincosilicates are prominent catalysts for the reaction since the charge of their framework heteroatom matches well with that of the exchanged ion which may hinder the side reactions catalyzed by un-exchanged, strong Brønsted acid sites.^[17] However, the substitution of zinc as heteroatom into different frameworks is still challenging. Especially, the easy formation of zinc oxide owing to precipitation of zinc species during synthesis does not allow large amount of zinc to incorporate in the zeolite frameworks.^[20,21] Also, zinc containing zeolites compared to aluminosilicates exhibit lower hydrothermal stability which restricts their usage in wide range of applications. Therefore, some zeolites (CHA, GME, and AEI) which contain zinc and aluminum in the same structure were prepared to bear not only Lewis acid characteristics but also durability against hydrothermal treatment.^[22]

In keeping with the above, we herein report a successful synthesis of zincoaluminosilicate MSE-type zeolites (MSE-TEA_{Znx}, x stands for Zn/(Zn+Al) ratios ranging from 0 to 1.0) by applying a co-precipitated gel technique^[23] in the previously developed rational seed-directed synthesis method using the simple OSDA (TEAOH).^[24] This is the first time for direct crystallization of zincoaluminosilicate MSE-type zeolites, and/or zincoaluminosilicate zeolites possessing both medium and large pores. Noteworthy, the prepared gels play a key role for this achievement since their homogeneously dispersed zinc and aluminum species tend to form zeolitic frameworks instead of hydrolyzing and precipitating. In addition, the physicochemical characterization and divalent-cation exchange performance of the successfully obtained samples were examined and detailed for bringing better understanding to the MSE-TEA_{Znx}.

3.2. Experimental section

3.2.1. Materials

The following commercially available raw materials for seed, aluminosilicate and zincoaluminosilicate MSE-type zeolite synthesis were used as provided: colloidal silica (Ludox[®] HS-40, 40 wt.% in water, DuPont); aluminum hydroxide (Al(OH)₃, Pfaltz, and Bauer); zinc acetate (Zn(CH₃COO)₂, Wako); potassium hydroxide (KOH, 50 wt.% in water, Wako) and sodium hydroxide solution (NaOH, 50 w/v% in water, Wako); tetraethylammonium hydroxide solution (TEAOH, 35 wt.% in water, Aldrich) as the OSDA; and deionized water. Additionally, TEBOP²⁺(Γ)₂ was prepared to be used as an OSDA for seed synthesis from the following chemicals: exo,exo-bicyclo[2.2.2]oct-7-ene-2,3:5,6-tetracarboxylic anhydride (Aldrich), ethylamine solution (70 wt.% in water, KANTO CHEMICAL), lithium aluminum hydride (LiAlH₄, Wako), tetrahydrofuran (THF, JIS Special Grade, KANTO CHEMICAL), benzene (JIS Special Grade, Wako), iodoethane (JIS Special Grade, Wako), ethanol (JIS Special Grade, Wako), and acetone (JIS Special Grade, Wako).

To prepare the zincoaluminosilicate gels, the following chemicals were used as received: sodium silicate solution (JIS No.3, Fuji Kagaku), aluminum sulphate solution (Taimei Chemicals), zinc sulphate (Wako) and sulphuric acid solution (64 wt %, Wako).

3.2.2. Synthesis of MCM-68 seed crystals

As previously reported,^[8] MCM-68 seed crystals synthesis were performed a gel with a composition of 1.0SiO₂: 0.05Al₂O₃: 0.375KOH: 0.1TEBOP²⁺(Γ)₂: 30H₂O. Firstly,

colloidal silica and $\text{Al}(\text{OH})_3$ were dissolved in deionized water. Then, KOH solution was added to this starting mixture and stirred for 30 min. $\text{TEBOP}^{2+}(\Gamma)_2$, which was synthesized as reported elsewhere,^[25] was subsequently mixed with the solution and stirred for additional 4 h. Finally, the obtained gel was loaded in a 125 mL Teflon[®]-lined autoclave (No. 4749, Parr Instrument) and maintained at 160 °C for 16 days under static conditions. After obtaining solid products, they were calcined at 650 °C with a rate of 1 K min^{-1} and further kept at this temperature for 10 h to be used as seed crystals.

3.2.3. Preparation of zincoaluminosilicate gels

As previously reported,^[23] the homogenous zincoaluminosilicate gels (Gel_{Zn_x} , x stands for $\text{Zn}/(\text{Zn}+\text{Al})$ ratios containing constant $\text{Si}/(\text{Zn}+\text{Al})$ ratio of 15 with various $\text{Zn}/(\text{Zn}+\text{Al})$ ratios ($x = 0, 0.2, 0.4, 0.6, 0.8, \text{ and } 1.0$) were synthesized by applying co-precipitation method. For doing this, a mixture of sodium silicate solution (9.37 wt% Na_2O , 28.96 wt% SiO_2), and sulphate solution containing aluminum sulphate solution, sulphuric acid solution and zinc sulphate were prepared. In order to keep media approximately neutral, the sodium silicate and sulphate solutions were mixed in a continuous flow vessel at 40°C via liquid pumps with a feeding rate of 60 cm^3/min and 15 cm^3/min , respectively. The obtained mixture maintained in the vessel around 15 min to become a gel slurry which then continuously flowed out to the collecting vessel. After all, the collected gel slurry is centrifuged to separate the gel from mother liquid, and simultaneously washed with distilled water to remove by-produced sodium sulphate. In order to calculate the water content of obtained gels from weight loss, a certain amount of sample taken from gels was calcined at 600 °C with a rate of 7 K min^{-1} and further kept at this temperature for 2 h.

3.2.4. Synthesis of MSE-type zeolites using zincoaluminosilicate gels and tetraethylammonium hydroxide as a simple organic structure-directing agent

The synthesis gels of MSE-type zeolites were prepared by using the preceding zincoaluminosilicate gels (Gel_{Znx}), TEAOH as an OSDA, NaOH and KOH solutions, and distilled water. Firstly, organic and inorganic solutions were mixed under stirring for ca. 10 min, then the zincoaluminosilicate gel was subsequently added. The resulting mixture was homogenized by stirring for additional 5 min. Thereafter, the synthesis gel was loaded to a 23 mL Teflon[®]-lined stainless steel autoclave (No. 4749, Parr Instrument), which was heated at 80 °C for 24 or 48 h. The chemical composition of the synthesis gels had the following molar ratios: 30SiO_2 : $(1-y)\text{Al}_2\text{O}_3$: $2y\text{ZnO}$: $8.25(\text{K}_2\text{O}+\text{Na}_2\text{O})$: $3.30(\text{TEA})_2\text{O}$: $450\text{H}_2\text{O}$ (where $y = 0, 0.2, 0.4, 0.6, 0.8, 1.0$, and $\text{K}_2\text{O}/(\text{K}_2\text{O}+\text{Na}_2\text{O}) = 0.25$). After cooling the autoclave to room temperature, 20 wt.% of calcined MCM-68 seed crystals relative to the silica source were added into the preheated synthesis gel. The resultant mixture was hydrothermally treated at 160 °C for 144 h under static conditions in a preheated air circulated oven. After crystallization, the solid products were centrifuged and subsequently washed with distilled water until the filtrate pH became neutral. Recovered products were dried at 80 °C overnight. In order to obtain the calcined powder, the as-synthesized product was heated at 550 °C for 10 h under flowing dry air. The solid yield of the obtained zeolite was described as the weight ratio percentage ($\text{g/g} \times 100$) of the solid product to the sum of the SiO_2 , Al_2O_3 , ZnO and calcined seeds in the reaction gel. Relative crystallinities were calculated based on the ratio of the integrated intensity of the sum for the four peaks in the X-ray diffraction ($2\theta = \text{ca. } 19.45, 21.68, 22.47, \text{ and } 22.99$) for solid products to those of seed crystals.

3.2.5. Synthesis of comparison sample by using zinc acetate

The initial gel for the synthesis of comparison sample (MSE-TEA_{ZnAc0.2}) was prepared with using Al(OH)₃, Zn(CH₃COO)₂, NaOH, KOH, and TEAOH solutions and fumed silica. For doing this, aluminum hydroxide and zinc acetate powder was dissolved in an aqueous alkali solution under stirring for ca. 10 min, and fumed silica was subsequently added slowly. The resulting mixture was homogenized using a mortar and a pestle for additional 30 min. Thereafter, this synthesis mixture was transferred to a 23 mL Teflon[®]-lined stainless steel autoclave (No. 4749, Parr Instrument), which was heated at 80 °C for 24 h. After cooling the autoclave to room temperature, calcined MCM-68 seed crystals were added as 20 wt.% of relative to the silica source. The resultant mixture was hydrothermally treated at 160 °C for 6 days under static conditions in a preheated air circulated oven. After the prescribed synthesis time, the solid product was centrifuged and subsequently washed with distilled water until the filtrate pH became neutral. Recovered products were dried at 80 °C overnight for further characterizations.

3.2.6. Ion-exchange

The ion exchange capacities of the samples were measured by the following methods. First, the calcined sample is converted to its NH₄ form by stirring at 80 °C for 2h using 0.1 mol/L NH₄NO₃ (Wako) solution that had been pH adjusted to 7.0 using 28 wt.% of NH₄OH solution (Wako). For each exchange, 400 mg of samples were added into 250 mL of solution. After 2 h, the samples were centrifuged. Then, the recovered samples were added to the fresh solution, and the same procedure was applied two more times. At the end, the samples were washed and dried in 80 °C oven for overnight.

Ni²⁺ ion exchange was performed at 80 °C for 2 h using a 0.05 M solution of Ni(CHCOO)₂ (hexahydrate, Wako) that had been pH-adjusted to 7.0 by using 28 wt.% of

NH₄OH solution (Wako). For each exchange, 200 mg of samples were added to 100 mL of solution. The materials were then separated from the Ni(CH₃COO)₂ solution via centrifugation, washed with deionized water, and dried at 80 °C oven. After the Ni²⁺ exchange, the color of samples turned from white to a pale green.

3.2.7. Characterization

Powder X-ray diffraction (XRD) patterns were recorded on a Rigaku Ultima IV diffractometer using CuK α radiation with a D/Tex Ultra detector (0.015406 nm, 40 kV, 40 mA). The machine was arranged to obtain each scan at a speed of 20°/min with step width of 0.02° for 2θ values from 3° to 40°. Elemental analysis was measured on a Thermo Scientific iCAP-6300 inductively coupled plasma-atomic emission spectrometer (ICP-AES) system after dissolving the products in a potassium hydroxide solution or hydrofluoric acid solution. Additionally, a Hitachi Z-2000 atomic absorption spectrometer equipped with a heated graphite tube atomizer was used for the determination of Na and K contents of each sample and gel after dissolving them in KOH and NaOH solutions, respectively. CHN elemental analyses were carried out on a CE-440 elemental analyser (Exeter Analytical) to measure the carbon, hydrogen, and nitrogen percentage of the samples which are related to the amount of organic substance in zeolite pores. Thermogravimetric analysis (TGA) was performed on a Rigaku Thermo plus TG 8120 from 30 to 800 °C at a heating rate of 10 K min⁻¹ under a flow (200 mL min⁻¹) of 10% O₂/90% He gas mixture. Nitrogen adsorption/desorption isotherms of the calcined samples were obtained on an Autosorb-iQ2-MP instrument (Quantachrome Instruments) at liquid nitrogen temperature. Prior to the measurements, the samples were degassed at 400 °C for 6h under vacuum. The crystal sizes and morphologies of the obtained products were observed on a JSM- 7500FA (JEOL) field emission scanning electron microscope (FE-SEM) after Os coating over the powder samples on the carbon tape at an accelerating

voltage of 20 kV. Diffuse reflectance (DR) UV–Vis spectra were recorded using a JASCO V-670 spectrometer in 190–800 nm wavelength range at a scan rate of 100 nm/min using BaSO₄ as a reference. The observation of FT-IR spectra using pyridine as a probe molecule was carried out at using a Jasco FT-IR 6100 spectrometer equipped with a mercury cadmium telluride (MCT) detector (JASCO corp., Japan). Spectra in 4000–700 cm⁻¹ range were acquired with 4 cm⁻¹ resolution. For the measurement, samples (15-18 mg) were pressed at around 30 MPa for 5 min to form self-standing pellets with a diameter of 2 cm. The pellets are placed in vacuum IR cell. While evacuating, the samples are heated to 500 °C (10 °C/min), where it was held for 1h for pretreatment. Then, the cell was cooled to 80 °C and probe molecule, pyridine (Wako chemical) was dosed to the samples until the spectra become unchanged. Then, the cell was evacuated again at 80 °C for 30 min., and FT-IR spectra was obtained. Then, the cell was heated to 200 °C, 300 °C and 400 °C under vacuum. After each temperature was held for 30 min, the samples were cooled to 50 °C, and FT-IR spectra was acquired. The resulting spectra were baseline-corrected by subtracting the spectrum at 50 °C without dosing molecules.

3.3. Result and discussion

3.3.1. Characterization of zincoaluminosilicate gels

The chemical compositions of the zincoaluminosilicate gels (Gel_{Zn_x}) synthesized from the mixture of silicate and sulphate solutions by applying co-precipitation technique are summarized in Table 3.1. The $\text{Zn}/(\text{Zn}+\text{Al})$ and $\text{Si}/(\text{Zn}+\text{Al})$ ratios of each prepared gel were same as those of their initial solution mixture. As above-mentioned, tetrahedral Zn usually creates two anionic charges. Contrary to this general idea, the calculated $\text{Na}/(\text{Zn}+\text{Al})$ ratios of those gels by ranging between 1.00 to 1.09 showed that many of the Zn species in prepared gels present one charge as in the case of tetrahedral Al. Indeed, Orazov et al. has already reported this behavior of framework Zn atoms as monocation ion-exchangeable sites, which may occur depending on the synthesis conditions of zincosilicates.^[19] Therefore, it can be said that Zn and Al species in our co-precipitated gels resulted similar anionic charge effect no matter Zn contents of those gels.

Moreover, the coordination state of the calcined zincoaluminosilicate gels and zinc oxide as a reference material were investigated by DR UV–Vis spectrum as depicted in Figure 3.1. As shown, pure ZnO exhibited a broad absorption band around 360 nm assigned to the $\text{O}^{2-} \rightarrow \text{Zn}^{2+}$ ligand to metal charge transfer transition.^[26,27] The diffuse

Table 3.1 Summary for prepared co-precipitated zincoaluminosilicate gels.

Gels ^a	Gel Compositions		
	$\text{Zn}/(\text{Zn}+\text{Al})^b$	$\text{Si}/(\text{Zn}+\text{Al})^b$	$\text{Na}/(\text{Zn}+\text{Al})^{b,c}$
$\text{Gel}_{\text{Zn}0}$	0.00	15.0	1.00
$\text{Gel}_{\text{Zn}0.2}$	0.20	14.5	1.03
$\text{Gel}_{\text{Zn}0.4}$	0.39	14.7	1.07
$\text{Gel}_{\text{Zn}0.6}$	0.60	15.0	1.08
$\text{Gel}_{\text{Zn}0.8}$	0.77	14.7	1.07
$\text{Gel}_{\text{Zn}1.0}$	0.99	15.0	1.09

^aGels were prepared from the mixtures with constant $\text{Si}/(\text{Zn}+\text{Al})$ ratio at 15. ^bSi, Al and Zn contents were quantified by ICP-AES. ^cNa measurement were carried out using AAS.

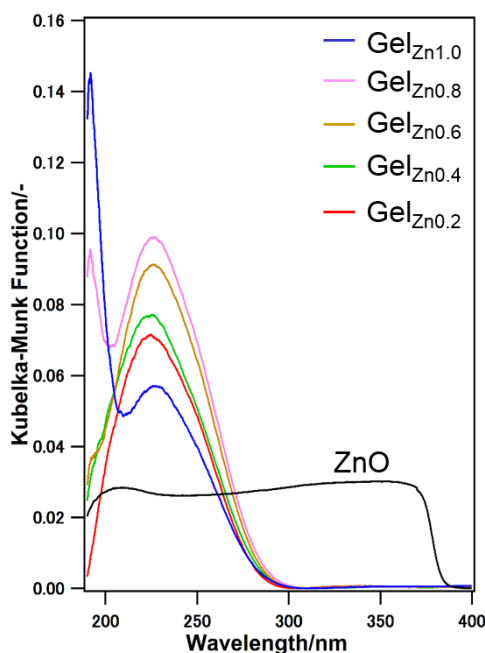


Figure 3.1 Diffuse reflectance UV–Vis spectra of zincoaluminosilicate gels and zinc oxide as reference material.

reflectance spectra of the zincoaluminosilicate gels showed two strong absorption bands centered at 195 and 230 nm which are completely different from that of pure ZnO. Based on these results, it can be assumed that the co-precipitation technique is very useful for homogenous dispersion of Zn and Al species in the gels which brings higher stability against the formation of ZnO than the direct mixing of zinc and silica sources.

3.3.2. Characterization of zincoaluminosilicate MSE-type zeolites

3.3.3. Structural evaluation

The samples were synthesized by using co-precipitated zincoaluminosilicate gels after hydrothermal treatment at 160 °C for 6 days with different preheating period at 80 °C. Figure 3.2 shows the XRD patterns of the as-synthesized series of MSE-TEA_{Zn x} (where x stands for Zn/(Zn+Al) ratios) from the gels containing constant Si/(Zn+Al) ratio of 15 and various Zn/(Zn+Al) ratio of 0, 0.2, 0.4, 0.6, 0.8 and 1.0 by applying preheating at 80 °C for 1 day. As shown, the samples with Zn/(Zn+Al) ratio up to 0.4 showed the

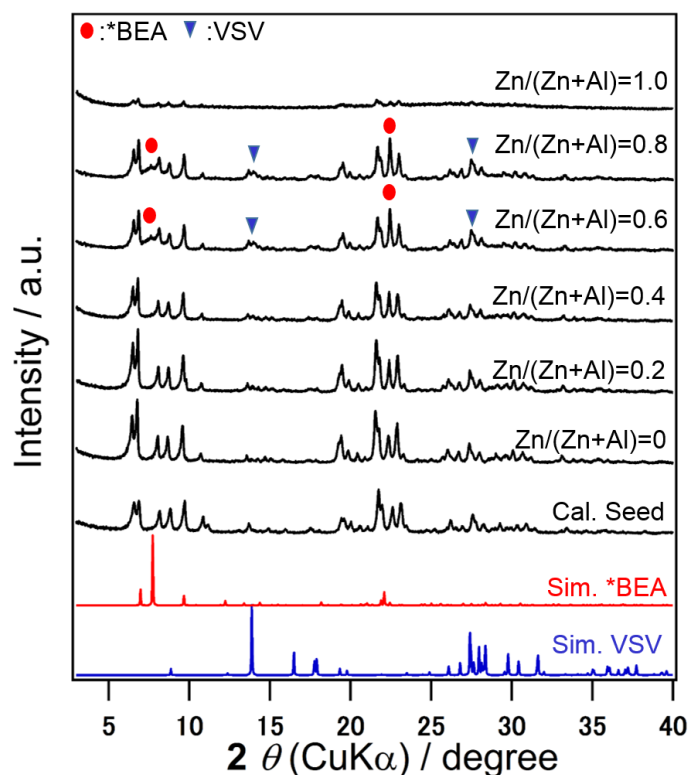


Figure 3.2 Powder XRD patterns of MSE-TEA_{Znx} which were synthesized using co-precipitated zincoaluminosilicate gels containing various Zn/(Zn+Al) ratios by preheating at 80 °C for 1 day, and subsequently hydrothermal treatment at 160 °C for 6 days.

characteristic patterns of MSE structure without any peak related to ZnO ($2\theta = 31.6^\circ$, 34.2° , 36.1° , 56.6°), indicating the zinc species were dispersed in the zeolite. On the other hand, the samples such as MSE-TEA_{Zn0.6} and MSE-TEA_{Zn0.8} exhibited the mixtures of MSE with *BEA and VSV-type zeolites. As previously stated,^[24] the preheating time is one of the key factors to suppress the easy formation of *BEA from the gels containing TEAOH. Thus, we could remove the traces of *BEA impurity by extending the time of preheating for 1 more day as shown in Figure 3.3.

Even though remarkable changes have been made in the synthesis conditions to obtain pure products with Zn/(Zn+Al) ratio of 0.6, VSV phase always appeared as a stable sodium zincosilicate. This result may be ascribed to an unfavorable effect of the

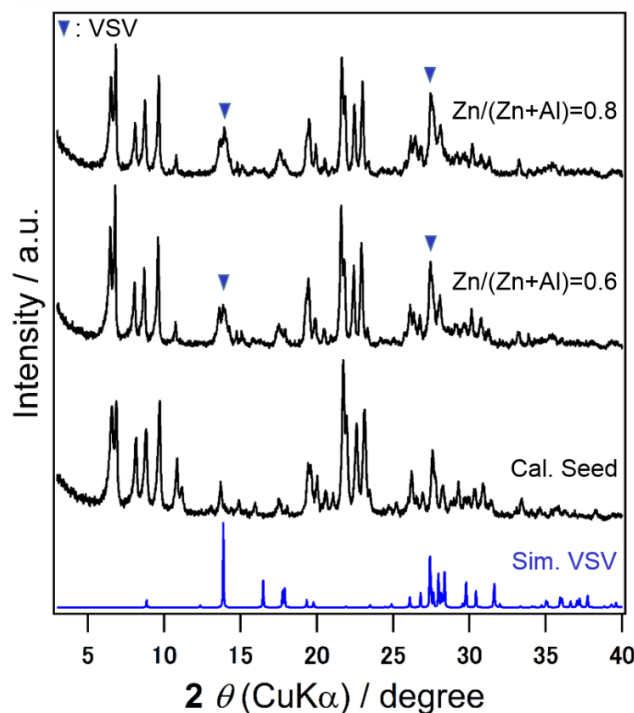


Figure 3.3 Powder XRD patterns of as-synthesized MSE-TEA_{Zn0.6} and MSE-TEA_{Zn0.8} after prolonging preheating time to 2 days, and subsequently hydrothermal treatment for 6 days.

excess amount of Zn content which could not incorporate into MSE framework. Also, MSE-TEA_{Zn1.0} prepared as zincosilicate sample yielded amorphous phase along with minor amount of remained MCM-68 seed crystals due to insufficient hydrothermal conditions in which crystal growth may not occur for any type of structure. Therefore, it is clear to say that the successful synthesis of MSE structure with zinc in the framework can be realized from a gel containing Zn/(Zn+Al) ratio up to 0.4. The reason behind can be that a certain amount of Al is required to be used for the successful crystallization of MSE structure in a narrow synthesis window.^[3]

Furthermore, the morphology of the successful MSE-TEA_{Znx} samples is shown in Figure 3.4. It can be seen that the samples prepared by using zincoaluminosilicate gels exhibit smooth rectangular facets as seed crystals. FE-SEM images of the samples containing a certain amount of zinc content revealed that the obtained products were composed crystal

particles approximately 300–400 nm in size, which seems larger than those of MSE-TEA (200–300 nm) and seed crystals (50–100 nm). As we previously stated in the case of MSE-TEA,^[9] obtaining large crystals can be a result of the seed-directed method since the crystal growth probably occurs on the surfaces of remaining seed crystals. This can be the case for MSE-TEA_{Zn_x} samples. Also, Tatsumi et. al. proposed the core-shell growth mechanism for the seed-directed system based on the TEM-EDX and XPS analysis.^[28] It is well-known in our system that the usage and remaining of seed-crystals after partially dissolved in the reaction gel are essential to obtain pure MSE phase. Although further investigations are required for better understanding, we may assume that the center or core of the obtained products are aluminosilicate since aluminosilicate MCM-68 seed crystals are utilized in the zincoaluminosilicate MSE synthesis, while edge or shell are zincoaluminosilicate.

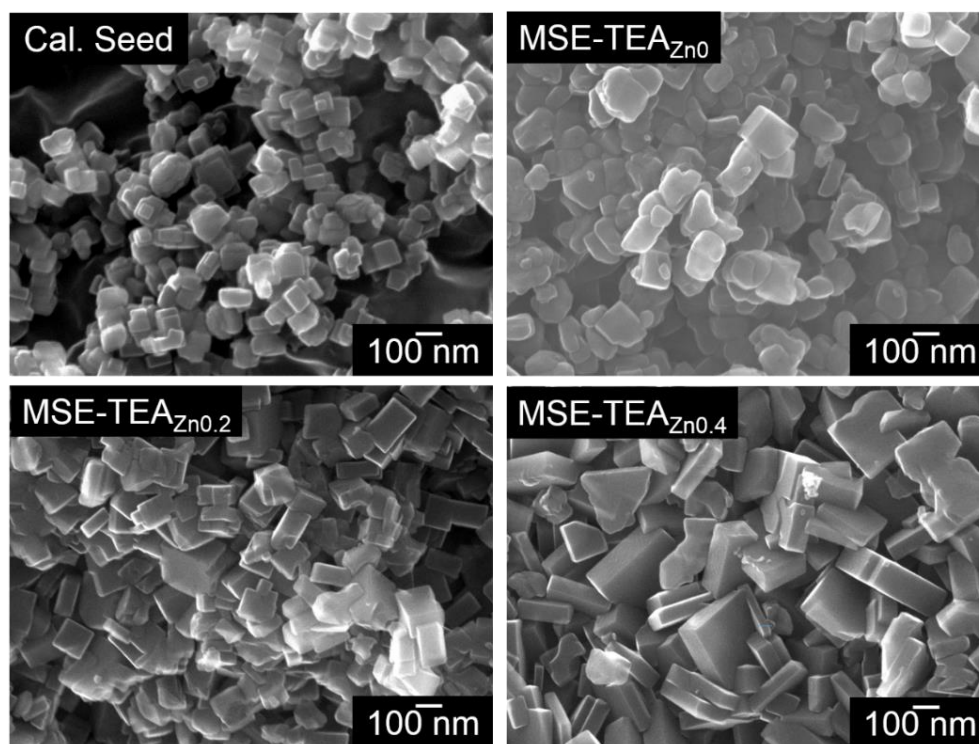


Figure 3.4 FE-SEM images of calcined MCM-68 seed crystals, MSE-TEA_{Zn0}, MSE-TEA_{Zn0.2}, and MSE-TEA_{Zn0.4} samples.

In order to study the effect of the co-precipitation technique and seed crystals in crystal growth of MSE structure, two different control experiments were carried out. Firstly, a sample using zinc acetate (MSE-TEA_{ZnAc0.2}) was prepared from the synthesis gel containing zinc acetate, fumed silica, and amorphous aluminum hydroxide as respectively Zn, Si, and Al sources in the same synthesis gel composition, preheating and hydrothermal conditions which were described above for MSE-TEA_{Zn0.2} sample. The other control experiment was also prepared by using the same synthesis conditions with MSE-TEA_{Zn0.2} sample including the co-precipitated gel with Zn/(Zn+Al) ratio of 0.2 but without adding any seed crystals. In Figure 3.5 (a), the XRD pattern of MSE-TEA_{ZnAc0.2} sample showed that the obtained product consisted of mostly MSE phase with a minor amount of *BEA impurity. It is probably a result of the inhomogeneous distribution of Al and Zn species in the synthesis gel since the synthesis gel prepared by using zinc

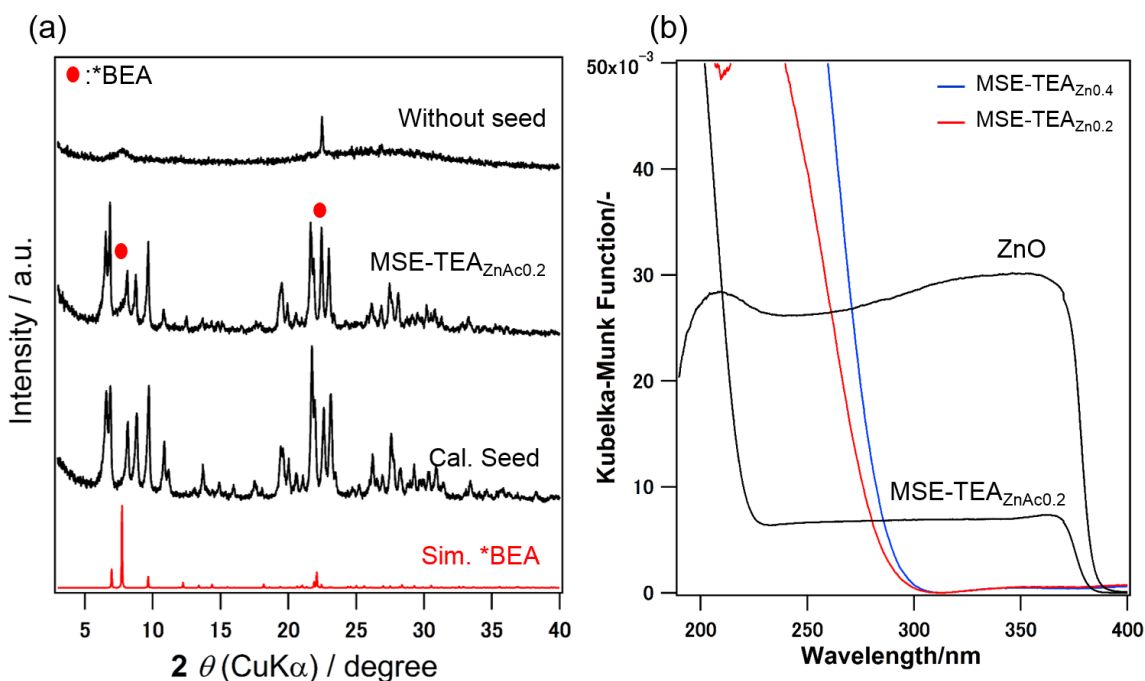


Figure 3.5 (a) The XRD pattern of MSE-TEA_{ZnAc0.2} and the sample prepared without seed crystals for comparison. (b) UV-Vis spectra of MSE-TEA_{ZnAc0.2} sample.

acetate and fumed silica showed ZnO formation during the synthesis (see Figure 3.5 (b)). As seen, the sample prepared without seed crystals also exhibited totally different results from MSE-TEA_{Zn0.2} sample since the absence of seed crystals led to the onset of *BEA instead of MSE nucleation from the same gel composition. Thus, it is worth to note that the combined use of the seed-directed method with co-precipitation gel technique on its own is an effective means of allowing the MSE-type zeolite as desired product with zinc content in a proper range.

Moreover, DR UV–Vis spectra were recorded in order to understand the coordination states of Zn species in the zincoaluminosilicate samples. Also, MSE-TEA, MCM-68 seed crystals, and proton form of MSE-TEA_{Zn0} (H-MSE-TEA_{Zn0}) were shown to be compared with. As depicted in Figure 3.6, the band corresponding to bulk ZnO

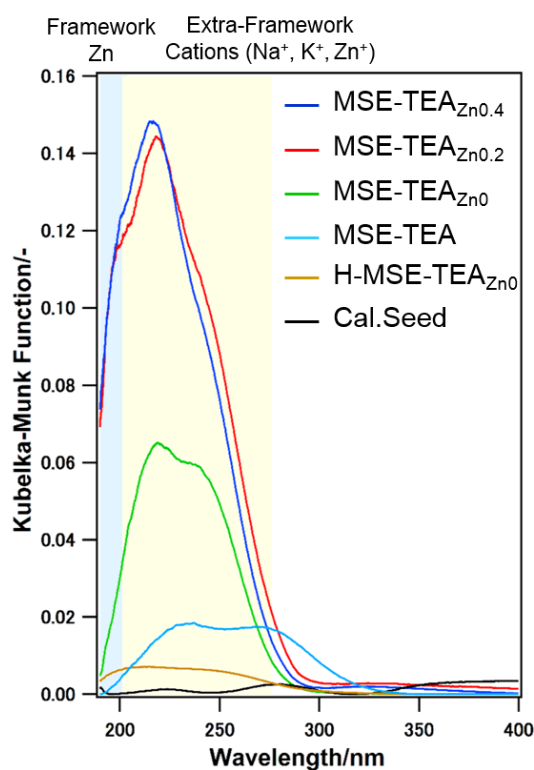


Figure 3.6 Diffuse reflectance UV–Vis spectra of as-synthesized MSE-TEA_{Zn0.4}, MSE-TEA_{Zn0.2}, MSE-TEA_{Zn0}, MSE-TEA, calcined MCM-68 seed crystals, and proton form of MSE-TEA_{Zn0} (H-MSE-TEA_{Zn0}).

cannot be found in the spectra of any as-synthesis samples, suggesting that the zinc species as either in isolated or ion-exchange positions. Both zincoaluminosilicate materials displayed a broad band in which an evident maximum absorption at 217 nm along with a shoulder around 197 nm, whereas MSE-TEA_{Zn0}, MSE-TEA, and MCM-68 seed crystals showed two maxima centered at ca. 224 and 240 nm. According to these results, the appearance of the shoulder below 200 nm is distinctive for the zincoaluminosilicate samples which might therefore be assigned to the framework zinc species. On the other hand, the bands observed between 200 and 280 nm can be attributed to the extraframework cations such as Na⁺, K⁺, and Zn²⁺ which are possibly in ion-exchange position since those peaks could be detected only slightly in the case of H-MSE-TEA_{Zn0} (Na/(Al+Zn) < 0.01 and K/(Al+Zn) < 0.02). Therefore, it can be assumed from these results, a certain amount of Zn species could be incorporated into MSE framework, although the exact states of Zn species cannot be understood in detail since absorptions of UV depends on many factors such as particle size and degree of hydration.^[29,30] Other evidence such as ion-exchange capacities for successful incorporation of zinc into zeolite framework will be discussed in the following section.

Aiming for removing the OSDA occluded into pores, calcination is applied to the samples synthesized using co-precipitated gels for a given period. As shown in Figure 3.7 (a), the crystallinity of MSE-TEA_{Zn0.4} sample slightly decreased after calcination compared to that of the as-synthesized sample, while MSE-TEA_{Zn0.2} exhibited highly crystalline MSE structure even after calcination. Moreover, the DR UV-Vis spectra of calcined MSE-TEA_{Zn0.4} sample figured a large band at visible region which is likely due to carbonaceous residues formed during calcination process, while MSE-TEA_{Zn0.2} sample exhibited almost similar bands even after the elimination of TEA⁺ (see Figure 3.7 (b)). Referring to the back, we mentioned that zinc containing zeolites demonstrates lower

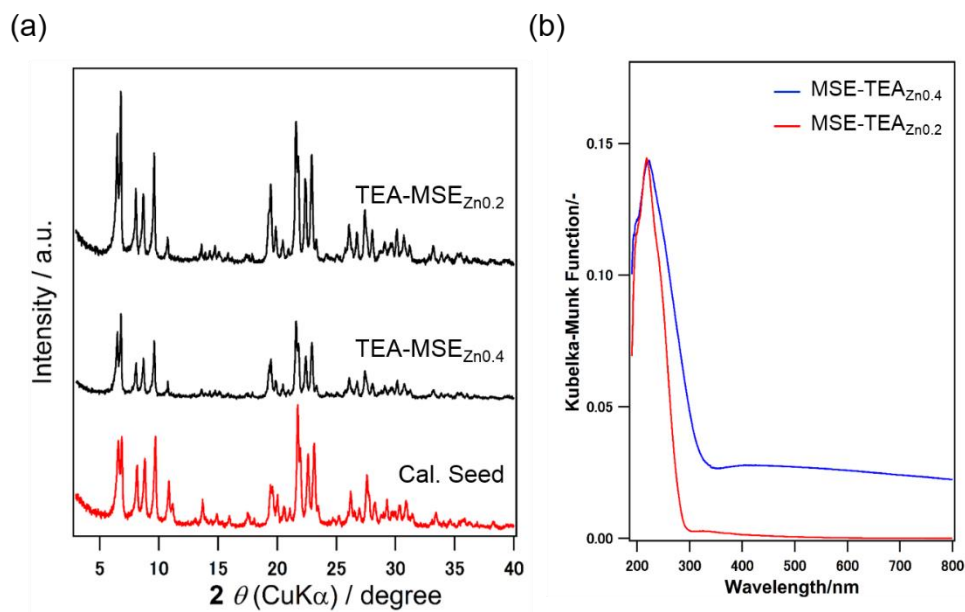


Figure 3.7 (a) The XRD pattern and (b) UV-Vis spectra of calcined MSE-TEA_{Zn0.2} and MSE-TEA_{Zn0.4}.

hydrothermal stability than those with aluminum in their frameworks. Therefore, these results suggested that a certain amount of Zn heteroatom is successfully inserted in the MSE framework as single site species since they would come out and form Zn–O–Zn extra-framework species after calcination. This might also be an indirect reason to claim the presence of Zn incorporation into MSE structure.

Chemisorption of Lewis basic molecules, pyridine, was applied to investigate the Lewis and Brønsted acidic properties of the prepared MSE samples through FTIR spectroscopy. The characteristic vibrational modes of pyridine coordinated to a Lewis acid sites and pyridinium ion generated from protonation of pyridine by a Brønsted acid sites allow identifying the presence of the two kinds of acid sites. Figure 3.8 compares pyridine adsorption onto MSE-TEA_{Zn0} and MSE-TEA_{Zn0.2}. In the IR bands, characteristic of pyridine interaction with Lewis acid sites (ca. 1450, 1490 and 1620 cm⁻¹, shown as ‘L’) and Brønsted acid sites (ca. 1490 and 1545 cm⁻¹, shown as ‘B’) are observed.^[31,32] The bands assigned to hydrogen bonded pyridine are also shown as ‘Py-H’. The bands at ca.

1490 cm^{-1} and 1545 cm^{-1} are generally used for the quantitative identification of Lewis acid sites and Brønsted acid sites, respectively.^[32] In the case of MSE-TEA_{Zn0}, characteristic band of the Brønsted acid sites (ca. 1547 cm^{-1}) and small band of the Lewis acid sites (ca. 1451 cm^{-1}) were observed. However, both bands, especially the bands correspond to Lewis acid sites, were not particularly seen after evacuation at high temperatures up to 300 °C. On the other hand, in the case of MSE-TEA_{Zn0.2}, significant band of Lewis acid sites (ca. 1451 cm^{-1}) was observed even after evacuation at up to 400 °C, together with small band characteristic of Brønsted acid sites. This result indicates

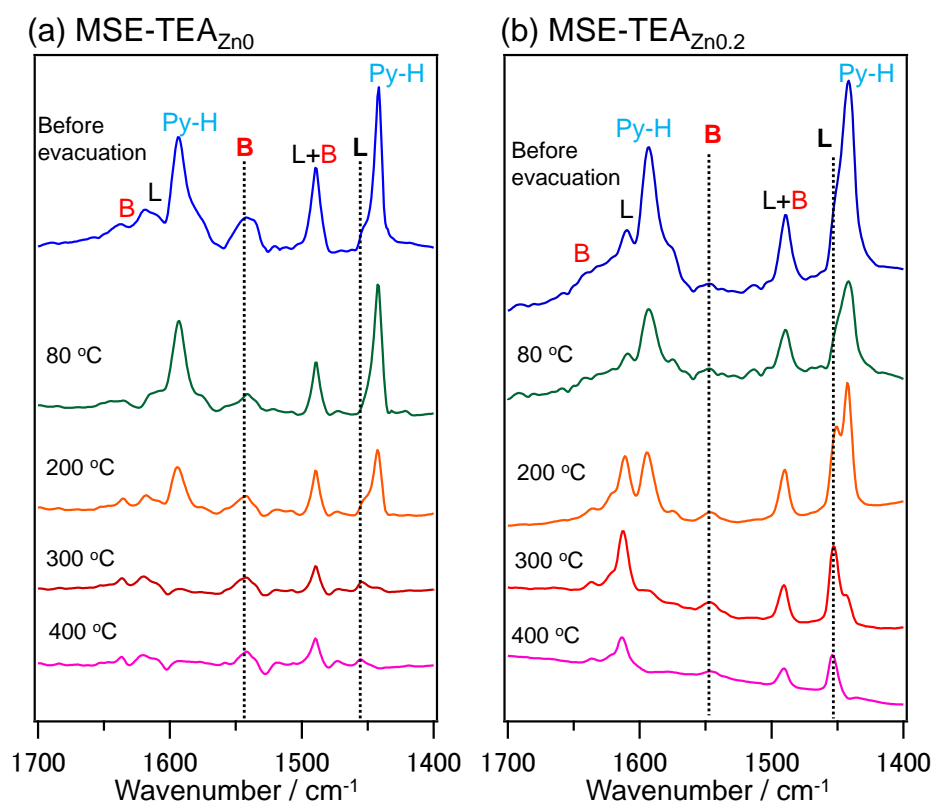


Figure 3.8 FTIR spectra of pyridine adsorbed on (a) MSE-TEA_{Zn0} and (b) MSE-TEA_{Zn0.2}. Peaks corresponding to pyridine coordinated to Lewis acid (L), Brønsted acid (B) sites and hydrogen bonded pyridine (Py-H) are marked. Blue: Spectra corrected at 80 °C before evacuation, Green: Spectra corrected after evacuation at 80 °C for 30 min, Orange: Spectra corrected after evacuation at 200 °C for 30 min, Red: Spectra corrected after evacuation at 300 °C for 30 min, Pink: Spectra corrected after evacuation at 400 °C for 30 min.

the presence of strong Lewis acid sites in the Zn-containing MSE sample, which is in consistent with the previous report.^[19]

3.3.4. Chemical and textural evaluation

The organic content of the samples prepared using co-precipitated gels was determined by using TGA analysis. As seen in Figure 3.9, the elimination of the occluded TEA⁺ is completed at around 700, 670, and 650 °C for MSE-TEA_{Zn0}, MSE-TEA_{Zn0.2}, and MSE-TEA_{Zn0.4} samples, respectively. It is previously reported that the occluded organic cation can be removed from zincosilicate framework at lower temperatures than that of aluminosilicates since the interaction between the cation and stepwise decrease in the elimination temperatures of TEA⁺ by increasing zinc content in the samples as another demonstrative for zinc insertion into MSE framework. Also, these zeolitic structure is weaker for the zincosilicate case.^[33] Thus, it can be assumed from the thermal data allow us to calculate the organic weight loss of MSE-TEA_{Zn0}, MSE-TEA_{Zn0.2}, and MSE-TEA_{Zn0.4} samples as about 16.1, 15.9, and 15.2 wt.%, respectively.

Further characterizations were performed on the successful MSE-TEA_{Znx}, MSE-TEA, and MCM-68 seed crystals with a view to examining the chemical compositions and microporosity. The results along with solid yield of those samples are summarized in Table 3.2. As seen, the obtained products synthesized from the co-precipitated gels by using TEAOH as OSDA had solid yield ranging between 31.6 and 57.5 wt.%. Regarding ICP-AES results, MSE-TEA_{Znx} series exhibited slightly lower Zn/(Zn+Al) molar ratio than that in their co-precipitated zincoaluminosilicate gels. Also, the Si/(Zn+Al) ratios of those samples decreased by increasing zinc content. Generally, it is speculated that the usage of a certain amount of Al in the synthesis gels is essential for direct crystallization of MSE-type zeolites.^[34] Even though YNU-2P was synthesized by steam-assisted crystallization (SAC) method as pure silica MSE-type material, it still

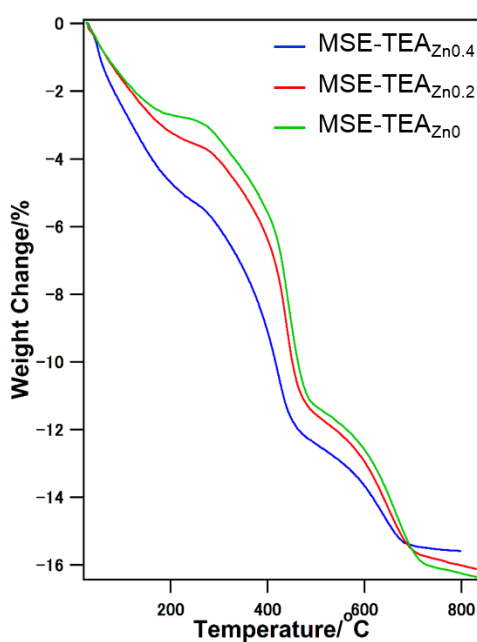


Figure 3.9 TGA patterns for MSE-TEA_{Zn0}, MSE-TEA_{Zn0.2} and MSE-TEA_{Zn0.4} samples.

requires some post-synthetic treatments to keep structure stable after calcination.^[35] Considering these points, the results suggested that the usage of homogenous heteroatom and aluminum source such as the co-precipitated gels is important to the insertion of a certain extent of heteroatom into MSE framework even by using TEAOH as OSDA. Moreover, the micropore volumes derived from a *t*-plot method of the calcined MSE-TEA_{Zn0}, MSE-TEA_{Zn0.2} are 0.19 and 0.18 cm³ g⁻¹, respectively. This means that MSE-TEA_{Zn0} and MSE-TEA_{Zn0.2} samples showed same value to that of calcined MCM-68 seed crystals (0.19 cm³ g⁻¹), suggesting a superior porosity of the products. Also, ICP-AES, TGA, and CHN elemental analysis data allow us to calculate the occluded OSDA per unit cell and Al for MSE-TEA_{Znx} samples as shown in Table 3.2. The results revealed that those samples prepared by using co-precipitated gels demonstrated decreasing OSDA/u.c. and OSDA/(Zn+Al) ratios by increasing the zinc content, even MSE-TEA_{Zn0} as aluminosilicate sample has lower those ratios compared to that of MSE-TEA. These results are likely because the increased incorporation of the Na⁺ and K⁺

Table 3.2 Summary of the chemical and textural features of prepared samples compared to MSE-TEA and seed crystals.

Sample	Zn/ (Zn+Al) ^a	Si/ (Zn+Al) ^a	Si/Zn ^a	Si/Al ^b	Na/ (Zn+Al) ^{a,b}	K/ (Zn+Al) ^{a,b}	OSDA/ (Zn+Al) ^c	(Na+K+OSDA)/ (Zn+Al) ^{a,b,c}	OSDA/ u.c ^c	Micropore volume (cm ³ g ⁻¹) ^f	Yield [wt.%] ^g
MSE-TEA _{Zn0.4}	0.28	6.86	24.2	9.56	0.6	0.4	0.4 ^d	1.4	5.9 ^d	-	57.5
MSE-TEA _{Zn0.2}	0.15	6.78	45.8	7.96	0.3	0.4	0.5 ^d	1.2	6.9 ^d	0.18	45.1
MSE-TEA _{Zn0}	0.0	6.98	∞	6.98	0.1	0.4	0.5 ^d	1.0	7.5 ^d	0.19	31.6
MSE-TEA	0.0	7.43	∞	7.43	0.2	0.2	0.6 ^d	1.0	8.1 ^d	0.21	43.6
Seed crystals	0.0	10.1	∞	10.1	0.0	0.4	0.5 ^e	0.9	5.0 ^e	0.19	-

^aSi, Zn and Al contents were quantified by ICP-AES. ^bNa and K measurements were carried out using AAS. ^cOSDA/(Zn+Al) and SDA⁺/u.c values were calculated from the ICP-AES, CHN and TGA results (u.c: unit cell of MSE consisting of 112 T-atoms). ^dThe SDA was TEA⁺. ^eThe SDA was TEBOP²⁺. ^fCalculated by *t*-plot method. ^gThe calculation of the solid yield was based on the oxides (excluding TEAOH and H₂O).

which were located along with TEA⁺ in the channels and super cage of the MSE structures, and balanced with anionic sites of the product framework. Regarding these results, it can be suggested that TEA⁺ may act as pore fillers rather than which were located along with TEA⁺ in the channels and super cage of the MSE structure-directing agents to stabilize the MSE structure. Moreover, Raman spectroscopy is applied to explore the possible influence of framework heteroatoms on the conformer distribution in the MSE cavities depending on the different framework element. The Raman spectra of MSE-TEA_{Zn0.4} and MSE-TEA_{Zn0.2} as zincoaluminosilicate and MSE-TEA_{Zn0} as aluminosilicate samples revealed that only *tt*.*tt* conformers of TEA⁺ are found in the MSE structure regardless the framework element, meaning that the conformational arrangement happened in the MSE-TEA structure with the intent of pore-filling considerations.

Moreover, in order to understand the zinc distribution in this newly grown MSE structure, ICP-AES and XPS results were compared as shown in Table 3.3. The accuracy of XPS confirmed by applying to seed crystals which presented almost similar results on their surface and bulk structure. However, in the case of zincoaluminosilicate sample, the surface showed higher zinc content compared to its bulk results. This result significantly indicates core-shell crystal growth for MSE-type zeolites, where shell was newly grown

Table 3.3 The comparison of chemical compositions of zincoaluminosilicate MSE sample and seed crystals by applying ICP-AES and XPS analysis.

	MSE-TEA _{Zn0.2}				Seeds			
	Si/ (Zn+Al)	Zn/ (Zn+Al)	Si/ Zn	Si/ Al	Si/ Al	Zn/ (Zn+Al)	Si/ (Zn+Al)	Si/ Zn
ICP-AES	6.78	0.15	45.8	7.96	10.1	-	10.1	∞
XPS	6.93	0.20	34.1	8.70	9.23	-	9.23	∞

zincoaluminosilicate structure, while the core was partially dissolved aluminosilicate seed crystals surface.

3.3.5. Ion-exchange characteristics

As aforementioned, the zinc containing zeolites synthesized in the presence of alkali cations might consist of two different zinc sites.^[19] The first one of those sites can generate only one anionic charge for each Zn atom as shown in Figure 3.10 (a), meaning that the anionic charge can be balanced with only one monocation (M^+) as Al atom in aluminosilicates. On the other hand, the second one creates two anionic charges per framework Zn atom to balance with two M^+ ions (see Figure 3.10 (b)). Therefore, the identification of the zinc species inserted into MSE framework is crucial for the obtained samples. Theoretically, if all zinc species in the framework exhibits the features of the first anionic site, M^+ per zinc ratio (M^+/Zn) should be 1. Otherwise, if framework Zn atoms behave as the second site, the M^+/Zn ratio should be 2. As shown in Table 3.2, the total sum of the balanced inorganic and organic monocation ratio to $(Zn+Al)$ is 1.0 for only aluminosilicate samples, while the samples with zinc content have a higher value than 1.0, and the ratio was getting higher by increasing incorporated Zn ratio. This result confirmed that zinc as heteroatom could be incorporated into MSE structure. Also, the calculated $(Na+K+OSDA)/(Zn+Al)$ ratios of MSE-TEA_{Zn0.2}, and MSE-TEA_{Zn0.4} samples

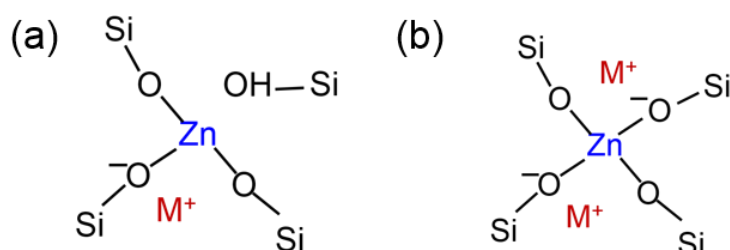


Figure 3.10 Possible zinc sites in zincoaluminosilicate MSE framework. Monovalent cations are described as M^+ which can be Na^+ , K^+ , and TEA^+ .

are respectively 1.2 and 1.4, suggesting that the most of the zinc species created two anionic charges in the framework.

Therefore, the divalent-cation exchange capacity of MSE-TEA_{Zn0} and MSE-TEA_{Zn0.2} samples were estimated by using nickel (Ni²⁺). As shown in Table 3.4, 0.5Ni/(Zn+Al) ratio of MSE-TEA_{Zn0.2} sample as 1.23 was higher than that of MSE-TEA_{Zn0} aluminosilicate sample (1.00), supposing that some of the zinc species inserted into MSE framework created two anionic charges, which can be suitable exchange sites for divalent-cations. Furthermore, noteworthy, the Si/(Zn+Al) ratio of the samples remained same even after cation exchange, suggesting high stability of framework Zn and/or absence of extra framework zinc species. Based on these results, MSE-TEA_{Zn0.2} sample can be proposed as a potential ion-exchangers for divalent-cations.

Table 3.4 Multivalent Ni²⁺ cations exchange capacity of the prepared samples.

Sample	Si/ (Zn+Al) ^a	Zn/ (Zn+Al) ^a	0.5 Ni/(Zn+Al) ^a
MSE-TEA _{Zn0.2}	6.78	0.15	1.23
MSE-TEA _{Zn0}	6.98	0.0	1.00

^aSi, Al, Zn and Ni measurements were carried out using ICP-AES.

3.4. Conclusion

This report reveals the successful enlargement of the rational seed-directed synthesis method from aluminosilicate to zincoaluminosilicate MSE-type zeolites by combining with the co-precipitated gel technique. The concept described herein is illustrated in Figure 3.10. Indeed, this is the first report for a direct crystallization of a medium and large pore zeolite with a certain amount of zinc content in its framework, so far. It should be pointed that the usage of co-precipitated gels is one of the critical factors to obtain pure products from the given gel compositions since those gels provide homogeneously dispersed zinc and aluminum species which can easily form a zeolitic framework. The physicochemical analysis of the products resulted that highly crystalline MSE structure could be obtained from the gels containing $Zn/(Zn+Al)$ ratios up to 0.4. As a notable exception of MSE-TEA_{Zn0.2} among those zincoaluminosilicate samples exhibited high stability against thermal treatment. The further characterizations of those samples confirmed that most of the zinc species are located in the MSE structure. The ion-exchange characteristics of MSE-TEA_{Zn0} and MSE-TEA_{Zn0.2} samples were identified from the balanced monocations ratios per zinc and aluminum. Additionally, the Ni²⁺ exchange results revealed the potential of their usage as divalent-cation exchangers. Based on overall results, it is demonstrated herein that the simplified synthesis path is

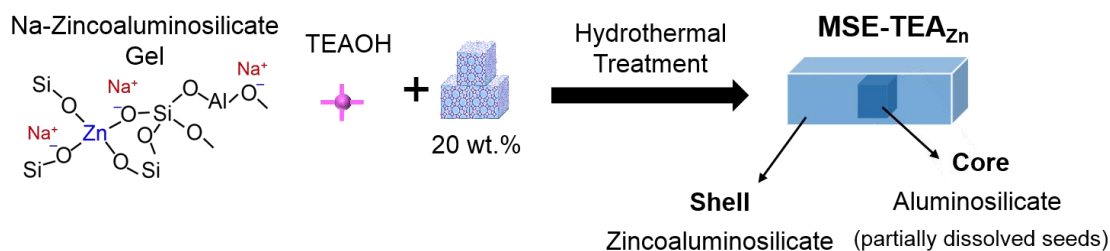


Figure 3.11 The illustration for the concept described in Chapter 3.

very effective alternative way to synthesize multipore zeolites containing medium and large pores in the frameworks with different heteroatoms.

3.5. References

- [1] C. Y. Chen, S. I. Zones, *Stud. Surf. Sci. Catal.* 135 (2001) 171.
- [2] C. B. Dartt, M. E. Davis, *Appl. Catal. A.* 143 (1996) 53–73.
- [3] Y. Kubota, Y. Koyama, T. Yamada, S. Inagaki, T. Tatsumi, *Chem. Commun.* (2008) 6224–6226.
- [4] M. Moliner, A. Corma, *Microporous Mesoporous Mater.* 164 (2012) 44–48.
- [5] M. Moliner, C. Martínez, A. Corma, *Angew. Chem. Int. Ed.* 54 (2015) 3560–3579.
- [6] C. Baerlocher, W. M. Meier, D. H. Olson, *Atlas of Zeolite Framework Types*; sixth ed.; Elsevier, Amsterdam, 2007.
- [7] N. Žilková, M. Bejblová, B. Gil, S. I. Zones, A.W. Burton, C.-Y. Chen, M. Musilová-Pavlavčková, G. Košová, J. Čějka, *J. Catal.* 266 (2009) 79–91.
- [8] B. Gil, G. Košová, J. Čějka, *Microporous Mesoporous Mater.* 129 (2010) 256–266.
- [9] T. Shibata, S. Suziki, H. Kawagoe, K. Komura, Y. Kubota, Y. Sugi, Kim, G. Seo, *Microporous Mesoporous Mater.* 116 (2008) 216–226.
- [10] T. Shibata, N. H. Kawagoe, K. Komura, Y. Kubota, Y. Sugi, *J. Mol. Catal. A: Chem.* 297 (2009) 80–85.
- [11] S. Inagaki, K. Takechi, Y. Kubota, *Chem. Commun.* 46 (2010) 2662–2664.
- [12] Y. Koyama, T. Ikeda, T. Tatsumi, Y. Kubota, *Angew. Chem. Int. Ed.* 47 (2008) 1042–1046.
- [13] M. Moliner, *Dalton Trans.* 43 (2014) 4197–4208.
- [14] H. Y. Luo, J. D. Lewis, Y. Roman-Leshkov, *Annu. Rev. Chem. Biomol. Eng. Volume. 7* (2016) 663–692.
- [15] P. Y. Dapsens, C. Mondelli, J. Perez-Ramírez, *Chem. Soc. Rev.* 44 (2015), 7025–7043.
- [15] J. Penzien, A. Abraham, J. A. van Bokhoven, A. Jentys, T. E. Müller, C. Sievers, J. A. Lercher, *J. Phys. Chem. B* 108 (2004) 4116–4126.
- [16] X. Collard, P. Louette, S. Fiorillic, C. Aprile, *Phys. Chem.* 17 (2015) 26756–26765.
- [17] M. A. Deimund, J. Labinger, M. E. Davis, *ACS Catal.* 4 (2014) 4189–4195.
- [18] X. Collarda, P. Louette, S. Fiorillic, C. Aprile, *Phys. Chem. Chem. Phys.* 17 (2015) 26756–26765.
- [19] M. Orazov, Mark E. Davis, *Chem. Sci.* 7 (2016) 2264–2274.
- [20] J.L. Guth, H. Kessler, R. Wey, *New Developments in zeolite science and technology*, in: Y. Murakami, A. Lijima, J. W. Ward (Eds.), *Studies in Surface Science Catalysis*, vol. 28, Elsevier,

Amsterdam, 1986, pp 121.

- [21] M. Dong, J. Wang, Y. Sun, *Microporous Mesoporous Mater.* 43 (2001) 237–243.
- [22] M. J. Dusselier, M. E. Davis, US 20160243531 A1, August 25, 2016.
- [23] N. Koike, S. P. Elangovan, K. Itabashi, JP 2016-200613, 2016.
- [24] S. Sogukkanli, K. Iyoki, S. P. Elangovan, K. Itabashi, M. Takano, Z. Liu, S. Inagaki, T. Wakihara, Y. Kubota, T. Okubo, *Microporous Mesoporous Mater.* 245 (2017) 1–7.
- [25] S. Inagaki, K. Takechi, Y. Kubota, *Chem. Commun.* 46 (2010) 2662–2664.
- [26] C. Cristiani, P. Forzatti, *J. Chem. Soc. Faraday Trans.* 85 (1989) 895–906.
- [27] S. Bordiga, C. Lamberti, G. Ricchiardi, L. Regli, F. Bonino, A. Damin, K.-P. Lillerud, M. Bjorgen, A. Zecchina, *Chem. Commun.* (2004) 2300–2301.
- [28] T. Yokoi, M. Yoshioka, H. Imai, T. Tatsumi, *Angew. Chem. Int. Ed.* 48 (2009) 9884–9887.
- [29] Y. Ni, A. Sun, X. Wu, G. Hai, J. Hu, T. Li, G. Li, *Microporous Mesoporous Mater.* 143 (2011) 435–442.
- [30] M. Yoshikawa, S. L. Zones, M. E. Davis, *Microporous Mesoporous Mater.* 11 (1997) 137–148.
- [31] J.C. Lavalley, *Cat. Today* 27 (1996) 377–401.
- [32] S. W. Choi, W. G. Kim, J. S. So, J. S. Moore, Y. Liu, R. S. Dixit, J. G. Pendergast, C. Sievers, D. S. Sholl, S. Nair, C. W. Jones, *J. Cat.* 345 (2017) 113–123.
- [33] T. Takewaki, L. W. Beck and M. E. Davis, *Topics in Catalysis* 9 (1999) 35–42.
- [34] Y. Kubota, S. Inagaki, *Topics in Catalysis* 58 (2015) 480–493.
- [35] Y. Koyama, T. Ikeda, T. Tatsumi, Y. Kubota, *Angew. Chem. Int. Ed.* 47 (2008) 1042–1046.

Chapter 4. Synthesis of Aluminoborosilicate CON-type Zeolites

4.1. Introduction

CIT-1 is the first reported pure CON-type borosilicate zeolite with intersecting $12 \times 12 \times 10$ -R channels system. The zeolite has molecular access to the crystal interior through 10 ($5.1 \text{ \AA} \times 5.1 \text{ \AA}$) and 12-R ($6.4 \text{ \AA} \times 7.0 \text{ \AA}$) pores, which are also connected to form a large void at intersections as shown in Figure 4.1.^[1-3] Because of its structure providing high accessibility and stability, CIT-1 is found to exhibit unique catalytic activities in hydrocarbon conversion reactions.^[4-6] Also, the existence of strong Brønsted acid sites in its channels provides a specific cracking behavior which makes the zeolite an attractive component for the fluid catalytic cracking (FCC) process.^[7,8] Additionally, its potential use as hydrocarbon trap^[9] was discovered by replacing

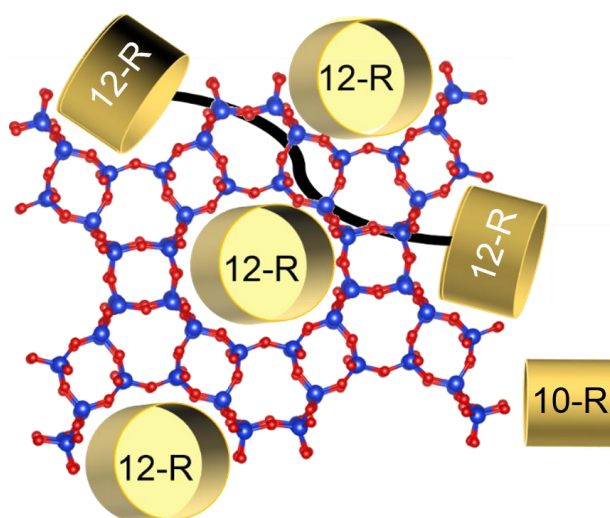


Figure 4.1 Illustration of CON structure with intersecting $12 \times 12 \times 10$ -R channels system.

boron as a framework element with aluminum via post-synthetic treatments.^[1,2] More recently, the direct preparation of aluminum containing CON-type borosilicate zeolite could be also achieved by developing a novel synthesis path.^[10] Indeed, the Al insertion in CON framework by either post-synthetic or direct methods opened a new door for the zeolite to be utilized as catalyst for methanol to olefin (MTO) reaction,^[11,12] in which the directly synthesized one exhibited superior performance compared with post-synthetic one, zeolite beta, and ZSM-5 in terms of duration and propene selectivity.^[10] Despite those attractive capabilities of the CIT-1, the actual challenge, as Corma pointed in 1997,^[8] is to synthesize the material by a method inexpensive enough to make it feasible for its usage in all above-mentioned applications.

The conventional synthesis of either aluminoborosilicate or borosilicate CIT-1 requires using a specially designed, expensive OSDA which is named as *N,N,N*-Trimethyl(-)-cis-myrtanylammmonium hydroxide (TMMAOH).^[1,2] As referred to back, the necessity of using such complex OSDAs in the synthesis of multipore zeolites is a significant hurdle for their practical applications. Even though some attempts have been made on simplifying the synthesis route for CIT-1, none of them seem to get ahead yet. On the contrary, the obtained results have been strongly implied that TMMA⁺ cation, as well as boron as framework element play strong structure-directing roles in the crystallization of CON-type zeolites.^[10]

Hereupon, we have attempted to develop a simple and low-cost production method for aluminoborosilicate CON-type zeolites using less expensive OSDA instead of conventional TMMAOH. For this objective, the proposed rational synthesis method for MSE-type zeolites is modified to suppress undesired product formation and make CON crystal growth favorable. Considering the extended CBU hypothesis,^[13] it is found that CON structure shares common CBUs with *BEA and MFI (see Figure 4.2) which

are traditionally synthesized by using simple quaternary ammoniums such as TEOH and TPAOH as OSDAs, respectively. In the literature, it is also reported that MFI structure can be directed from the synthesis gels containing TEOH.^[14] Based on these results, it is assumed that TEOH can be a candidate to apply in the simplified synthesis of CON-type zeolites. However, when TEOH is utilized as OSDA in the aluminosilicate gels, zeolite beta is mostly obtained under very broad synthesis conditions.^[15] Therefore, in order to reverse the dominant role of TEOH in nucleation of *BEA versus CON, we started modifying our rational synthesis by introducing boron, then tuning reaction composition and controlling kinetics. By applying this strategy, we herein present the first success on the simplified synthesis of aluminoborosilicate CON-type zeolites, in which as-synthesized borosilicate CIT-1 seeds, TEOH, and Na-K balance play critical roles for phase selectivity.

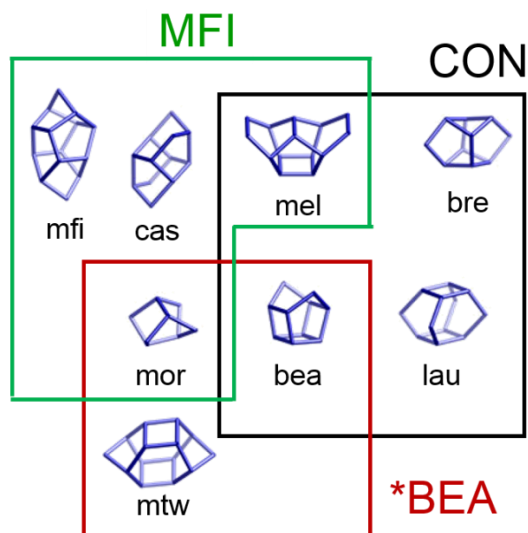


Figure 4.2 The correlation of the common composite building units between CON, *BEA, and MFI structures.

4.2. Experimental section

4.2.1. Materials

The following commercially available raw materials for boron beta seed, boron CIT-1 seed, aluminoborosilicate CON-type zeolite synthesis were used as provided: colloidal silica (Ludox[®] AS-40, 40 wt.% in water, DuPont) and fumed silica (Cab-O-Sil[®] M5, Cabot) as silicon sources; sodium tetraborate decahydrate ($\text{Na}_2\text{B}_4\text{O}_7 \cdot 10\text{H}_2\text{O}$, Wako) and boric acid ($\text{B}(\text{OH})_3$, Wako and Sigma Aldrich) as boron sources; aluminum hydroxide ($\text{Al}(\text{OH})_3$, Sigma Aldrich) as aluminum source; potassium hydroxide (KOH, 50 wt.% in water, Wako) and sodium hydroxide solution (NaOH, 50 w/v% in water, Wako); tetraethylammonium hydroxide solution (TEAOH, 35 wt.% in water, Aldrich) as the OSDA; and deionized water. Additionally, TMMAOH was prepared to be used as an OSDA for boron CIT-1 seed synthesis from the following chemicals: (-)-*cis*-myrtanylamine (98 wt% in water, Sigma Aldrich), iodomethane (JIS Special Grade, Wako), potassium carbonate (K_2CO_3 , Wako), tetrahydrofuran (THF, JIS Special Grade, Wako), chloroform (JIS Special Grade, Wako), and methanol (JIS Special Grade, Wako).

4.2.2. Preparation of *N,N,N*-Trimethyl(-)-*cis*-myrtanylammmonium as organic structure directing agent

According to a previous report,^[2] the typical synthesis of *N,N,N*-Trimethyl(-)-*cis*-myrtanylammmonium is carried out as follows: 10 g of (-)-*cis*-myrtanylamine((1*S*)-[1 α ,2 β ,5 α]-2-methanamine-6,6-dimethylbicyclo[3.1.1]heptane) was dissolved in 100 mL methanol, then 27 g of K_2CO_3 and 55 g of methyl iodide were added into this solution. The mixture was stirred for overnight at room temperature in the absence of light. Later, the reaction mixture was filtered, and the solid filtrate was

washed with additional 50 mL of methanol to remove unreacted K_2CO_3 . In order to separate the methanol from the solid material, the combined solution was heated at 50 °C by using evaporator. A white solid was formed in the flask which is then extracted with 2 portions each of 100 mL of chloroform. The combined chloroform solution which contains trimethylmyrtanylammonium were filtered again and were heated in an evaporator until the chloroform was evaporated. Generally, a very viscous oily liquid was obtained after the evaporation of chloroform. In this case, the ammonium salt can be easily recrystallized by the addition of 50 mL of diethyl ether. After the solid was formed, the crystals were washed with 200 mL of additional ether. Then, the ether was allowed to be evaporated from the solid at room temperature in a hood. Later, the recovered solids were recrystallized from a 9:1 tetrahydrofuran/methanol solution, approximately 17 g white crystals of *N,N,N*-Trimethyl-(–)-cis-myrtanylammonium iodide were recovered. The ^{13}C NMR of this iodide salt is: ^{13}C NMR $\delta = 23.2, 23.7, 25.6, 27.2, 31.5, 35.6, 38.2, 40.2, 47.6, 53.8, 76.9$ ppm. Finally, ion exchange was accomplished from iodide form to hydroxide.

4.2.3. Synthesis of borosilicate beta seed crystals

The synthesis of borosilicate beta zeolite was performed by using the general dry gel technique as previously reported.^[11,12] In a typical synthesis procedure, the prepared gel with the molar composition was $1.0SiO_2: 0.033B_2O_3: 0.056NaOH: 1.0$ TEAOH. First, an appropriate amount of TEAOH was mixed with colloidal silica under continuous stirring, and was further stirred for 10 min. Then, NaOH was added in this mixture, and continued stirring for extra 30 min. Meanwhile, sodium tetraborate decahydrate was dissolved in a certain amount of deionized, distilled water, then added into the above mixture. The final mixture was further stirred for 2h. Then the gel was dried at 80 °C by using a hot plate with continuous stirring, allowing evaporation of

water. When the gel became thick and viscous, it was homogenized by hand using a teflon rod until it dried. After formation of white solid, it was ground into a fine powder, and the powder was poured into a small teflon cup (20 mm × 20 mm). Later, this teflon cup was placed in a Teflon-lined autoclave (No. 4749, Parr Instrument) which had 0.25 g water as the source of steam to avoid direct contact between gel and water. The crystallization of the dry gel was carried out at 175 °C for 96 hours in autogenous pressure. After the crystallization was over, the solid products could be recovered by consecutively washing with deionized water, centrifuging, and drying at 80 °C for overnight.

4.2.4. Synthesis of borosilicate CIT-1 seed crystals

CIT-1 seed crystals were synthesized according to a previous report^[2] from a gel with the following composition: 1.0SiO₂: 0.02B₂O₃: 0.12NaOH: 0.24TMMAOH: 60H₂O. First, sodium tetraborate decahydrate, NaOH, and TMMAOH were dissolved in distilled water under stirring for 30 min. Then, fumed silica was added into this solution, and the mixture was further stirred to homogenize for 6 hours. Later, as-synthesized either borosilicate or aluminosilicate beta seed crystals using 1 wt% respect to the initial silica weight were added in this gel, and stirred for additional 15 min. Lastly, the obtained gel was placed in a 125 mL Teflon[®]-lined autoclave (No. 4749, Parr Instrument) and maintained at 160 °C for 12 days in a convection oven. After the hydrothermal treatment, the solution was cooled to room temperature and the solid products were separated by centrifugation, washed with deionized water several times, and finally dried at 80 °C overnight. In order to remove the OSDA occluded in the pores, the as-synthesized CIT-1 was heated to 650 °C at a rate of 5 K min⁻¹ and maintained at this temperature for 4 h.

4.2.5. Synthesis of aluminoborosilicate CON-type zeolites using tetraethylammonium hydroxide as an organic structure-directing agent

The initial gels for the synthesis of CON-type zeolites (i.e., CON-TEA) using TEAOH as an OSDA were prepared with using $\text{Al}(\text{OH})_3$, $\text{B}(\text{OH})_3$, NaOH, KOH, and TEAOH solutions and fumed silica. In a typical synthesis, aluminum hydroxide and boric acid powder was dissolved in an aqueous alkali solution under stirring for ca. 30 min, and fumed silica was subsequently added slowly. The resulting mixture was homogenized under stirring for additional 6 hours. The starting gel had the following molar ratios: 1.0SiO_2 : $x\text{Al}(\text{OH})_3$: $y\text{B}(\text{OH})_3$: $z(\text{KOH}+\text{NaOH})$: 0.22TEAOH : $60\text{H}_2\text{O}$ (where $x = 0-0.04$, $y = 0-0.04$, $z = 0-1.0$, and the $\text{KOH}/(\text{KOH}+\text{NaOH})$ ratio ranged from 0 to 1.0). After proper homogenization, as-synthesized either borosilicate or aluminosilicate CIT-1 seed crystals (from 0 to 20 wt.% relative to the silica source) were added into the synthesis gel, and continued stirring for extra 30 min. Thereafter, this synthesis mixture was transferred to a 23 mL Teflon[®]-lined stainless steel autoclave (No. 4749, Parr Instrument), which was hydrothermally treated at 160 °C for 168 h under static conditions in a preheated air circulated oven. After the prescribed synthesis time, the solid products were centrifuged and subsequently washed with distilled water until the filtrate pH became neutral. Recovered products were dried at 80 °C overnight. In order to obtain the calcined powder, the as-synthesized product was heated at 550 °C for 10 h under flowing dry air. The solid yield of the obtained zeolite was described as the weight ratio percentage ($\text{g/g} \times 100$) of the solid product to the silica in the starting gel. Relative crystallinities were calculated based on the ratio of the area of the five peaks in the

the X-Ray diffraction (2 theta ca. 20.52, 21.54, 22.12, 23.02, and 23.18) for solid products to those of seed crystals.

4.2.6. Characterization

Powder X-Ray diffraction (XRD) patterns were recorded on a Rigaku Ultima IV diffractometer using CuK α radiation with a D/Tex Ultra detector ($\lambda = 0.015406$ nm, 40 kV, 40 mA). The amounts of silicon and aluminum in the products were measured on a Thermo Scientific iCAP-6300 inductively coupled plasma-atomic emission spectrometer (ICP-AES) system after dissolving the products in a potassium hydroxide solution. Additionally, a Hitachi Z-2000 atomic absorption spectrometer equipped with a heated graphite tube atomizer was used for the determination of sodium and potassium after dissolving them in hydrofluoric acid. Na and K hollow cathode lamps operating at 6.5 mA were used as the radiation sources. CHN elemental analyses were carried out on a CE-440 elemental analyzer (Exeter Analytical). Thermogravimetric and differential thermal analysis (TG-DTA) were performed on a Rigaku Thermo plus TG 8120 from 30 to 800 °C at a heating rate of 10 K min⁻¹ under a flow (200 mL min⁻¹) of 10% O₂/90% He gas mixture. Raman spectra of the solid products were collected on a device NRS-5100 (JASCO) by using a 532 nm laser. Nitrogen adsorption-desorption isotherms of the calcined samples were obtained on an Autosorb-iQ2-MP instrument (Quantachrome Instruments) at liquid nitrogen temperature. The crystal sizes and morphologies of the obtained products were observed on a JSM-7500FA (JEOL) field emission scanning electron microscope (FE-SEM) after Os coating over the powder samples on the carbon tape.

4.3. Result and discussion

4.3.1. Chemical and textural evaluation

The synthesis of CON-type zeolites by using TEAOH as a simple OSDA was performed from the modified rational synthesis conditions and gel composition to promote the crystal growth of CON phase. As it mentioned previously boron is one of the key factors for successful synthesis of CON-type zeolites. Since borosilicate zeolites are well-known with their low hydrothermal stabilities compared to aluminosilicates,^[16] we applied as-synthesized borosilicate CIT-1 seed crystals (amount of seed crystals was 20 wt% relative to silica source) instead of calcined ones to prevent complete dissolution of the seed-crystals and to provide more growth surface during crystallization. In order to reach the successful gel composition, the boron is first introduced into the rational synthesis, which has the gel composition of 1SiO_2 : $x\text{B}(\text{OH})_3$: $y\text{Al}(\text{OH})_3$: 0.125KOH : 0.375NaOH : 0.22TEAOH : $15\text{H}_2\text{O}$. As shown in Figure 4.3(a), the synthesis gels containing different $\text{B}/\text{Si} = x$ and $\text{Al}/\text{Si} = y$ ratios resulted great alteration in the product from zeolite beta to alpha quartz by increasing boron content in the gel composition, suggesting ineligible conditions for crystal growth for any type of zeolites. This made us consider the typical synthesis of aluminoborosilicate CIT-1 which requires using the gels with high boron ($\text{B}/\text{Si} = 13\text{--}50$, $\text{Al}/\text{Si} = 100\text{--}200$) and water contents ($\text{H}_2\text{O}/\text{Si} = 60$) to be applied under wide ranging synthesis conditions.^[10] However, when the water content in the reaction gel ($\text{B}/\text{Si} = 0.04$) increased, the nucleation of kenyaite (layered silica) is observed from amorphous matter along with a minor amount of remaining CIT-1 seed crystals (see Figure 4.3 (b)). In fact, kenyaite may occur from the gels containing less alkalinity under long hydrothermal treatment. As shown in Figure 4.4 (a), we applied the same gel composition without preheating,

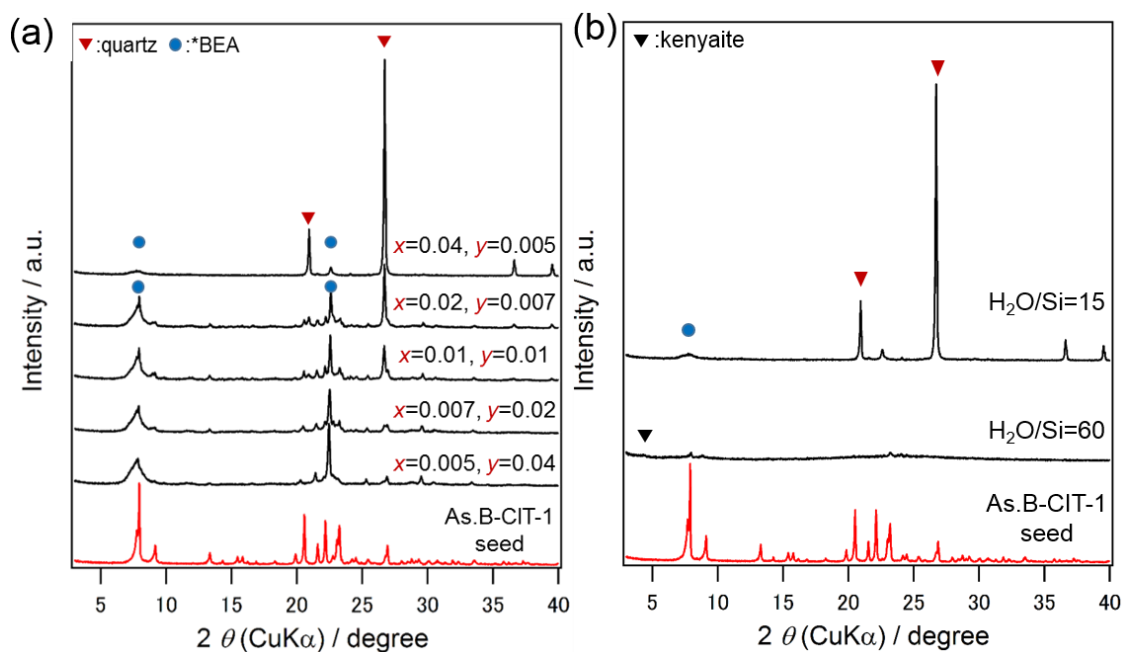


Figure 4.3 XRD patterns of the products synthesized from the rational synthesis gels with different boron and aluminum contents.

which resulted the formation of zeolite beta besides remaining seed crystals. Although not the entire synthesis conditions were affected by the preheating, we also adjusted the alkalinity of the gels. By doing this, highly crystalline pure CON-phase (CON-TEA-1) with a solid yield of 28 wt. % is preferentially formed from the synthesis gels containing high alkalinity. On the other hand, the products prepared from gels with lower alkalinity were contaminated by either *BEA or kenyaite structures, suggesting that strong alkalinity is necessary to enhance the crystallization of CON structure. Moreover, the successful synthesis of CON-TEA product could be done by varying the $\text{Si}/(\text{Al}+\text{B})$, $(\text{KOH}+\text{NaOH})/\text{Si}$, and $\text{KOH}/(\text{KOH}+\text{NaOH})$ ratios. Furthermore, the SEM images revealed that CON-TEA-1 sample is composed of aggregated wide-width crystals (Figure 4.4 (b)) which indicate alteration in the crystal shape compared to seed-crystals of acute-square prisms (Figure 4.4 (c)), showing the crystal growth proceeded on the partially dissolved seed crystals, as it is well-recognized for seed-directed synthesis.^[17]

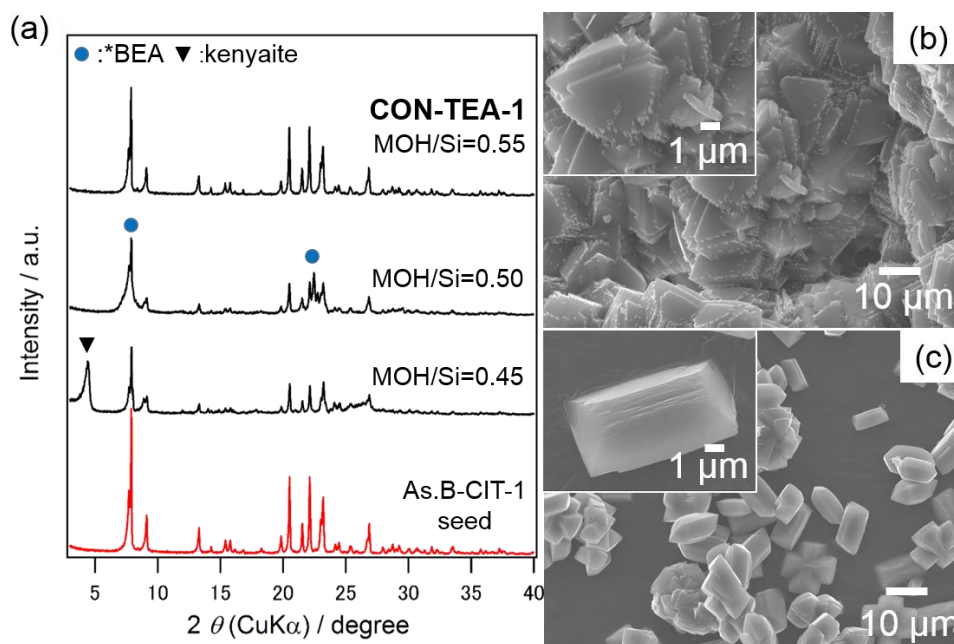


Figure 4.4 (a) Powder XRD patterns of the samples containing different MOH/SiO₂ ratios. FE-SEM images of: (b) CON-TEA-1, (c) as-synthesized B-CIT-1 seed crystals.

It is worth noting that the highly-crystalline, the pure product could be obtained from the gel containing both K⁺ and Na⁺ in an exact KOH/(KOH+NaOH) ratio of 0.25, while typical synthesis mixture of CIT-1 contains only Na⁺ as an alkaline metal cation. Therefore, it can be assumed that the rational synthesis of CON-type zeolites might require a mixture of alkaline sources to prevent the formation of byproducts and promote crystal growth of the target material.

Although significant changes in synthesis conditions including gel compositions have been done, increasing the obtained yield could not be successful from the system mentioned up to this point. As it is reported in various papers,^[19,20] the presence of seed crystals in synthesis media eliminates the induction period, and allows to go through the secondary nucleation via the initial breeding mechanism. Also, it is claimed that the size of seed crystals significantly influences the formation of secondary nuclei, since small seed crystals provide large surfaces for the newly growing crystals. As shown in Figure

4.5 (a), highly crystalline small borosilicate CIT-1 crystals ca. 2 μ m could be obtained by applying as-synthesized aluminosilicate beta seed crystals instead of borosilicate in the same synthesis composition of conventional CIT-1. By applying those crystals in the rational synthesis, a pure CON-TEA-2 product with a max. solid yield of 36 wt. % could be obtained, indicating smaller seed crystals provides more surface for crystal growth (see Figure 4.5. (b)). In order to study the role of the seed crystals and OSDA in the synthesis, some experiments were carried out. Figure 4.5 (c) displays the XRD patterns of the samples prepared with as-synthesized seed amounts lower than 20 wt.% (based on silica amount) and calcined seed crystals. As shown here, low amount of seeding to the synthesis gels resulted low crystalline CON-TEA products along with amorphous matter which increases by decreasing the additive seed amount. These results indicate that

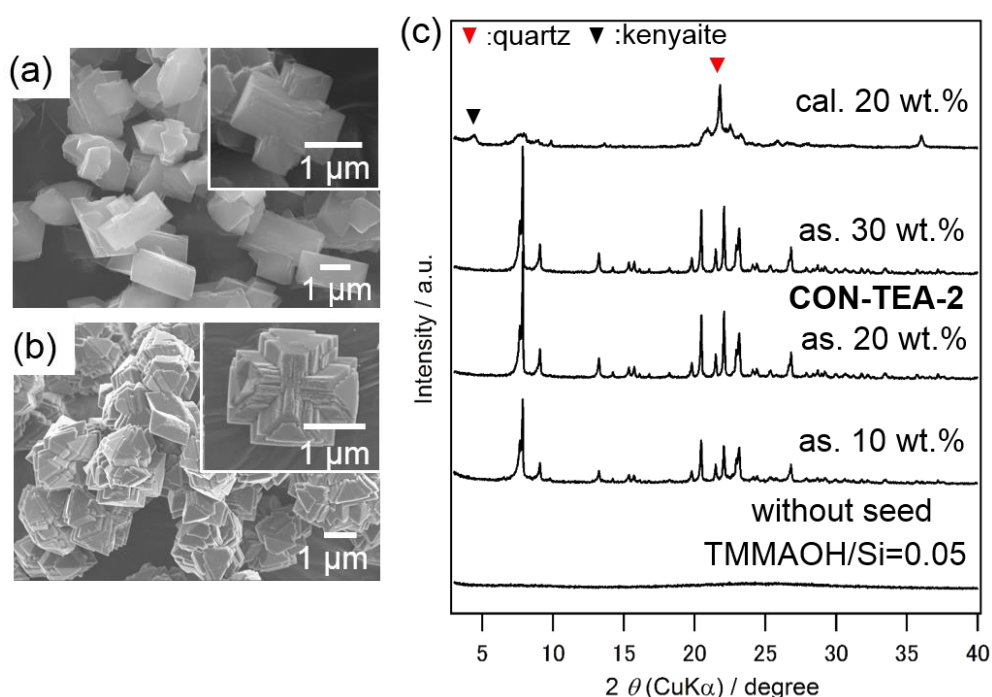


Figure 4.5 FE-SEM images of (a) small borosilicate CIT-1 seed crystals and (b) CON-TEA-2. (c) XRD patterns of the samples prepared by using various amount of as-synthesized, 20 wt.% calcined CIT-1 seed crystals, the same amount of TMAOH as occluded in the as-synthesized seed crystals instead of them.

optimum seeding is necessary to obtain fully crystalline pure products since seed crystals act as growth centers during the synthesis. Therefore, it can be said that the essential role of the seed crystals is to accelerate the crystal growth and prior to spontaneous nucleation. Moreover, the gel seeded using 20 wt% of calcined CIT-1 crystals resulted a mixture of kenyaite and quartz with so less amount of remained seed crystals. As it is previously reported,^[18] under harsh conditions, the calcined zeolite crystals tend to dissolve faster than the one having occluded OSDAs in their cavities as a result of the stabilization role of the OSDAs. Therefore, the difference in the products synthesized using as-synthesized and calcined seed crystals can be explained with the dissolution rate difference of those crystals. Since the seed crystals were exposed to the highly alkaline hydrothermal environment in our synthesis system, the use of as-synthesized seed crystals would allow partially dissolution and facilitate the promotion of CON growth. Also, to understand either as-synthesized seed crystals or the occluded TMMAOH in their structure are having effect in crystallization of CON-type zeolites, the sample prepared using the same amount of TMMAOH as occluded in the seed crystals instead of seed crystal itself resulted totally amorphous matter (see Figure 4.5 (c)). These results exhibit that a small amount of TMMAOH (TMMAOH/Si=0.05) added into this seedless gel had almost no effect on the structural direction of CON-type zeolites.

Moreover, to investigate the effect of type and amount of applied simple OSDA, some control samples were first prepared by using TMAOH and TPAOH. As seen in Figure 4.6 (a), the XRD patterns showed that those OSDAs resulted strong structure-directing effect for RUT and MFI-type zeolites, respectively. Regarding these results, one may also think either TEAOH can also direct CON structure due to its having relatively intermediate charge density (see Figure 4.6 (b)). However, when different amount of TEAOH was applied to the synthesis as shown in Figure 4.6 (c), it is found

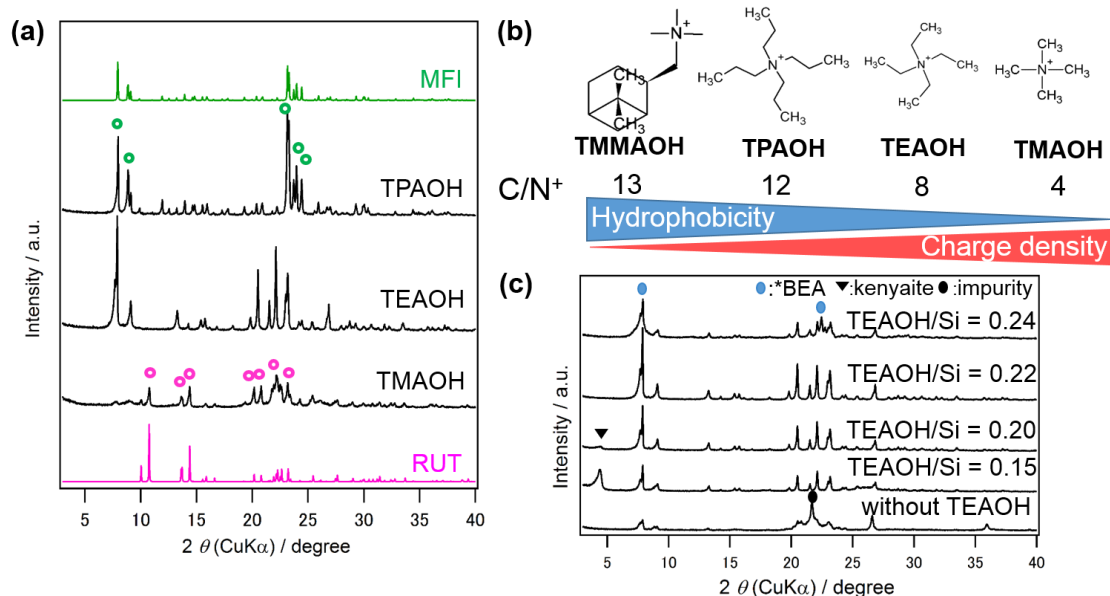


Figure 4.6 XRD patterns of the samples prepared by using (a) different type of simple OSDAs and (c) different amount of TEAOH. (b) C⁺/N ratio of the applied simple OSDAs.

that only a certain amount of TEAOH can favor CON growth in the seed-directed synthesis. Also, it can be seen that TEAOH is one of the indispensable factors to obtain pure CON product since the sample prepared in OSDA-free manner yielded quartz as dominant with a small amount of residue seed crystals. These results once again indicate that a certain amount of seed crystals along with TEAOH as a simple OSDA are having a collaborative growth effect in the rational synthesis of CON-type zeolites as well.

For a better understanding the crystallization mechanism, the crystallization kinetics were studied by synthesizing the samples at different period of hydrothermal treatment. In Figure 4.7 (a), the crystallinity curve presented that the as-synthesized product had approximately 15% relative crystallinity after 6 hours of heating which is possibly due to the residual CIT-1 seed crystals. After prolonging the synthesis time up to 24, 72, and 120 hours, the crystallinity of the as-synthesized CON-type zeolite product gradually increased, and the maximum crystallinity could be attained at 168 hours of heating. FE-SEM images of those samples in Figure 4.7 (b) also exhibited that seed

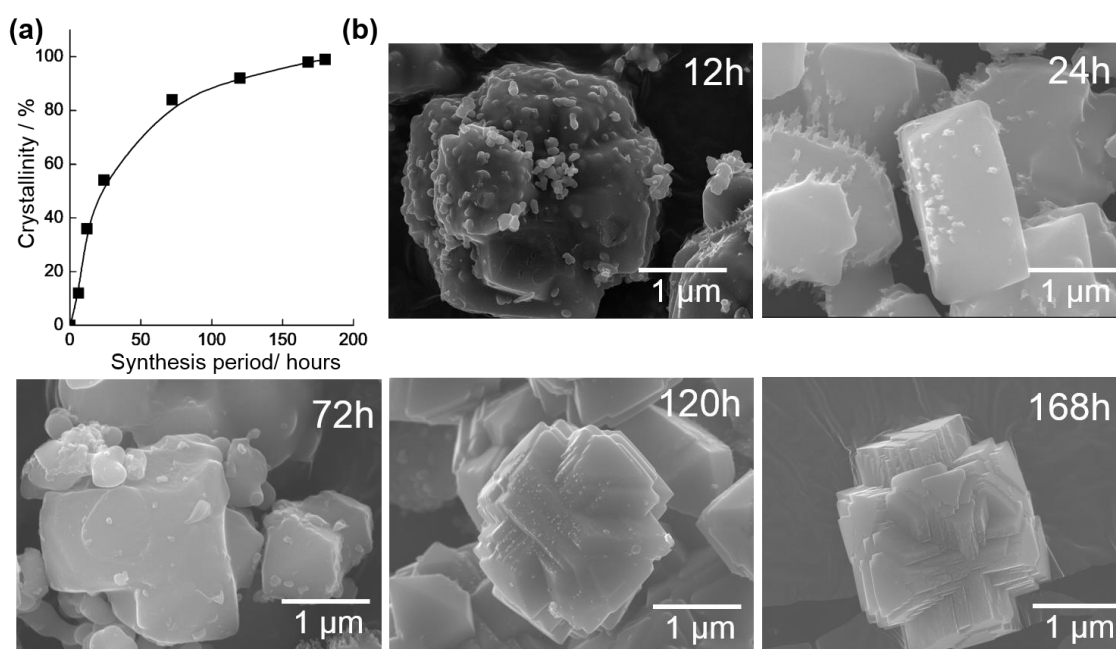


Figure 4.7 (a) Evolution of the crystallinity curve of CON-TEA product. (b) FE-SEM images of the as-synthesized products obtained by the hydrothermal treatment of rational synthesis gel for CON-type zeolites for various periods of time at 160 °C, in the presence of 20 wt% of as-synthesized CIT-1 seed crystals.

crystals were embedded with the round-shaped amorphous matter which induces the crystallization of CON-type zeolite by extending the hydrothermal treatment after 24, 72, 120 hours, and eventually completes the crystallization at 168 hours. Regarding these results, it can be said that seed crystals have an essential role to kinetically accelerate the crystal growth of CON-type zeolites which might occur on partially dissolved seed surfaces.

Furthermore, the structural and physicochemical properties of obtained CON-TEA sample were investigated by conducting ^{27}Al and ^{11}B MAS NMR, and N_2 adsorption-desorption measurement. As shown in Figure 4.8 (a), CON-TEA-2 sample displayed type I isotherms, which is corresponding to micropore characteristics as described in the International Union of Pure and Applied Chemistry (IUPAC)

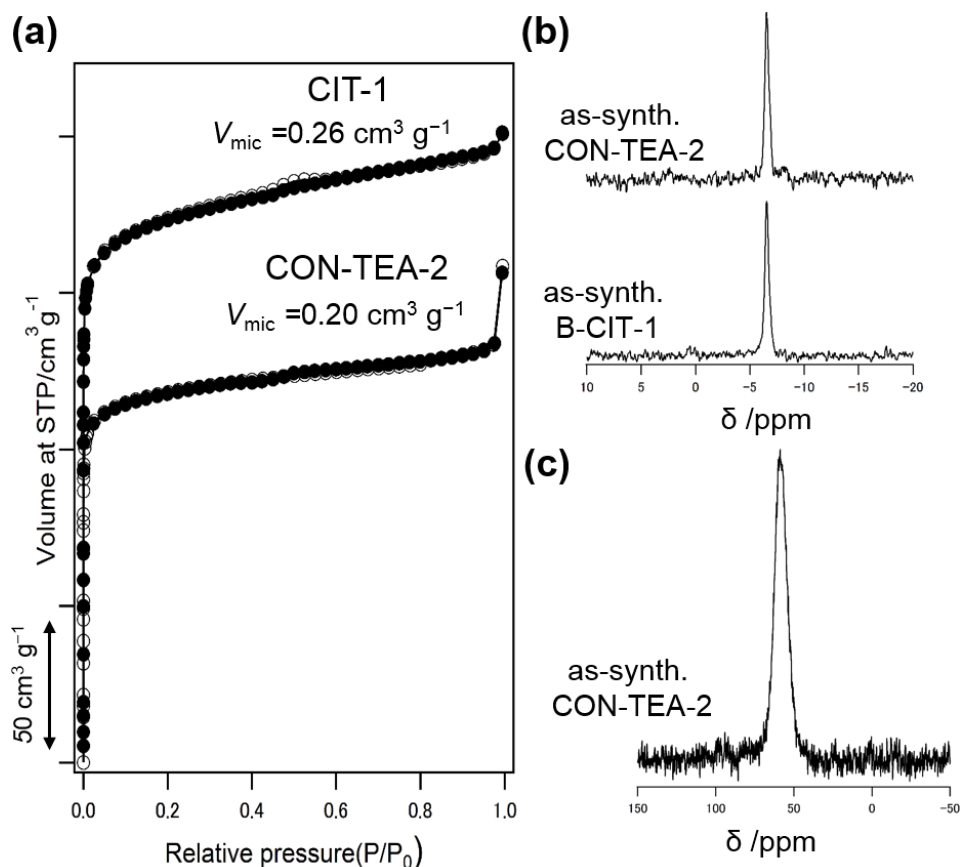


Figure 4.8 (a) Nitrogen adsorption-desorption isotherm of CON-TEA and borosilicate CIT-1 seed crystals. (b) ^{11}B and (c) ^{27}Al MAS NMR spectra of the as-synthesized CON-TEA-2 sample and for comparison CIT-1 seed crystals.

classification.^[21] Regarding these isotherm results, the calcined aluminoborosilicate CON-TEA sample displayed pore volume as $0.20\text{ cm}^3\text{ g}^{-1}$, which is similar to the reported values of conventionally synthesized H-type aluminoborosilicate CIT-1 ($0.21\text{ cm}^3\text{ g}^{-1}$), while borosilicate CIT-1 seed crystals have $0.26\text{ cm}^3\text{ g}^{-1}$.^[10] Therefore, it can be said that obtain CON-TEA sample revealed comparable micropore characteristics of conventional aluminoborosilicate CON-type zeolite. Moreover, ^{11}B and ^{27}Al MAS NMR spectra of the products revealed a strong peak at -3 ppm (see Figure 4.8 (b)) and 57 ppm (see Figure 4.8 (c)), respectively. These results confirmed the presence of only tetrahedrally coordinated boron and aluminum elements in the product.

4.3.2. Characterization of occluded tetraethylammonium cations

As seen in Table 4.1, ICP-AES results revealed that CON-TEA samples consist of an aluminum-rich structure with its Si/Al ratio ranging from 125 to 130 compared to reported aluminoborosilicate CIT-1 having Si/Al ratio as 196,^[10] and unlike conventional borosilicate CIT-1.^[2] These results can be indicative for that a certain amount of Al is incorporated into the newly grown CON structure on the borosilicate CIT-1 seed surface from the gel containing TEAOH. Also, it is shown that the sample prepared by using smaller seed crystals showed higher Si yield than that of one prepared from larger seed crystals, suggesting the strong effect of seed surfaces on the structural growth. Moreover, AAS results confirmed that K⁺ is occluded along with Na⁺ cation in the cavities of CON-TEA structure, indicating charge balancing effect of Na⁺, K⁺ and TEA⁺ cations during the crystal growth of CON-TEA. These results also showed once again the usage of binary alkali cation system is required for successful crystallization of CON-type zeolites from the gels consisting of simple OSDA. Regarding the overall results of elemental analysis, it is found that 3 TEA⁺ cations are occluded per unit cell. By remaining constant regardless of Si/B and Si/Al ratios, it can be said that the occluded

Table 4.1 Summary of the chemical features of the obtained CON-TEA products and CIT-1 seed crystals for comparison.

Sample	Gel Composition				Product					
	Si/ B	Si/Al	Si/B ^a	Si/Al ^a	Si Yield [wt.%]	Al+B/ u.c. ^a	Na+/ u.c. ^b	K+/ u.c. ^b	SDA+/ u.c. ^c	M ⁺ +SDA+/ u.c. ^c
CON-TEA-1	25	200	16	125	27	3.6	0.42	0.13	3.1 ^d	3.6 ^d
CON-TEA-2	25	200	18	130	35	3.3	0.28	0.05	3.0 ^d	3.3 ^d
Seeds	25	-	22	-	~95	2.4	-	-	3.6 ^e	3.6 ^e

^aSi, B and Al contents were quantified by ICP-AES. ^bNa and K measurements were carried out using AAS. ^cSDA+/u.c. and M⁺+SDA+/u.c. values were calculated from the ICP-AES, CHN and TGA results (u.c: unit cell of CON consisting of 56 T-atoms). ^dThe SDA was TEA⁺. ^eThe SDA was TMMA⁺.

OSDAs stabilize especially the 12-R channel and the intersections of the CON structure. Raman spectroscopy was employed on the as-synthesized CON-TEA-2 sample with *BEA as a reference to assess the conformational information of TEA⁺ cation occluded into the CON cavities. As it is known, TEA⁺ in aqueous solution consisted of two conformers with all-trans (tt.tt) and trans-gauche (tg.tg) arrangements (see Figure 4.9 (a)) which exhibit two distinct Raman bands.^[22] As shown in Figure 4.9 (b), two Raman peaks corresponding to TEA⁺ and TMMA⁺ (at 630 cm⁻¹) cations were observed, indicating a small amount of TMMA⁺ along with TEA⁺ cations are occluded into the newly obtained CON-TEA-2 product. Also, the deconvolution of the peak related to TEA⁺ presented two distinctive peaks centered at 676.5 and 664.5 cm⁻¹ assigned to the conformations of TEA⁺ cation which are tt.tt and tg.tg, respectively. The area fraction of these two Raman bands of TEA⁺ cation revealed that ca. 60% of the occluded TEA⁺ cation in CON-TEA were formed by tt.tt conformers, while tt.tt conformers constituted 95 % of all occluded TEA⁺ cation in *BEA structure.^[23] These results suggest that TEA⁺ cations are occluded in the obtained CON-TEA product, and play an important role in crystal growth of CON-type zeolite.

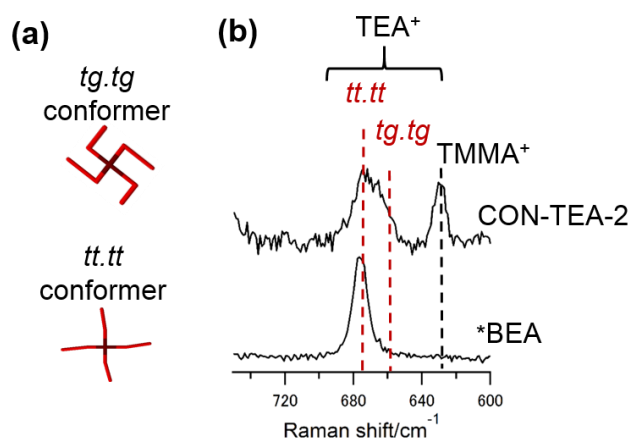


Figure 4.9 (a) Molecular model of TEA⁺ cation. (b) Raman spectra of CON-TEA and *BEA as a reference.

4.4. Conclusion

Synthesis of aluminoborosilicate CON-type zeolites was achieved from the Na-K gel containing TEAOH as a simple OSDA by the addition of as-synthesized borosilicate CIT-1 seed crystals. The obtained CON-TEA sample was composed of the crystals which are different from borosilicate CIT-1 seed crystals. This result confirms the crystal growth occurred on the partially dissolved seed crystal surfaces. Based on the physicochemical analysis, it is shown that the characteristics of the obtained CON-TEA material were comparable with those of conventional CIT-1, suggesting well-crystalline CON phase. Furthermore, the Raman spectra of CON-TEA sample revealed that TEA^+ is occluded into CON structure, and control experiments showed that it played an important role along with seed crystals for the crystal growth of CON-type zeolites as depicted in Figure 4.10. These results have also implied the validity of rational synthesis path for multipore zeolites containing medium and large pores in their structure.

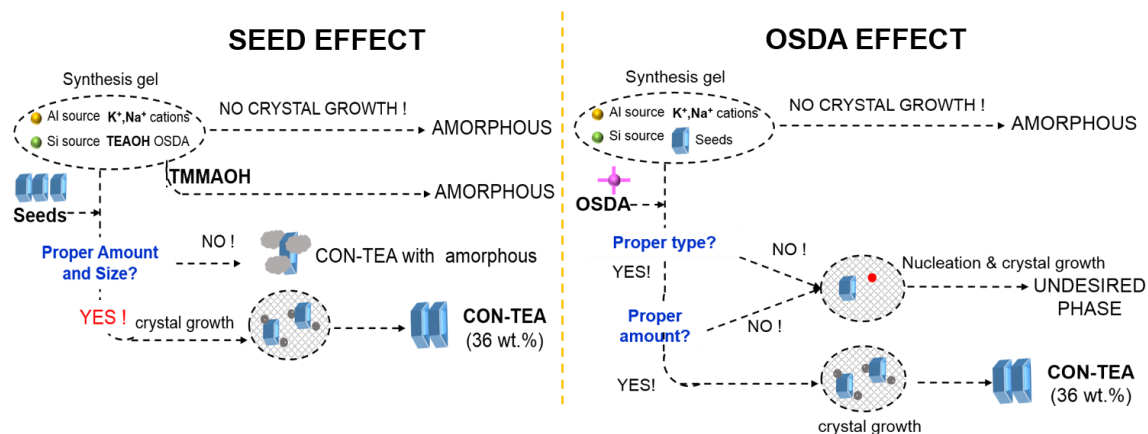


Figure 4.10 The effect of seed and OSDA in the rational synthesis of CON-type zeolites.

4.5. References

- [1] M. E. Davis, R. F. Lobo, U.S. Patent 5512267, 1996.
- [2] M. E. Davis, R. F. Lobo, *J. Am. Chem. Soc.* 117 (1995) 3766–3779.
- [3] J. M. Guil, R. Guil-López, J. A. Perdigón-Melón, A. Corma, *Microporous and Mesoporous Materials* 22 (1998) 269–279.
- [4] A. Corma, *Microporous and Mesoporous Materials* 21 (1998) 487–495.
- [5] B. Adair, C.Y. Chen, K. T. Wan, M. E. Davis, *Microporous Materials* 7 (1996) 261–270.
- [6] G. Sastre, N. Raj, C. R. A. Catlow, R. Roque-Malherbe, A. Corma, *J. Phys. Chem. B* 102 (1998) 3198–3209.
- [7] A. Corma, V. González-Alfaro, A.V. Orchillés, *Applied Catalysis A: General* 187 (1999) 245–254.
- [8] A. Corma, M. E. Davis, V. Fornés, V. González-Alfaro, R. F. Lobo, A. V. Orchillés, *J. Catal.* 167 (1997) 438–446.
- [9] T. Mathew, S. P. Elangovan, T. Yokoi, T. Tatsumi, M. Ogura, Y. Kubota, A. Shimojima, T. Okubo, *Microporous and Mesoporous Materials* 129 (2010) 126–135.
- [10] M. Yoshioka, T. Yokoi, T. Tatsumi, *ACS Catal.* 5 (2015) 4268–4275.
- [11] J. Q. Chen, A. Bozzano, B. Glover, T. Fuglerud, S. Kvisle, *Catal. Today* 106 (2005) 103–106.
- [12] C. D. Chang, C. T. W. Chu, R. F. Socha, *J. Catal.* 86 (1984) 289–296.
- [13] S. Sogukkanli, K. Iyoki, S. P. Elangovan, K. Itabashi, M. Takano, Z. Liu, S. Inagaki, T. Wakihara, Y. Kubota, T. Okubo, *Microporous Mesoporous Mater.* 245 (2017) 1–7.
- [14] J. E. Schmidt, D. Fu, M. W. Deem, B. M. Weckhuysen, *Angew. Chem. Int. Ed.* 55 (2016) 16044–16048.
- [15] T. Takewaki, L. W. Beck, M. E. Davis, *J. Phys. Chem. B* 103 (1999) 2674–2679.
- [16] M. W. Simon, S. S. Nam, W. -Q. Xu, S. L. Suib, J. C. Edwards, C. -L. O`Young, *J. Phys. Chem.* 96 (1992) 6381–6388.
- [17] K. Iyoki, K. Itabashi, T. Okubo, *Microporous Mesoporous Mater.* 189 (2014) 22–30.
- [18] Y. Kamimura, K. Itabashi, Y. Kon, A. Endo, T. Okubo, *Chem. Asian J.* 12 (2017) 530–542.
- [19] H. Kacirek, H. Lechert, *J. Phys. Chem.* 79 (1975) 1589–1593.
- [20] L. Gora, R.W. Thompson, *Zeolites* 15 (1995) 526–534.
- [21] M. Thommes, K. Kaneko, A. V. Neimark, J. P. Olivier, F. Rodrigues-Reinoso, J. Rouquerol, K. S. W. Sing, *Pure Appl. Chem.* 87 (2015) 1051–1069.

- [22] C. Naudin, F. Bonhomme, J. L. Bruneel, L. Ducasse, J. Grondin, J. C. Lassègues, L. Servant, *J. Raman Spectrosc.* 31 (2000) 979–985.
- [23] T. Ikuno, W. Chaikittisilp, Z. Liu, T. Iida, Y. Yanaba, T. Yoshikawa, S. Kohara, T. Wakihara, T. Okubo, *J. Am. Chem. Soc.* 137 (2015) 14533–14544.

Chapter 5. General Conclusion and Future Perspectives

During the last decades of porous material history, great efforts have been made to synthesize so-called “multipore” zeolites, which contain channels of different directions within the same crystalline structure. This is a very attractive subject since the presence of pores of different sized would favor the preferential diffusion of reactants and products through different channels, allowing unique catalytic activities for specific reactions. However, the synthesis of multipore zeolites frequently requires the use of complex and expensive OSDAs, which hampers to manufacture these zeolites. Therefore, there is always a call to develop the rational synthesis of existing multipore zeolites.

In Chapter 1, the general background and the rationalization of the objective and strategy of this dissertation are presented. In this dissertation, developing rational synthesis route for multipore zeolites with medium and large pores is described. This simplified synthesis is built on solely using commercially available quaternary ammonium as OSDA in the seed-directed method. In order to select the most suitable organic molecules and synthesis conditions, composite building unit (CBU) hypothesis is extended to obtain target multipore zeolite, and it is further called as “Extended CBU Hypothesis”. The concept applied in this research aims to suppress the formation of undesired products, and to efficiently promote the direct crystal growth on the partially

dissolved seed crystal surfaces with the help of using simple OSDAs. For doing this, the synthesis conditions were optimized by aging, modifying reaction composition and controlling the kinetics. These adjustments, combined with the advantages of simple OSDAs in the seed-directed method, allow obtaining highly crystalline pure multipore zeolites with satisfying solid yields which could not be achieved in any other alternative synthesis paths, so far.

In Chapter 2, the synthesis of aluminosilicate MSE-type zeolites is investigated. Unlike previous reports stating that costly and bulky organic molecules are essential to form MSE-type zeolites, a simplified and efficient synthesis route to these multi-dimensional, large-pore zeolites by using TEOAH as a simple OSDA is developed. Based upon CBU hypothesis, a clear relation was found among MSE, *BEA, and MOR framework types. According to this relation, TEOAH which is basically utilized for the industrial production of *BEA-type zeolite was determined to be used in a modified gel composition as an easily reachable and comparatively inexpensive OSDA. This novel approach allowed to obtain pure solid products with high yields by consecutively applying aging and hydrothermal synthesis steps. The series of characterizations revealed that the features of obtained products were similar to those of conventional MCM-68 with relatively better microporosity characteristics. Remarkably, the “second-generation” products can be synthesized via this novel route by optimizing the aging time. Considering the overall results, this method is assumed as the most simplified and efficient synthesis route for MSE-type zeolites.

In Chapter 3, the synthesis of zincoaluminosilicate MSE-type zeolites is studied. Simplified and efficient synthesis of MSE-type zeolites by using tetraethylammonium hydroxide (TEAOH) is extended from aluminosilicate to

zincoaluminosilicate by combining with co-precipitated gel technique. The direct crystallization of MSE-type zeolite could be realized from the synthesis gels containing co-precipitated gels in which homogeneously dispersed zinc and aluminum species having a $Zn/(Zn+Al)$ ratio up to 0.4. The overall characterizations revealed that most of the zinc species were incorporated as a heteroatom, and created anionic charges in MSE framework. Also, it is confirmed that the newly obtained zincoaluminosilicate MSE-type zeolite consists of a core-shell structure, in which shell as the newly grown zincoaluminosilicate, while core as residual aluminosilicate seed crystals. Based on the ion-exchange characteristics of those samples, it is found that the most of the inserted zinc species exhibited two anionic charges per atom, which is expected to be suitable sites for divalent-cation exchange. Since the sample prepared by using $Zn/(Zn+Al)$ ratio of 0.2 (MSE-TEA_{Zn0.2}) remained stable after thermal treatment, Ni²⁺ exchange was applied to that sample. These results revealed that MSE-TEA_{Zn0.2} sample exhibited the superior ion-exchange capacity to aluminosilicate MSE-TEA sample. Therefore, MSE-TEA_{Zn0.2} sample can be purposed as a potential divalent-cation exchanger. In this report, it is demonstrated that the simplified synthesis path is a very effective alternative way to synthesize multipore zeolites containing medium and large pores in the frameworks with different heteroatoms.

In Chapter 4, the synthesis of aluminoborosilicate CON-type zeolites is investigated. It is found that CON structure shares common CBUs with *BEA and MFI, which are traditionally synthesized by using simple quaternary ammoniums such as TEOH and TPAOH as OSDAs, respectively. Moreover, MFI can be fabricated from the synthesis gels containing TEOH, hence, TEOH is thought to be suitable simple and commercially available OSDA for crystal growth of CON-type zeolites. Regarding the

obtained results, it is found that rational synthesis is possible for CON structure which could not be synthesized other than conventional method thus far. The obtained highly crystalline CON-TEA sample exhibited larger crystals which are distinguishable than borosilicate CIT-1 seed crystals. This result confirms once more that the crystal growth occurs on the partially dissolved seed crystal surfaces. Regarding physicochemical analysis, it can be said that the characteristics of obtained materials were comparable with those of CIT-1 seed crystals, suggesting well-crystalline CON phase. Furthermore, the Raman spectra of CON-TEA sample revealed that TEA^+ is occluded into CON structure, and played an important role in the crystal growth of CON-type zeolites. These results showed the validity of rational synthesis path for other multipore zeolites containing medium and large pores in their structure.

Finally, in Chapter 5 general conclusions and future perspectives of this doctoral dissertation is presented. Overall results revealed that the present research proposed a new synthesis path involving the use of simple and commercially available quaternary ammoniums as OSDAs and a certain amount of seed crystals. The selection of those OSDAs has been done by considering shared composite building units between target multipore zeolite and another zeolite which can be synthesized using those simple OSDA. In this regard, the rational synthesis of MSE and CON as two different type multipore zeolites containing medium and large pores has been achieved by using TEAOH as an OSDA with reasonable solid yields, suggesting TEAOH as probably the most suitable simple OSDA for multipore zeolites. Moreover, the rational synthesis allowed the insertion of zinc species as a heteroatom in the aluminosilicate MSE-type zeolites which is the first direct synthesis of MSE or multipore zeolites with zinc in their framework.

As cited in this dissertation, the combination of seed-directed method and simple OSDAs, so-called rational synthesis, opened a new door for economical, high-yield synthesis of multipore zeolites containing medium and large pores. However, there are some key issues which are first required to be well-investigated for further extensions of the rational synthesis. These issues can be: (i) understanding the exact role of alkali cations during in crystallization, (ii) finding an OSDA that does not show any structure-directing effect for a specific structure, (iii) designing rational synthesis gels which can yield much higher solid product. After this investigation, it is surely expected that the applicability of rational synthesis can be expanded to other multipore zeolites containing various heteroatoms which require complex OSDAs to be synthesized. By doing this, we would be enabled to reach the existing multipore structures and bring them in the industries. Moreover, as shown in this dissertation, rational synthesis makes the insertion of different framework element possible, which would amplify their applications and introduce new industrial applications for those existing structures.

As a conclusion, it is clearly shown that the rational synthesis is valid for the multipore zeolites containing medium and large pores, and can be a way to improve the existing structures by the allowance of the insertion different atoms in the framework which may lead to open new windows to the zeolite world.

List of publications

Publications related to this dissertation

Chapter 2

1. S. Sogukkanli, K. Iyoki, S. P. Elangovan, K. Itabashi, M. Takano, Z. Liu, S. Inagaki, T. Wakihara, Y. Kubota and T. Okubo, “Rational Seed-Directed Synthesis of MSE-type Zeolite using a Simple Organic Structure-Directing Agent by Extending Composite Building Unit Hypothesis”, *Microporous and Mesoporous Materials*, 245, 2017, 1-7.

Chapter 3

2. S. Sogukkanli, K. Iyoki, S. P. Elangovan, K. Itabashi, M. Takano (0.1), N. Koike (0.1), Y. Kubota and T. Okubo, “Seed-Directed Synthesis of Zincoaluminosilicate MSE-type Zeolites using Homogenous Gels with Tetraethylammonium Hydroxide as Organic Structure Directing Agent”, *Microporous and Mesoporous Materials*, 2017, *In Press*.

Chapter 4

3. S. Sogukkanli, K. Iyoki, S. P. Elangovan, K. Itabashi, T. Okubo, “Seed-Directed Synthesis of CON-type Zeolite using Tetraethylammonium Hydroxide as a Simple Organic Structure-Directing Agent”, *Chemistry Letters*, 2017, <https://doi.org/10.1246/cl.170602>.
4. S. Sogukkanli, K. Iyoki, S. P. Elangovan, K. Itabashi, T. Okubo “Rational Synthesis for Multipore Zeolites with Medium and Large Pores”, *In Preparation*.

Acknowledgment

The written sentences in this pages are my deepest gratitude to all those who supported and encouraged me to complete my doctoral research in The University of Tokyo, Japan.

First and foremost, I would like to express my most heartfelt appreciation to my supervisor, Professor Tatsuya Okubo, for giving me the opportunity to be a member of Okubo-Wakihara Laboratory, and pursuing my Ph. D. He showed an ideal image of the professor to me by living his motto “ *Think globally, act locally!* ” in reality since the day I met him. I am wholeheartedly grateful for his moral support, steady encouragement, extraordinarily tolerant, and insightful advice not only my research but also daily life in Japan which made me moving forward and doing better research.

I would like to thank Associate Professor Toru Wakihara for his continuous encouragement, constructive advice and supports during my graduate study. The discussions with him were always cheerful and enjoyable.

My special thanks go to Dr. Keiji Itabashi who taught me the synthesis of zeolites. I always admired his creativity and hard work. In addition to academic research, his advice for my various difficulties was incredibly helpful. I will be forever thankful to Dr. Shanmungam Palavi Elangovan for his endless support, insightful discussions, and countless advice which I have greatly benefited.

I sincerely appreciate to Assistant Professor Kenta Iyoki for his companionship, encouragement, constructive comments toward improving my work. He is always offering his help whenever I need. I am also thankful to Assistant Professor Watcharop Chaikittisilp for his thoughtful advice, kind discussion, and experimental help. He is really brilliant and admirable person in research.

I appreciate the feedback provided by the committee members, Professor Kazunari Domen, Professor Masaru Ogura, Professor Kazuya Yamaguchi, and Associate Professor Masashi Okubo, also their valuable time and comments on my research.

I would like to express my greatest appreciation to all my co-workers, for their contributions and helps in laboratory works. I would like to thank Professor Yoshihiro Kubota, Associate Professor Satoshi Inagaki, and Ms. Miku Takano, Yokohama National University for their help in Chapter 2 and Chapter 3. Also, Professor Masaru Ogura and Ms. Natsume Koike, The University of Tokyo for the access to and performing FT-IR analysis in Chapter 3, respectively.

I would like to thank all the members in Okubo-Wakihara Laboratory for continuous experimental and daily life supports, which was really helpful for me to handle my life in Japan. Especially, our secretaries, Ms. Yoko Ohashi, Ms. Ayako Saito, Ms. Yoshie Hayashi, Ms. Ikuko Kinumatsu, and Ms. Kazuko Yokoyama. Also, I would like to send my deepest thanks to our international students, whom I had an amazing time.

I also address my sincere appreciation to Ministry of Education, Culture, Sports, Science, and Technology for the Monbukagakusho scholarship for the financial support which let me to have the chance for pursuing my Ph. D. at The University of Tokyo.

I am also greatly indebted to my dear friend Ms. Suheyla Koc who always supports me in any condition. Also, I owe to a special thanks to Mr. Mahdi Javanmardi who made life more beautiful.

Finally but not least, I would like to express my gratitude to my parents Ms. Necla Sogukkanli and Mr. Coskun Sogukkanli for their unconditional love, moral support, constant understanding, and sincere encouragement.

Benim canımı, ömrümü ve hayatımı adadığım tek varlığım olan aileme en içten teşekkür ve saygılarımla.

Sibel SOĞUKKANLI

シベル ソウグクカナル